次世代地上波デジタルTVシステムに関する研究

A Study on Next Generation Digital Terrestrial Television System.

平成 25 年度
博士論文

九州工業大学大学院
情報工学府
情報システム専攻
09792005

Nico Surantha

Contents

List of Figures

List of Tables

Summary

Currently the research about the digital terrestrial television is still progressing. The research is intended to realize the tranmission of high resolution digital television. ISDB-T is the standards that was developed by Japan in 1998. The standard has been implemented not only by Japan, but also by some South America countries. On the other hand, DVB-T is the first generation of digital terrestrial television that were proposed by several European countries. This standard has been used by most countries in the world.

The DVB-T2 system is a second generation of a digital terrestrial television standard based on the orthogonal frequency division multiplexing (OFDM) system. In this system, a multi input-single output (MISO) with Alamouti scheme has been included in order to increase a diversity gain that is essential for reception performance in low speed environment. However, in the future the mobil reception of digital terrestrial television in high speed environment, such as high speed train (TGV, Maglev, etc with commercial speed = 300 km/h) will become an important aspect in the competition with other digital broadcasting system, such as digital satellite. There is a need to provide information and on board entertainment services to high speed train passengers. In this case, the inclusion of MIMO scheme become necessary to increase the reception performance of high speed digital terrestrial television.

In a MISO/MIMO system based on the Alamouti scheme, it has been acknowledged that a channel estimation would hold the important role in maintaining the diversity gain that is provided by Alamouti scheme and maximal ratio combining scheme. If different signals are transmitted simultaneously from two transmitters, it will be received as a superposition of signals by the receiver. This will become one of the main challenge of channel estimation in MISO/MIMO system. In this thesis, the channel estimation for 2×1 MISO and 2×2 MIMO scheme in high speed mobile environment is proposed.

In order to cope with the parallelogram-shaped grid pilot pattern of the DVB-T2 system, we have employed the 2D filter with a non-rectangular spectrum. It was actually proposed for an image processing application. A single stage implementation of the the 2D filter continues to have a high complexity cost. Thus, we have divided the 2D filter into two stage of filtering in the time and frequency direction separately, resulting in lower complexity in hardware implementation. In order to optimize the performance of interpolation filter in a 2×2 MIMO system, we have proposed the 3-points diagonal averaging method. This method can shorten the distances between scattered pilots resulting in the improvement of channel estimation performance.

In this thesis, we have also done a research about synchronization for OFDM based Digital Terrestrial Television broadcasting. There are three problem of synchronization that we investigate here, i.e. symbol timing offset (STO), carrier frequency offset (CFO), and sampling frequency offset (SFO). An STO occurs because the receiver does not know exactly the arrival time of OFDM symbol, therefore there is an offset in determination of an OFDM symbol starting point. On the other hand, CFO and SFO are caused by a carrier frequency and a sampling frequency mismatch between the trans-

mitter and receiver local oscillators, respectively. All of this synchronization problem could introduce an intersymbol interference (ISI) and an intercarrier interference (ICI) to the signal received by a digital terrestrial television broadcasting receiver. The demodulation of signal that contains ICI and ISI will dramatically increase bit error rate.

In this thesis, we have proposed a joint-synchronization method for ISDB-T system in Multipath Fading Channel. This joint-synchronization method consists of three stages. In the first-stage, we have employed joint time and frequency synchronization using a simplified maximum likelihood method. In the second-stage, we have proposed a DFT window shift to avoid ISI. Both of this stage are implemented in time domain. In the third stage,we have proposed a frequency domain SFO estimation method that exploits scattered pilots to estimate an SFO. Since the value of SFO is usually very small (part per million (ppm) scale), the SFO estimation is very susceptible to a noise. Therefore, in this thesis, we have proposed an estimation method that can minimize the influence of noise in estimating the SFO.

Finally, we can summarize that the main contribution of this research is an implementation of low complexity and robust channel estimation method for very high speed mobile DVB-T2 system. The simulation results show that the proposed channel estimation method can optimize the diversity gain that is provided by multi-antenna techniques to improve the performance of the mobile DVB-T2 system. Another contribution is a robust synchronization method for OFDM based Digital Terrestrial Television Broadcasting in multipath fading channel. Simulation results show that the proposed synchronization method can produce high performance in multipath fading channel, while has lower complexity

Chapter 1

Introduction

1.1 Background

Currently the research about the digital terrestrial television is still progressing. The research is intended to realize the tranmission of high resolution digital television. There are many standards that are developed by many countries to implement the transmission of digital terrestrial television. ISDB-T is the standards that was developed by Japan in 1998. The standard has been implemented not only by Japan, but also by some South America countries. On the other hand, DVB-T is the first generation of digital terrestrial television that were proposed by several European countries. This standard has been used by most countries in the world.

The DVB-T2 system [1] is the second generation of a digital terrestrial television standard based on the orthogonal frequency division multiplexing (OFDM) system. It was developed in order to increase the capacity and quality of digital terrestrial broadcasting from a previous DVB-T system [2]. One of the modification that the DVB-T2 system had developed on top of DVB-T is the inclusion of multi transmitter antenna techniques, referred to as a 2×1 MISO based on Alamouti scheme [3], which can provide a diversity gain that is essential for the reception performance of a digital terrestrial television.

In a 2×1 MISO system based on the Alamouti scheme, it has been acknowleged that channel estimation would hold the important role in maintaining the diversity gain that is provided by Alamouti scheme [3]. If different signals are transmitted simultaneously from two transmitters, it will be received as a superposition of signals by the receiver. This will become one of the main challenge of channel estimation in a 2×1 MISO system.

However, as illustrated by Fig. 1.1 in the future the mobile reception of digital terrestrial television in high speed environment, such as high speed train (TGV, Maglev, etc with commercial speed $\approx$ 300 km/h) will become an important aspect in the competition with other digital broadcasting system, such as digital satellite. A particularly important commercial application is to provide information and onboard entertainment services to passengers. In this case, the inclusion of MIMO scheme become necessary to increase

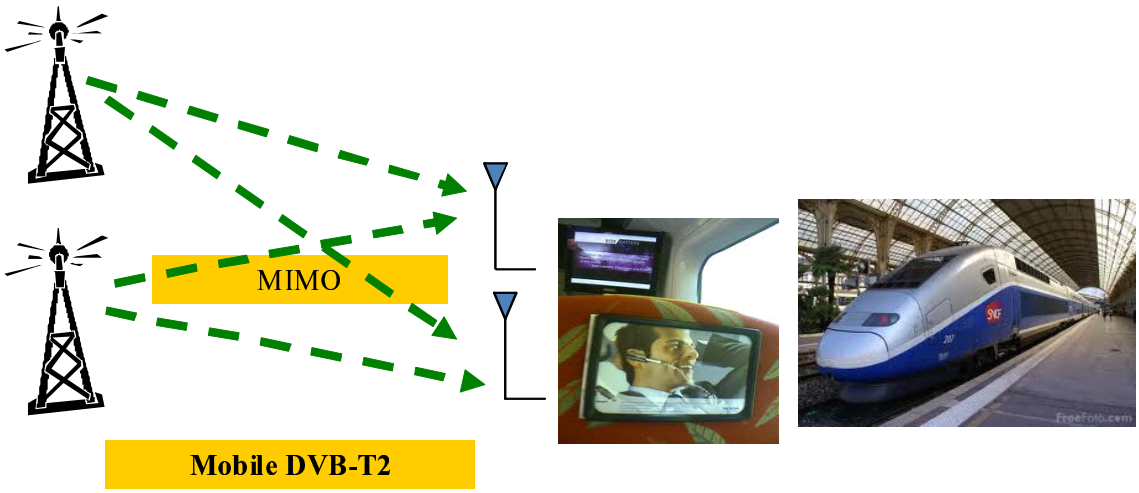

Figure 1.1: MIMO system for mobile reception DVB-T2 in high speed environment

the reception performance of high speed digital terrestrial television.

In a fixed reception, the channel estimation of OFDM systems would only need to deal with the frequency selectivity caused by multipath fading. On the other hand, in mobile reception, the systems also need to deal with the time varying channel due to a Doppler shift. This time variance factor will lead to an intercarrier interference (ICI), resulting in error floor as the doppler frequency increases. This will affect the performance of the pilot aided channel estimation (PACE), since the received pilot will be corrupted by ICI. It will also become another challenge of channel estimation in mobile DVB-T2 system. In this thesis, a channel estimation for a MIMO system in high speed mobile environment is proposed. Until now, many research works have been conducted regarding PACE for the multi antenna OFDM system. [4–6] proposed 1D channel estimation for the multi antenna OFDM systems, which is limited only to the frequency direction, as opposed to the 2D channel estimation method proposed by [7] that can track the variation of time varying channel even at high doppler frequencies. Reference [7] however, employed the Wiener filter which has a very high complexity cost.

In order to cope with the parallelogram-shaped grid pilot pattern of the DVB-T2 system, we have employed the 2D filter with a non-rectangular spectrum. It was actually proposed by [8] for an image processing application and has been successfully implemented in the Single Input Single Output (SISO) system channel estimation [9]- [10]. A single stage implementation of the the 2D filter continues to have a high complexity cost. Thus, we have divided the 2D filter into two stage of filtering in the time and frequency direction separately, resulting in lower complexity in hardware implementation.

We have also proposed the 3-points diagonal averaging method to optimize the performance of an interpolation filter in a MIMO system. This method can shorten the distances between scattered pilots resulting in the improvement of channel estimation performance. The combination between the proposed 3-points diagonal averaging method

and the two stage implementations of a 2D non-rectangular filter is proven to be robust in very high speed mobile environment and has a capability to optimize a diversity gain provided by the Alamouti Scheme.

In OFDM receiver, synchronization is also one of the main problem. There are three problem of sycnchronization that we investigate here, i.e. symbol timing offset (STO), carrier frequency offset (CFO), and sampling frequency offset (SFO). An STO occurs because the receiver does not know exactly the arrival time of OFDM symbol, therefore there is an offset in determination of an OFDM symbol starting point. On the other hand, CFO and SFO are caused by a carrier frequency and a sampling frequency mismatch between the transmitter and receiver local oscillators, respectively. All of this synchronization problem could introduce an intersymbol interference (ISI) and an intercarrier interference (ICI) to the signal received by a digital terrestrial television broadcasting receiver. The demodulation of signal that contains ICI and ISI will dramatically increase bit error rate.

In this thesis, we have proposed three-stages joint-synchronization for ISDB-T system in Multipath Fading Channel. In the first-stage, we have employed joint time and frequency synchronization using a simplified maximum likelihood method. In the second-stage, we have proposed a DFT window shift to avoid ISI. Both of this stage are implemented in time domain. In the third stage,we have proposed a frequency domain SFO estimation method that exploits scattered pilots to estimate an SFO. Since the value of SFO is usually very small (part per million (ppm) scale), the SFO estimation is very susceptible to a noise. Therefore, in this thesis, we have proposed an estimation method that can minimize the influence of noise in estimating the SFO.

1.2 Research Objectives

The objectives of this research is an implementation of low complexity and robust channel estimation method for very high speed mobile DVB-T2 System. In this research, we have investigated how the proposed channel estimation method can optimize the diversity gain that is provided by multi antenna technique in transmitter and receiver. We have also investigated how the proposed architecture can reduce the complexity of implementation compared to the conventional architecture. Another objective of this research is an implementation of low complexity and robust synchronization method for OFDM based system in multipath fading channel.

1.3 Thesis Hierarchy

This thesis consists of five chapters where the first chapter is devoted to the introduction of the thesis work. The following chapters are organized as follows.

Chapter 2 Digital Terrestrial TV Overview

This chapter provides the overview of Digital Terrestrial TV Standard that cur-

rently used all over the world. Then we discuss specificaly about european standard, DVB-T that is upgraded to DVB-T2. We explain briefly what is the motivation of DVB-T2 development and the benefit of this system over DVB-T. The OFDM baseband model and the MIMO system of DVB-T2 are also discussed in this chapter

Chapter 3 Pilot Aided Channel Estimation for DVB-T2 System

This chapter discusses about a channel estimation using scattered pilot for DVB-T2 System. We start with the overview of pilot pattern in SISO and MISO mode. Then, The Channel estimation in SISO and MIMO mode using scattered pilot is discussed in detail, including the proposed 3-point averaging method for MIMO DVB-T2 system. This chapter also provides the explanation about the proposed 2D non-rectangular filter and how to implement it with less complexity for channel estimation system

Chapter 4 Synchronization Method for DTTB System

This chapter discuss about symbol-timing, carrier-frequency, sampling-frequency synchronization in multipath fading channel. Firstly, we discuss about the effect of synchronization error for OFDM system. Then, we discuss about the conventional and proposed synchronization method.

Chapter 5 Simulation Results and Analysis

This chapter provides simulation results and analysis of the proposed method compared to the conventional method

Chapter 6 Conclusion and Future Work

This chapter provides a short summary of the whole report and the obtained results. Some recommendations are also given concerning the further development of this research topic.

Chapter 2

A Digital Terrestrial TV Overview

Digital terrestrial television (DTTV or DTT) is the technological evolution of broadcast television and an advancement of analog television. DTTV broadcasts land-based (terrestrial) signals. The purposes of digital terrestrial television, similar to digital versus analog in other platforms such as cable, satellite, and telecommunications, are to reduce use of spectrum and to provide more capacity than analog, provide better-quality picture, and to lower operating costs for broadcast and transmission after the initial upgrade costs. A terrestrial implementation of digital television (DTV) technology uses aerial broadcasts to a conventional television antenna (or aerial) instead of a satellite dish or cable television connections.

2.1 The Existing Digital Terrestrial TV Standard in The World

Competing variants of broadcast television systems are being used around the world. Some of the existing digital terrestrial tv standard are listed as follow:

- DVB-T

  DVB-T [2] is an abbreviation for Digital Video Broadcasting-Terrestrial which is DVB European-based consortium standard for broadcasting technology in digital terrestrial television. It was first published in 1997 and first broadcasted in UK in 1998. This system transmits compressed digital audio and digital video in an MPEG transport stream, using orthogonal frequency-division multiplexing(OFDM) modulation. In 2009, the DVB Group launched the second generation of digital terrestrial television [1]. This system was developed in order to transmit the high-definition television contents. This system offers an increased efficiency of 30-50% in its use of spectrum compared to DVB-T [2]. DVB-T and DVB-T2 has the biggest number of consumer country in the world as shown by Fig. 2.1. This system will be discussed more detail in sec. 2.2

- ISDB-T

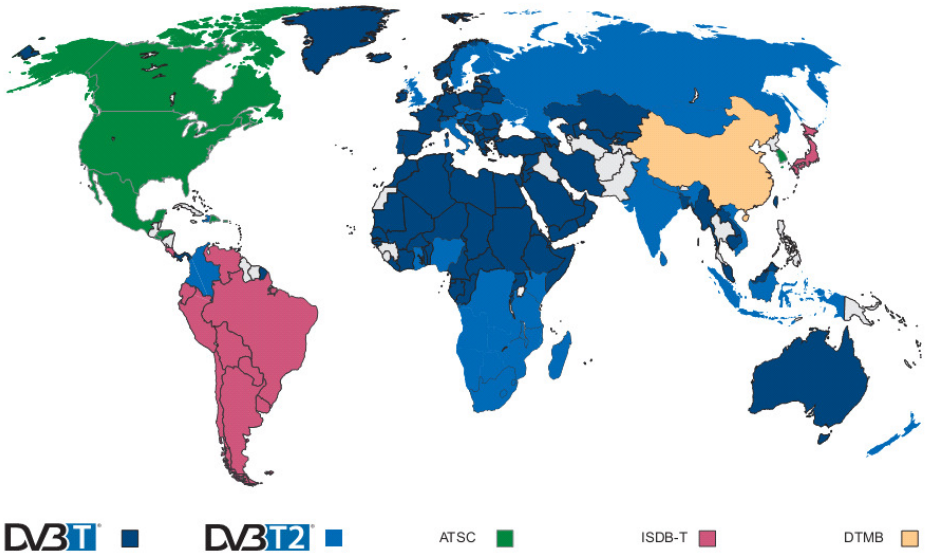

Figure 2.1: The map of digital terrestrial television standard [11]

ISDB-T [12] is an abbreviation for Integrated Services Digital Broadcasting-Terrestrial which is a Japanese standard for digital television and digital radio broadcasting. Similar to DVB-T, ISDB-T employ an OFDM as their modulation technique. This system was first launched in Japan in December 2003 and in Brazil in December 2007 [13].The number of the country which has adopted its standard is gradually increasing with the recognition of its technological advantage. ISDB-T has been adopted by almost all country in South America in 2009, such as Argentina, Peru, Chille, and Venezuela. One of the most technical advantage of ISDB-T is the OFDM segmented transmission that enables fixed, mobile, and portable transmission all in one channel. As a comparison, DVB-T and ATSC require another channel for portable reception service, on the other hand, ISDB-T enables fixed/mobile/portable service in same channel by one transmitter. It leads not only saving the frequency resource but also saving transmitter cost The transmitted signals are divided into 13 segments with a bandwidth of 5.57 MHz bandwidth. It enables us to broadcast for various different purposes because we can change the parameter in each segment. Using 12 of the 13 segments enables High Definition Television (HDTV) services and using 4 segments enables Standard Definition Television(SDTV) services. Moreover, one of the 13 segments is specially designed for onesegment reception, enabling ISDB-T transmission to mobile terminals by using only this segment.

- ATSC

  Advanced Television Systems Committee (ATSC) standards [14] are a set of standards developed by the Advanced Television Systems Committee for digital television transmission over terrestrial, cable, and satellite networks. The ATSC stan-

dards were developed in the early 1990s by the Grand Alliance, a consortium of electronics and telecommunications companies that assembled to develop a specification for what is now known as HDTV. ATSC formats also include standard-definition formats, although initially only HDTV services were launched in the digital format. This system is widely used in north america, parts of Central America, and South Korea. ATSC as implemented in the US uses 8VSB modulation, which requires less power to transmit, as opposed to the also proposed COFDM modulatiion (which is less prone to multipath distortion and therefore better received in mobile installations.

- DTMB

  DTMB (Digital Terrestrial Multimedia Broadcast) is the TV standard for mobile and fixed terminals used in the People's Republic of China, Hong Kong and Macau. The DTMB was created in 2004 and finally became an official DTT standard in 2006. The DTMB standard uses many advanced technologies to improve their performance, for example, a pseudo-random noise code (PN) as a guard interval that allows faster synchronization system and a more accurate channel estimation, Low-Density Parity-Check (LDPC) encoding to protect against mistakes, modulation Time Domain Synchronization - Orthogonal Frequency Division Multiplexing (TDS-OFDM) which allows the combination of broadcasting in SD, HD and multimedia services, etc. This system gives flexibility to the services offered to support the combination of single-frequency networks (SFN) and multi-frequency networks (MFN). The different modes and parameters can be chosen depending on the type of service and network's environment.

2.2 The ISDB-T system

2.2.1 The Overview of ISDB-T System

The Integrated Services Digital Broadcasting-Terrestrial (ISDB-T) system is designed to provide reliable high-quality video, sound, and data broadcasting not only for fixed receivers but also for mobile receivers. The system is also designed to provide flexibility, expandability, and commonality/interoperability for multimedia broadcasting. The system is rugged because it uses orthogonal frequency division multiplexing (OFDM) modulation, two-dimensional (frequency-domain and time-domain) interleaving, and concatenated error-correcting codes. Its modulation scheme is called Band Segmented Transmission-OFDM (BST-OFDM), and it consists of 13 OFDM segments. The system has a wide variety of transmission parameters for choosing the carrier modulation scheme, coding rate of the inner error-correcting code, length of time interleaving,

Table 2.1: Basic Transmission Parameters for ISDB-T [12]

Transmission Parameter	Mode 1	Mode 2	Mode 3
No. of OFDM segments	13		
Bandwidth	5.5575 MHz	5.573MHz	5.572 MHz
Carrier interval	3.968kHz	1.984 kHz	0.992 kHz
No. of carriers	1405	2809	5617
Carrier modulation	QPSK, 16QAM, 64QAM, DQPSK		
Effective symbol length	252 μs	504 μs	1.008 ms
Guard Interval length	1/4, 1/8, 1/16, 1/32 of effective symbol length		
No. of symbols per frame	204		
Time Interleave	Maximum 4 values: 0, 0.1, 0.2, 0.4 sec		
Frequency interleave	Intra-segment and inter-segment interleaving		
Inner code	Convolutional coding (1/2, 2/3, 3/4, 5/6, 7/8)		
Outer code	RS (204, 188)		
Information bit rate	3.65 Mbps - 23.23 Mbps		
Hierarchical transmission	Maximum 3 level (Layer A, B, C)		

2.2.2 Basic Transmission Parameters

ISDB-T features three transmission modes having different carrier intervals in order to deal with a variety of conditions such as the variable guard interval as determined by the network configuration and the Doppler shift occurring in mobile reception. Table 2.1 lists the basic parameters of each mode. One OFDM segment corresponds to a frequency spectrum having a bandwidth of 6/14 MHz (about 430 kHz). In Mode 1, one segment consists of 108 carriers, while Modes 2 and 3 feature two times and four times that number of carriers, respectively. Television broadcasting employs 13 segments with a transmission bandwidth of about 5.6 MHz. Terrestrial digital audio broadcasting, on the other hand, uses one or three segments. A digital signal is transmitted in sets of symbols. One symbol consists of 2 bits in QPSK and DQPSK, 4 bits in 16QAM, and 6 bits in 64QAM. Here, effective symbol length is the reciprocal of carrier interval-this is the condition preventing carriers in the band from interfering with each other. The guard interval is a time-redundant section of information that adds a copy of the latter portion of a symbol to the symbol ' s " front porch " with the aim of absorbing interference from multipath-delayed waves. Accordingly, increasing the guard-interval ratio in the signal decreases the information bit rate.

An OFDM frame consists of 204 symbols with guard intervals attached regardless of the transmission mode. The time interleave length in real time depends on the parameters set at the digital-signal stage and on the guard-interval length, and the values shown in the table for this parameter are consequently approximate values. Error-correction

schemes are concatenated codes, namely, Reed-Solomon (204, 188) code for the outer code and a convolutional code for the inner code. The information bit rate takes on various values depending on the selected modulation scheme, inner-code coding rate, and guard-interval ratio. The range shown in the table reflects the minimum and maximum values for 13 segments.

2.3 The DVB-T System

2.3.1 The Overview of DVB-T System

The DVB-T terrestrial digital video broadcasting standard (ETSI, 1997) is replacing the former analogue systems in many countries around the world. The benefits of digital coding and transmission techniques allow perfect signal recovery in all the serviced areas avoiding the effects of the wireless channel and noise. Considering the physical level of the communications, the digital data sequences, which contain MPEG video, audio and other information streams, are transmitted using coded orthogonal frequency division multiplexing (COFDM) modulation. The information bits are coded, interleaved, mapped to a quadrature amplitude modulation (QAM) constellation and grouped into blocks. All the symbols in a block are transmitted simultaneously at different frequency subcarriers using an inverse fast Fourier transform (IFFT) operation. The number of IFFT points, which can be either 2048 (2K) or 8192 (8K), determines the transmission mode and the number of the available subcarriers in the transmission bandwidth. Some of these subcarriers are not used to allow for guard frequency bands whereas others are reserved for pilot symbols, which are necessary to acquire the channel information required for signal recovery.

Fig.2.2 shows the main diagram of a DVB-T transmitter. As it can be seen, the data bit stream is scrambled, processed by an outer Reed-Solomon (RS) coder, an interleaver and an inner convolutional coder. The first coding stage removes possible error floors at high signal-to-noise-ratio (SNR) values, whereas the second reduces the bit error rate (BER) at the receiver by including more redundant information depending on the selected coding rate (CR), which can range from 1/2 to 5/6. The coded information bits are interleaved again in order to allocate consecutive bits to different subcarriers. The resulting information bits are then arranged by blocks, mapped and modulated using OFDM, which involves an IFFT operation and the addition of a cyclic prefix to enable a guard interval (GI) that avoids interference between consecutive blocks. The use of coding and interleaving processes over OFDM provides an efficient and robust transmission method in multipath scenarios enabling time and frequency diversity.

2.3.2 The Limitation of DVB-T System

Despite the many benefits achieved by the deployment of the DVB-T network, its limitations became clear from the beginning. First, the number and bit rates of the transmitted

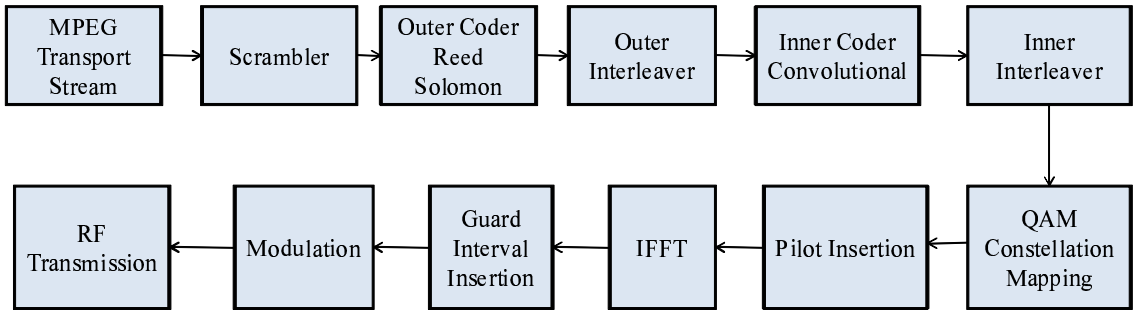

Figure 2.2: The DVB-T Block Diagram [2]

channels are limited in comparison with new wireless transmission techniques. A new standard was soon required to broadcast more channels and high-definition television (HDTV) using the same frequency spectrum. Second, a new information system was required to allow more interaction with the user. Third, the DVB-T standard, which had been designed for fixed scenarios, had a very bad performance in mobile or portable environments, so it could not be properly implemented in scenarios such as moving vehicles. Last but not least, the deployment of the DVB-T network has been and still is a true nightmare in SFN scenarios, where interferences between repeaters, which transmit the same information on the same frequency bands, may destroy the received signal avoiding its reception in areas with good reception levels. Considering the new advances in signal processing, modulation and coding, the DVB consortium has published a draft standard named DVB-T2 aiming to extend the capabilities of the aforementioned DVB-T standard.

2.4 The DVB-T2 System

2.4.1 The Motivation of the DVB-T2 System

DVB-T is the most popular way to distribute TV in Europe and many other parts in the world. However, its success has been under pressure after the introduction of the MPEG5 compression standard and the new digital video broadcasting standard for satellite transmission DVB-S2 [15], which are driving the first adoption of high definition television (HDTV) on satellite and cable networks. Therefore, in 2006, the terrestrial TV broadcasting community felt the need for an improved system. DVB-T2 [1] is a second-generation terrestrial transmission system for digital terrestrial broadcasting. It builds one the technologies used as part of the first-generation system, DVB-T [2], developed over a decade ago. DVB-T2 extends the range of most of the parameters of DVB-T and significantly reduces overhead to build a system with a throughput close to theoretical channel capacity, with the best possible ruggedness of transmission. The key motivation behind this new standard was the desire in several European countries to offer HDTV services as efficiently and effectively as possible. The move to HDTV

inevitably brings with it a change of source coding, necessating the introduction of new domestic reception equipments (set-top boxes and TV sets), and therefore offers an ideal opportunity to upgrade the transmission system simultaneously.

2.4.2 The Commercial Requirement of DVB-T2

The DVB organisation defined a set of commercial requirements which acted as a framework for the T2 developments. As written by [16], These commercial requirements included:

- T2 transmissions must be able use existing domestic receive antenna installations and must be able to re-use existing transmitter infrastructures. (This requirement ruled out the consideration of MIMO techniques which would involve both new receive and transmit antennas.)
- T2 should primarily target services to fixed and portable receivers.
- T2 should provide a minimum of 30% capacity increase over DVB-T working within the same planning constraints and conditions as DVB-T.
- T2 should provide for improved single-frequency-network (SFN) performance compared with DVB-T.
- T2 should have a mechanism for providing service-specific robustness; i.e. it should be possible to give different levels of robustness to some services compared to others. For example, within a single 8 MHz channel, it should be possible to target some services for roof-top reception and target other services for reception on portables.
- T2 should provide for bandwidth and frequency flexibility.
- There should be a mechanism defined, if possible, to reduce the peak-to-average-power ratio of the transmitted signal in order to reduce transmission costs.

2.4.3 The Key Technologies of DVB-T2

Based on recent research results and a set of commercial requirements, the DVB consortium concluded that there were suitable technologies which could provide increased capacity and robustness in the terrestrial environment, mainly for HDTV transmission. Therefore, a new standard named DVB-T2 has been designed primarily for fixed receptors, although it must allow for some mobility, with the same spectrum characteristics as DVB-T. Fig. 2.3 shows the main stages of a DVB-T2 transmitter, where dashed lines represent optional stages.

DVB-T2 system contain major feature improvement compared to DVB-T2. The key technologies of DVB-T2 [17] are listed as follow:

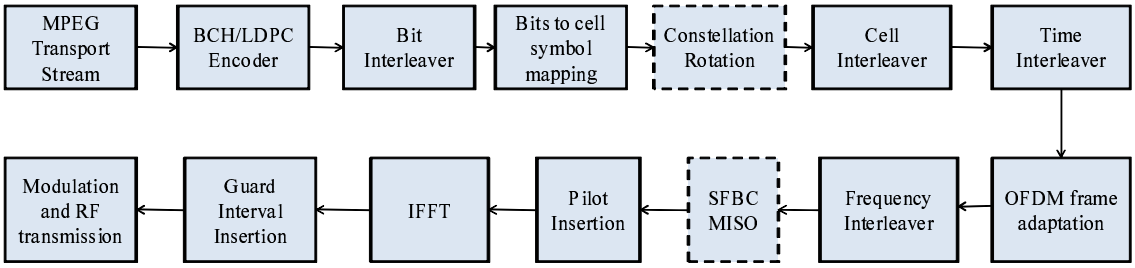

Figure 2.3: Elementary transmission chain of DVB-T2 [1]

- Error protection coding
  The first remarkable novelty lies on the error correction strategy, since DVB-T2 uses the same channel codes that were designed for DVB-S2. The coding algorithms, based on the combination of LDPC and Bose-Chaudhuri-Hocquenghem (BCH) codes, offer excellent performance resulting in a very robust signal reception. LDPC-based forward error correction (FEC) techniques can offer a significant improvement compared with the convolutional error correcting scheme used in DVB-T.

- Scheduling
  DVB-T2 enables lower power consumption for receivers as receivers can choose to only decode one particular program instead of an entire multiplex of programs [18]. Each program can be sent through its own physical layer pipe (PLP) with its own modulation, coding and time interleaving [16]. This enables DVB-T2 to also deliver a specific level of robustness per service. Together with a new frame structure that allows for faster channel scanning and acquisition, DVB-T2 aims to deliver an enhanced user experience.

- Modulation techniques
  DVB-T2 uses coded OFDM (COFDM), as used by the DVB-T, digital audio broadcasting (DAB), terrestrial integrated services digital broadcasting (ISDB-T), and digital radio mondiale (DRM) broadcast standards, and by other radio systems such as IEEE 802.11a/n and the Long Term Evolution (LTE) of 3GPP. A wider range of OFDM parameters is offered than for DVB-T, while coding is also changed. There are 1 K, 2 K, 4 K, 8 K, 16 K, and 32 K FFT sizes, and each subcarrier, in each symbol, is modulated using QAM constellations. A range of options is available for payload data: 4-, 16-, 64-, and 256-QAM. The combination of 256-QAM with the new LDPC error correction offers increased throughput with performance roughly comparable with 64-QAM in DVB-T.

- Rotated constellations
  The LDPC codes of DVB-T2 offer adequate performance in non-selective channels using a higher code rate than DVB-T. However, frequency selective channels need extra redundancy previously given by a lower-rate code. DVB-T2 in-

Table 2.2: The Comparison between DVB-T and DVB-T2 Specification [20]

	DVB-T	DVB-T2
Forward Error Correction (FEC) Code Rate	Convolutional Coding + Reed Solomon 1/2, 2/3, 3/4, 5/6, 7/8	LDPC + BCH 1/2,**3/5**,2/3,3/4,**4/5**,/5/6
Modes	QPSK,QAM-16, QAM-64	QPSK,QAM-16, QAM-64, **QAM-256**
Guard Interval	1/4, 1/8, 1/16, 1/32	1/4, **19/256**, 1/8, **19/128** ,1/16, 1/32, **1/128**
FFT Size	2k,8k	**1k**,2k,**4k**,8k,**16k**,**32k**
Scattered Pilots	8% of total	**1%**,**2%**,**4%**, or 8% of total
Continual Pilots	2.6% of total	0.35% of total

cludes the option of another kind of redundancy, rotated constellations, making the throughput advantage of high-rate LDPC available even for frequency selective channels. In regular QAM, different information is mapped onto the I and Q axes, with no correlation between the axes. Rotating the constellation by a suitable angle means that every constellation point maps onto a different point on each of the I and Q axes. So a 16-QAM constellation has 16 different values for both of I and Q.

- PAPR reduction
  OFDM has the disadvantage that the transmitted signal increasingly resembles Gaussian noise as the number of sub-carriers increases, with the consequence that the peakto- average-power-ratio is high. This places demands on the transmitter's power amplifier. DVB-T2 includes two optional features which can reduce PAPR. Active constellation extension (ACE) modifies some of the transmitted constellations by selectively moving their outer points to positions having greater amplitude [19]. ACE reduces PAPR without throughput loss, but is not used together with rotated constellation. Reserved-carrier PAPR reduction sacrifices a small amount of throughput by reserving some sub-carriers, which do not carry data [19]. They are used instead to carry arbitrary values, which permit the synthesis of a peak-canceling waveform.

The comparison between DVB-T and DVB-T2 is specified more detail by table 2.2

2.4.4 The Benefit of DVB-T2 over DVB-T System

As a result of the technologies introduced in DVB - T2, the potential gain in capacity that could be achieved in the UK is nearly 50% compared to the current UK mode of DVB- T (see table 2.3). In addition to the increased capacity, the proposed DVB-T2

Table 2.3: Potential capacity increase of almost 50% compared with current highest capacity DVB -T mode used in the UK

	Current UK Mode	**DVB-T2**
Modulation	QAM-64	QAM-256
FFT size	2K	32K
Guard Interval	1/32	1/128
FEC	2/3 CC + RS	3/5 LDPC + BCH
Scattered Pilots	8.3%	1.0%
Continual Pilots	2.0%	0.53%
L1 Overhead	1.0%	0.53%
Carrier mode	Standard	Extended
Capacity	24.1 Mbit/s	36.1 Mbit/s
NOTE 1:Includes only Continual Pilot cells which are not also Scattered Pilots. NOTE 2:TPS for DVB-T; L1-signalling, P1 and extra P2 overhead for DVB-T2.		

mode is expected to offer greater tolerance of multipath and impulsive interference than the current DVB- T mode. Even greater increases in capacity could be achieved in modes designed for single- frequency network (SFN) operation, because of the large fractional guard intervals used in these modes. Table 2.4 shows the comparison between DVB - T2 and DVB - T for a long guard interval (SFN) mode, with the same absolute guard interval in both cases. This provides a 67% increase in capacity for DVB-T2 over DVB- T. A longer guard interval mode is also available (nearly 20% increase), which would give improved SFN coverage for only a small loss of capacity (around 3%).

2.5 DVB-T2 Baseband OFDM System

The baseband model of a 2×2 MIMO OFDM system that has been developed for this research work is shown in Fig. 2.4. The binary data are first mapped according to the modulation that is used by the signal mapper. Then, the mapped data are processed by the MISO encoder to generate input for each transmitter antenna. The complete process of the MISO encoder is presented in subsection 2.6.1. After that, the reference pilots are inserted into the data. One of the main function of including the reference pilot in this system is to conduct the channel estimation, especially the scattered pilots.

An OFDM baseband symbol is generated by modulating N complex data using the inverse fast fourier transform (IFFT) on N subcarriers. In order to prevent inter symbol interference (ISI), guard interval (GI) which is chosen to be larger than delay spread is inserted at the beginning of each symbol. It makes every OFDM symbol has $N + N_g$

Table 2.4: Potential capacity increase of almost 67% for an SFN mode

	DVB-T	**DVB-T2**
Modulation	QAM-64	QAM-256
FFT size	8K	32K
Guard Interval	1/4	1/16
FEC	2/3 CC + RS	3/5 LDPC + BCH
Scattered Pilots	8.3%	4.2%
Continual Pilots	2.0%	0.39%
L1 Overhead	1.0%	0.65%
Carrier mode	Standard	Extended
Capacity	19.9 Mbit/s	33.2 Mbit/s
NOTE 1:Includes only Continual Pilot cells which are not also Scattered Pilots. NOTE 2:TPS for DVB-T; L1-signalling, P1 and extra P2 overhead for DVB-T2.		

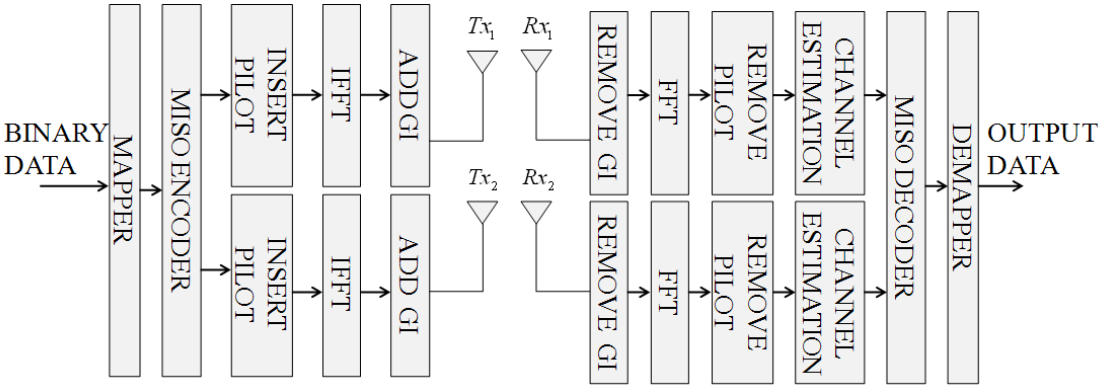

Figure 2.4: Baseband Alamouti 2×2 MIMO DVB-T2 OFDM System

samples. The transmitted symbol is given by (2.1)

$$x_i(t) = x_{i,n,l} = \frac{1}{N} \sum_{k=-N/2+1}^{N/2} X_{i,k,l} e^{\frac{j2\pi nk}{N}} \qquad (2.1)$$
$$n = -N_g, ..., N-1$$

where $x_i(t)$, $x_{i,n,l}$, and $X_{i,k,l}$ are the continuous time-domain, the n-th discrete time-domain, and k-th complex frequency-domain transmitted signal of the l-th symbol and i-th transmit antenna, respectively. The continuous time-domain signal $x_i(t)$ is obtained from the discrete time-domain signal $x_{i,n,l}$ through Digital to Analog Converter (DAC). It is then transmitted through multipath fading channel as given by (2.2)

$$h_{ij}(t,\tau) = \sum_{d=1}^{D} h_{ij,d}(t)\delta(\tau - \tau_{ij,d}(t)) \qquad (2.2)$$

where $h_{ij,d}(t), \tau_{ij,d}(t)$ are the complex channel coefficient and delay of the d-th path and i-th transmit antenna and j-th receive antenna, respectively. τ and D denote the time-delay variable and the total number of channel paths.

At receiver, the time-domain received signal is obtained by convolving the transmitted signal $x_i(t)$ with channel impulse response $h_{ij}(t, \tau)$ and adding the Additive White Gaussian Noise (AWGN) $w_j(t)$. It can be expressed as (2.3).

$$y_j(t) = \sum_{i=1}^{I} \sum_{d=1}^{D} h_{ij,d}(t) x_i(\tau - \tau_{ij,d}(t)) + w_j(t) \tag{2.3}$$

After removal of GI, the receiver transforms the remaining N sample into frequency-domain by using fast fourier transform(FFT). Finally, the k-th frequency-domain received signal can be represented as shown by (2.4)

$$Y_{j,k,l} = \sum_{i=1}^{I} X_{i,k,l} H_{ij,k,l} + W_{j,k,l} \tag{2.4}$$

where $X_{i,k,l}$ and $H_{ij,k,l}$ denote the frequency-domain transmitted signal and channel frequency response at k-th subcarrier, l-th symbol of $i-$th antenna. $W_{j,k,l}$ denotes the AWGN at k-th subcarrier and l-th symbol. From here, channel estimation and MISO decoding are performed to decode the received signal.

2.6 Multi-Antenna DVB-T2

2.6.1 Modified Alamouti SFBC Coding

The DVB-T2 system defined the transmit diversity based on the Alamouti Coding [3], but it was slightly modified to allow a backward compatibility with the SISO system. Since this scheme exploits diversity in space and frequency-domain, therefore it has been termed as space frequency block coding (SFBC). The modified Alamouti SFBC coding is shown in Table 2.5.

If $S_{k,l}$ represents the pre-coding transmitted signal of k-th subcarrier and l-th symbol, then the received signal for the first pair of MIMO cell, $Y_{j,k,l}$ and $Y_{j,k+1,l}$ can be derived as shown by (2.5)-(2.6)

$$\begin{aligned} Y_{j,k,l} &= X_{1,k,l} H_{1j,k,l} + X_{2,k,l} H_{2j,k,l} + W_{j,k,l} \\ &= S_{k,l} H_{1j,k,l} - S^*_{k+1,l} H_{2j,k,l} + W_{j,k,l} \end{aligned} \tag{2.5}$$

$$\begin{aligned} Y_{j,k+1,l} &= X_{1,k+1,l} H_{1j,k+1,l} + X_{2,k+1,l} H_{2j,k+1,l} + W_{j,k+1,l} \\ &= S_{k+1,l} H_{1j,k+1,l} + S^*_{k,l} H_{2j,k+1,l} + W_{j,k+1,l} \end{aligned} \tag{2.6}$$

where $H_{1j,k,l}, H_{1j,k,l}$ and $W_{j,k,l}$ are the channel frequency response between Tx_1 and Rx_j, the channel response between $\mathrm{Tx}_2$and Rx_j, and AWGN in k-th subcarrier and l-th symbol, respectively.

Table 2.5: Modified Alamouti Scheme

	k-th subcarrier	$(k+1)$-th subcarrier
Tx_1	$S_{k,l}$	$S_{k+1,l}$
Tx_2	$-S^*_{k+1,l}$	$S^*_{k,l}$

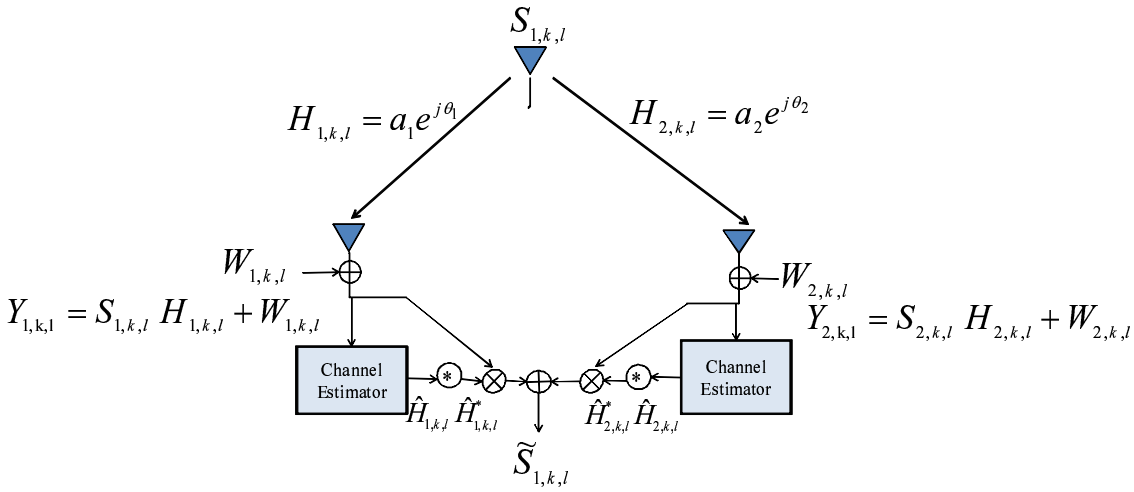

Figure 2.5: Maximal Ratio Combining

Equation (2.5)-(2.6) can be represented in a matrix as shown by (2.7)

$$\begin{bmatrix} Y_{k,l} \\ Y^*_{k+1,l} \end{bmatrix} = \begin{bmatrix} H^1_{k,l} & -H^2_{k,l} \\ H^{2*}_{k+1,l} & H^{1*}_{k+1,l} \end{bmatrix} \begin{bmatrix} S_{k,l} \\ S^*_{k+1,l} \end{bmatrix} + \begin{bmatrix} W_{k,l} \\ W^*_{k+1,l} \end{bmatrix} \tag{2.7}$$

From this matrix representation, the decoding can be conducted in simpler way.

2.6.2 Maximal-Ratio Combining

In order to improve the performance of mobile DVB-T2 system, we include the receiver diversity technology, i.e. maximal ratio combining [21] in our system. The maximal ratio combining method is illustrated by Fig. 2.5. The transmit signal $S_{1,k,l}$ is transmitted to receiver 1 and 2 through channel $H_{1,k,l}$ and $H_{2,k,l}$. The signal is also effected by the thermal noise in both receiver, i.e. $W_{1,k,l}$ and $W_{2,k,l}$. The received signal in both antenna are expressed by 2.8-2.9

$$Y_{1,k,l} = S_{1,k,l} H_{1,k,l} + W_{1,k,l} \tag{2.8}$$

$$Y_{2,k,l} = S_{1,k,l} H_{2,k,l} + W_{2,k,l} \tag{2.9}$$

After arrived in receiver, the receiver decode the transmit signal by multiplying the received signal with the conjugate of estimated channel $\hat{H}_{1,k,l} = \alpha H_{1,k,l}$ and $\hat{H}_{2,k,l} = \alpha H_{2,k,l}$. The decoded signal is expressed by

$$\begin{aligned}\tilde{S}_{1,k,l} &= Y_{1,k,l}\hat{H}^*_{1,k,l} + Y_{2,k,l}\hat{H}^*_{2,k,l} \\ &= (a_1^2 + a_2^2)\alpha S_{1,k,l} + \hat{H}^*_{1,k,l}W_{1,k,l} + \hat{H}^*_{2,k,l}W_{2,k,l}\end{aligned} \tag{2.10}$$

In 2.10, we obtain the decoded transmit signal with diversity gain $(a_1^2 + a_2^2)$. Normalizing 2.10 with the gain, we obtain 2.11

$$\begin{aligned}\tilde{S}_{1,k,l} &= Y_{1,k,l}\hat{H}^*_{1,k,l} + Y_{2,k,l}\hat{H}^*_{2,k,l} \\ &= S_{1,k,l} + \frac{\hat{H}^*_{1,k,l}W_{1,k,l} + \hat{H}^*_{2,k,l}W_{2,k,l}}{(a_1^2 + a_2^2)}\end{aligned} \tag{2.11}$$

Since a_1^2 and a_2^2 are equivalent with $|H_{1,k,l}|^2$ and $|H_{2,k,l}|^2$, eq. 2.11 can be also expressed as 2.12

$$\begin{aligned}\tilde{S}_{1,k,l} &= Y_{1,k,l}\hat{H}^*_{1,k,l} + Y_{2,k,l}\hat{H}^*_{2,k,l} \\ &= S_{1,k,l} + \frac{\hat{H}^*_{1,k,l}W_{1,k,l} + \hat{H}^*_{2,k,l}W_{2,k,l}}{(|H_{1,k,l}|^2 + |H_{2,k,l}|^2)}\end{aligned} \tag{2.12}$$

In this form we succesfully decode the transmit and also weaken the noise by normalizing them with the diversity gain obtained by the received signal.

2.7 Summary

In this section, we have discussed about the digital terrestrial television standard, especially, DVB-T2. DVB-T/T2 has the largest number of customer in the world. DVB-T2 has been developed to increase the capacity of DVB-T that was developed a decade ago. DVB-T2 can increase the system capacity until 50% compared to the DVB-T. In order to improve the reception performance of digital terrestrial TV, DVB-T2 introduced the transmitter diversity using modified Alamouti. However, in the future the mobile reception of digital terrestrial television in high speed environment, such as high speed train (TGV, Maglev, etc with commercial speed $\approx$ 300 km/h) will become an important aspect in the competition with other digital broadcasting system, such as digital satellite. There is a need to provide information and onboard entertainment services to high speed train passengers. In this case, the inclusion of MIMO scheme become necessary to increase the reception performance of high speed digital terrestrial television. In this section, we have discussed the antenna diversity method for DVB-T2, i.e. modified Alamouti scheme (transmitter diversity) and maximal-ratio combining (receiver diversity).

Chapter 3

Pilot Aided Channel Estimation for DVB-T2 System

3.1 DVB-T2 Scattered Pilot Pattern

3.1.1 The Pilot Pattern of SISO mode

The DVB-T system introduced parallelogram-shaped grid scattered pilot pattern that is especially used for channel estimation [1]. If DVB-T proposed the same scattered pilot pattern for every FFT size and Guard Interval size scenario, DVB-T2 has chosen a more flexible approach by defining eight different scattered pilot patterns which are dependent on the size of FFT and GI. This approach reduces the pilot overhead while assuring the channel estimation quality. The position of scattered pilot of Tx_1 in l-th symbol and k-th subcarrier is given as (3.1)

$$k \bmod (D_X D_Y) = D_X (l \bmod D_Y) \tag{3.1}$$

where D_X and D_Y are the distances of pilot bearing subcarriers forming a periodic pattern in frequency and time direction, respectively. The D_X and D_Y of the eight scattered pilot pattern are defined by table 3.1. The combinations of scattered pilot patterns, FFT size and guard interval which are allowed to be used are defined in table 3.2 for SISO mode. On the other hand the amplitudes of the scattered pilot A_{sp} depend on the scattered pilot pattern as shown in table 3.3 the phase of the scattered pilots of Tx_1 in l-th symbol and k-th subcarrier is given as (3.2)

$$P_{1,k,l} = 2A_{sp}(0.5 - r_{k,l}) \tag{3.2}$$

where $r_{k,l}$ and A_{sp} denote a reference sequence for generating pilot and amplitude of scattered pilot, respectively. A_{sp} is defined in table A_{sp} .

Table 3.1: Parameters defining the scattered pilot patterns [1]

Pilot pattern	**Separation of pilot in frequency domain D_X**	**Separation of pilot in timed domain D_Y**	**SP Overhead**
PP1	3	4	8.33%
PP2	6	2	8.33%
PP3	6	4	4.17%
PP4	12	2	4.17%
PP5	12	4	2.08%
PP6	24	2	2.08%
PP7	24	4	1.04%
PP8	6	16	1.04%

3.1.2 The Pilot Pattern of MISO mode

The DVB-T2 standard proposed a modified pilot pattern for MISO case. Since the received signal contains the mixture of channel from Tx_1 and Tx_2, a DVB-T2 system introduced a few modifications on the pilot from a Tx_2 in order to estimate the channel from both transmitter antenna. In one subset (symbol 0, 2, 4,.., $2N$), pilots are transmitted in the same phase from both transmitters, allowing the addition of two channel responses to be estimated. In another subset (symbol 1, 3, 5,.., $2N$+1), the pilots from the second transmitter are inverted from the one in the first transmitter, allowing the substraction of channel responses to be estimated. In the case of a 2K FFT and 1/8 of GI that has been selected for this paper, the pattern of scattered pilot for a 2×2 MIMO is that of a PP1 pattern [1] as shown by Fig.3.1.

The combinations of scattered pilot patterns, FFT size and guard interval for MISO mode which are allowed to be used are defined in table 3.4. The inverted phase of scattered pilot of Tx_2 is given by (3.3)

$$P_{2,k,l} = (-1)^{k/Dx} P_{1,k,l} \tag{3.3}$$

3.2 SISO DVB-T2 Channel Estimation

3.2.1 Overview

The received carrier amplitudes output by the receiver are not in general the same as the transmitted since they are affected by the channel through which the signal has passed on its way from the transmitter. If $X_{k,l}$ represent transmitted signal from Tx, then the received signal is expressed by (3.4)

$$Y_{k,l} = X_{k,l} H_{k,l} + W_{k,l} \tag{3.4}$$

Table 3.2: Scattered pilot pattern to be used for each FFT size and guard interval combination in SISO mode [1]

FFT size	**Guard Interval**						
	1/128	1/32	1/16	19/256	1/8	19/128	1/4
32K	PP7	PP4 PP6	PP2 PP8 PP4	PP2 PP8 PP4	PP2 PP8	PP2 PP8	NA
16K	PP7	PP7 PP4 PP6	PP2 PP8 PP4 PP5	PP2 PP8 PP4 PP5	PP2 PP3 PP8	PP2 PP3 PP8	PP1 PP8
8K	PP7	PP7 PP4	PP8 PP4 PP5	PP8 PP4 PP5	PP2 PP3 PP8	PP2 PP3 PP8	PP1 PP8
4K,2K	NA	PP7 PP4	PP4 PP5	NA	PP2 PP3	NA	PP1
1K	NA	NA	PP4 PP5	NA	PP2 PP3	NA	PP1

Table 3.3: Amplitudes of the scattered pilots [1]

Scattered pilot pattern	**Amplitude** (A_{sp})	Equivalent boost (dB)
PP1,PP2	4/3	2.5
PP3,PP4	7/4	4.9
PP5,PP6,PP7,PP8	7/3	7.4

where $H_{k,l}$ and, $W_{k,l}$ are the channel response between Tx and Rx; and the AWGN (Additive White Gaussian Noise), respectively. An SISO system is illustrated by Fig.3.2

The receiver needs the knowledge of channel, $H_{k,l}$, if it wants to interpret the $Y_{k,l}$ in the best way. The channel estimate can be derived using the known information or reference signal inserted in transmitted symbol. In this system, the known information or reference signal from transmitted symbol is the scattered pilot that is discussed in section 3.1. The channel estimate can be expressed as follow:

$$\hat{H'}_{k,l} \approx Y_{k,l}/Xref_{k,l} \tag{3.5}$$

where $Xref_{k,l}$ is the reference signal in k-th subcarrier and l-th symbol. To obtain the estimates of the channel response for every data cell, the conventional approach is to interpolate between value $\hat{H'}_{k,l}$ that is only available in every scattered pilot position to provide values for every cell.

Table 3.4: Scattered pilot pattern to be used for each FFT size and guard interval combination in MISO mode [1]

FFT size	Guard Interval						
	1/128	1/32	1/16	19/256	1/8	19/128	1/4
32K	PP8 PP4 PP6	PP8 PP4	PP2 PP8	PP2 PP8	NA	NA	NA
16K	PP8 PP4 PP5	PP8 PP4 PP5	PP3 PP8	PP3 PP8	PP1 PP8	PP1 PP8	NA
8K	PP8 PP4 PP5	PP8 PP4 PP5	PP3 PP8	PP3 PP8	PP1 PP8	PP1 PP8	NA
4K,2K	NA	PP4 PP5	PP3	NA	PP1	NA	NA
1K	NA	NA	PP3	NA	PP1	NA	NA

3.2.2 Fundamental Limits

The channel response $H_{k,l}$ in general varies with both time (symbol index l) and and frequency (carrier index k). The temporal variation corresponds to external causes such as Doppler shift and spread. The variation within frequency direction corresponds to channel selectivity due to multipath fading.

In effect, the receiver samples the $H_{k,l}$ by measuring it for the cells (k,l)within which the scattered pilot has been transmitted. The scattered pilot constitute a form of 2-D sampling grid and in consequence there are limits, according to Nyquist's criterion, on the rates of variation of the channel response with time and frequency that can be measured using scattered pilot. Section 3.1 defines various scattered pilot patterns of

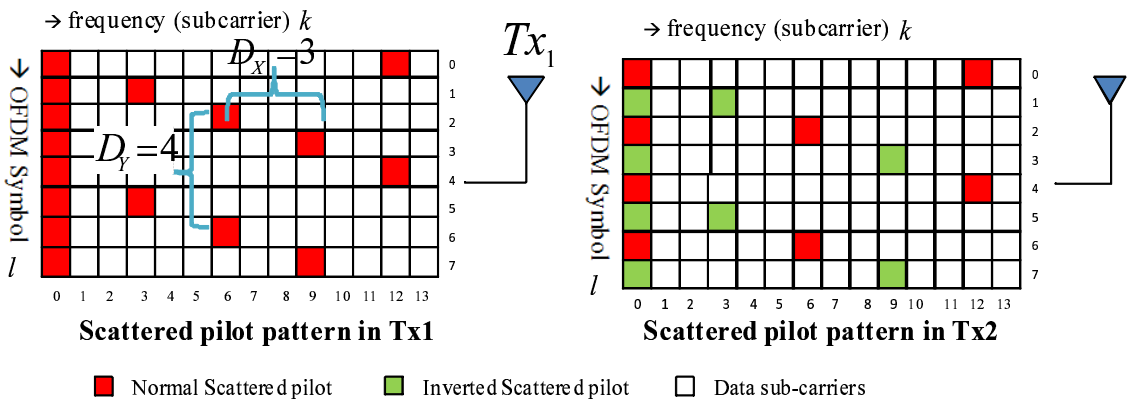

Figure 3.1: Scattered Pilot Pattern for Tx_1 and Tx_2

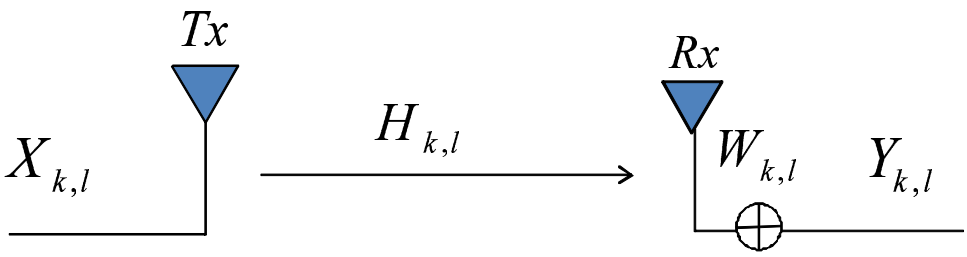

Figure 3.2: an SISO system

DVB-T2 and introduces terms D_X and D_Y to characterize them. As we know, Symbol occurs at the rate

$$f_s = 1/T_S = 1/(T_U + T_G) \tag{3.6}$$

where T_S,T_U,T_G are the total symbol period, symbol period without guard interval, and guard interval period,respectively. The Nyquist limit for temporal channel variation that can be measured is $\frac{\pm 1}{2D_Y(T_U+T_G)}$ Hz. Given suitable temporal interpolation, then we have an interpolated estimate of the channel response for every cell on the pilot-bearing carries. Estimates for the remaining cells can then be found by frequency interpolation between the pilot-bearing carriers. Since these are spaced by D_X carriers, or $D_X f_U = D_X/T_U$ Hz, it follows that the maximum Nyquist channel extent, or spread between the first and last paths in a channel that can be supported, is T_U/D_X sec.

Note that this approach is variables-separables one leading to a rectangular Nyquist area on a diagram of Doppler versus delay. This rectangular area corresponds to a (dimensionless) timewidth-bandwidth product with the value

$$\frac{1}{D_Y(T_U + T_G)}\frac{T_U}{D_X} = \frac{1}{D_X D_Y(1 + GIF)} \tag{3.7}$$

where $GIF = T_G/T_U$ is the guard-interval fraction,.

It can be shown that the same sampling grid of channel measurements can be interpreted to produce other shapes of supportable 'are', in general non-rectangular, but whose total area remains the same.

3.2.3 Interpolation

After obtaining the channel estimate in scattered pilot position $\hat{H}'_{k,l}$ as shown by (3.5), we estimate the channel in every data cell by doing the interpolation. There are two kinds of interpolation method that we can implement for this system:

- 2D (two-dimensional) interpolation

  The direct 2D interpolation can be implemented using the 2D filter. The weakness of this interpolation method is the high complexity of the 2D filter implementation. The process of 2D interpolation is described in Fig. 3.3

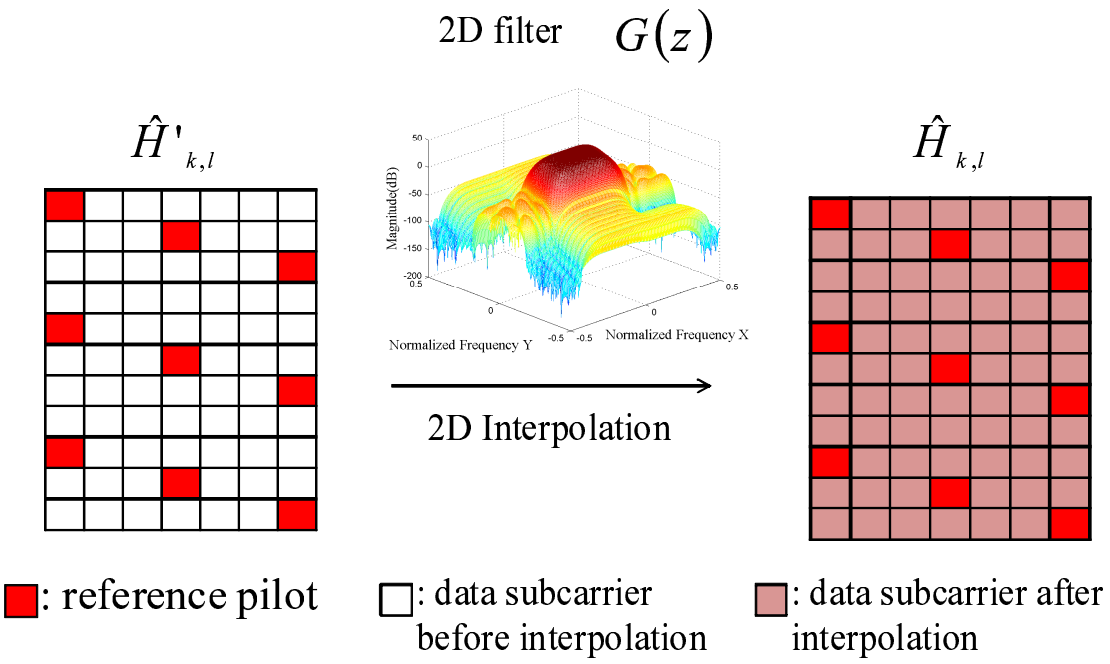

Figure 3.3: 2D interpolation process

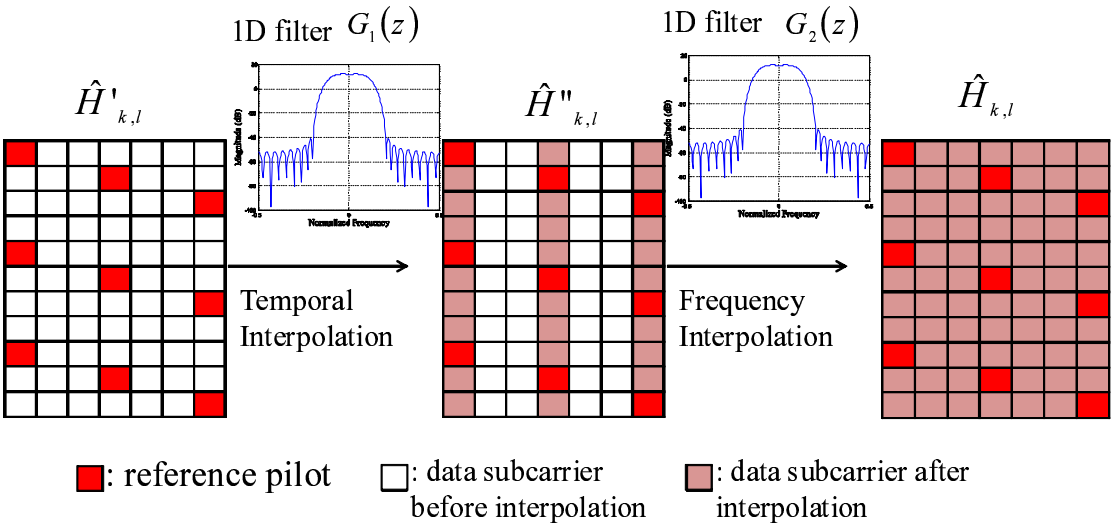

Figure 3.4: 2×1D interpolation process

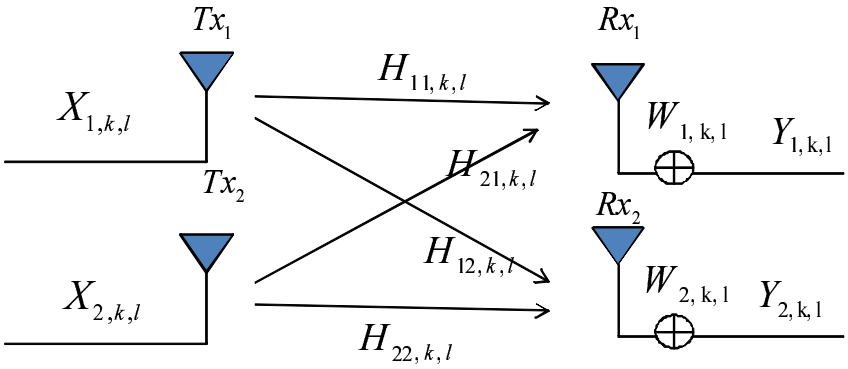

Figure 3.5: a 2×2 MIMO

- 1D temporal interpolation - 1D frequency interpolation

  This interpolation method will produce lower complexity of interpolation method. In this method, the length of the temporal interpolator is tightly limited by the fact that the main signal stream awaiting equalisation has to be delayed while the measurements to be input into the temporal interpolator are gathered. This delay has a large cost in terms of memory needed, but also in terms of the delay it introduces before the programme material can be delivered to the viewer. The temporal interpolator is thus usually much more constrained in its size than the frequency interpolator. This interpolation process is shown by Fig. 3.4

3.3 MIMO DVB-T2 Channel Estimation

3.3.1 Overview

In this section, we present the PACE for a 2×2 MIMO DVB-T2 system. This method supports the interpolation filter that is discussed in chapter 3.4.

If $X_{1,k,l}$ and $X_{2,k,l}$ represent transmitted signal from Tx_1 and Tx_2, then the received signal at j-th antenna is expressed by (3.8)

$$Y_{j,k,l} = X_{1,k,l}H_{1j,k,l} + X_{2,k,l}H_{2j,k,l} + W_{j,k,l} \tag{3.8}$$

where $H_{1j,k,l}$, $H_{2j,k,l}$, and, $W_{j,k,l}$ are the channel response between Tx_1 and Rx_j, channel response between Tx_2 and Rx_j, and AWGN of Rx_j, respectively.

For a 2×2 MIMO, the received signal in Rx_1 and Rx_2 are expressed by (3.9) and (3.10)

$$Y_{1,k,l} = X_{1,k,l}H_{11,k,l} + X_{2,k,l}H_{21,k,l} + W_{1,k,l} \tag{3.9}$$

$$Y_{2,k,l} = X_{2,k,l}H_{12,k,l} + X_{2,k,l}H_{22,k,l} + W_{2,k,l} \tag{3.10}$$

A 2×2 MIMO system is illustrated by Fig.3.5

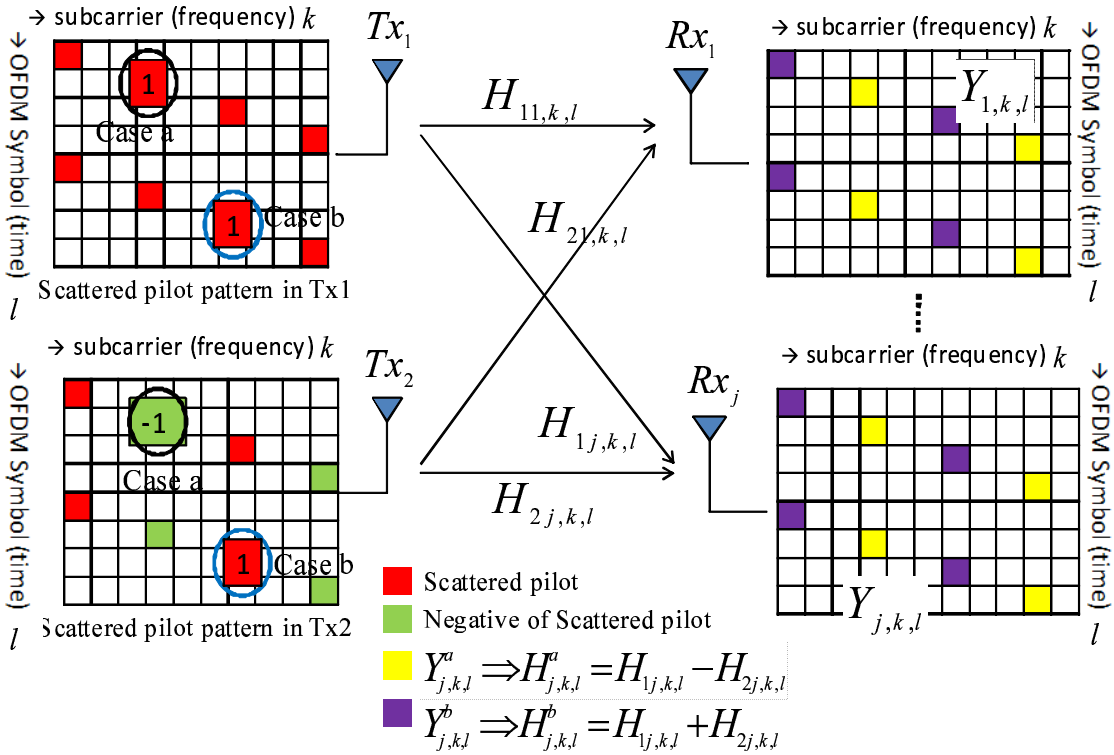

Figure 3.6: Scattered Pilot Association for Tx_1 and Tx_2

There are two cases to be considered to estimate the channel as shown by Fig.3.6. In the first case, the transmitted pilots from the Tx_2 are the invert of the pilot from Tx_1, $X_{1,k,l} = -X_{2,k,l} = X^a_{k,l}$. The received signal for case A is given by (3.11)

$$Y^a_{j,k,l} = X^a_{k,l}(H_{1j,k,l} - H_{2j,k,l}) + W_{j,k,l} \tag{3.11}$$

In another case, the transmitted pilots from Tx_2 are completely similar to the pilots from Tx_1 in given subcarriers, $X_{1,k,l} = X_{2,k,l} = X^b_{k,l}$. The received signal for case B is given by (3.12)

$$Y^b_{j,k,l} = X^b_{k,l}(H_{1j,k,l} + H_{2j,k,l}) + W_{j,k,l} \tag{3.12}$$

Based on this condition, the conventional method [16], the 2-point averaging [22], and the proposed 3-point diagonal averaging method is discussed in section 3.3.2-3.3.4.

3.3.2 The Conventional Method

The conventional method of PACE for a 2×2 MIMO DVB-T2 system is described briefly in [16]. The complete processes of the conventional method are illustrated in Fig. 3.7-3.9. This method consists of several steps,i.e:

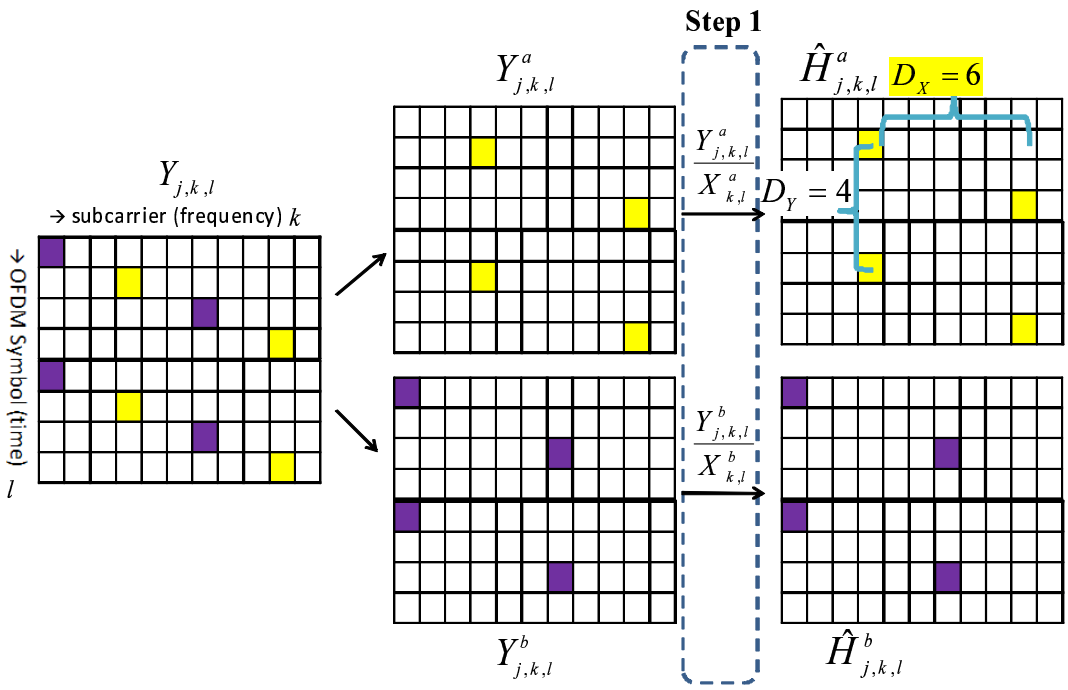

Figure 3.7: The illustration of conventional PACE for a 2×1 MISO OFDM system [16] Step 1

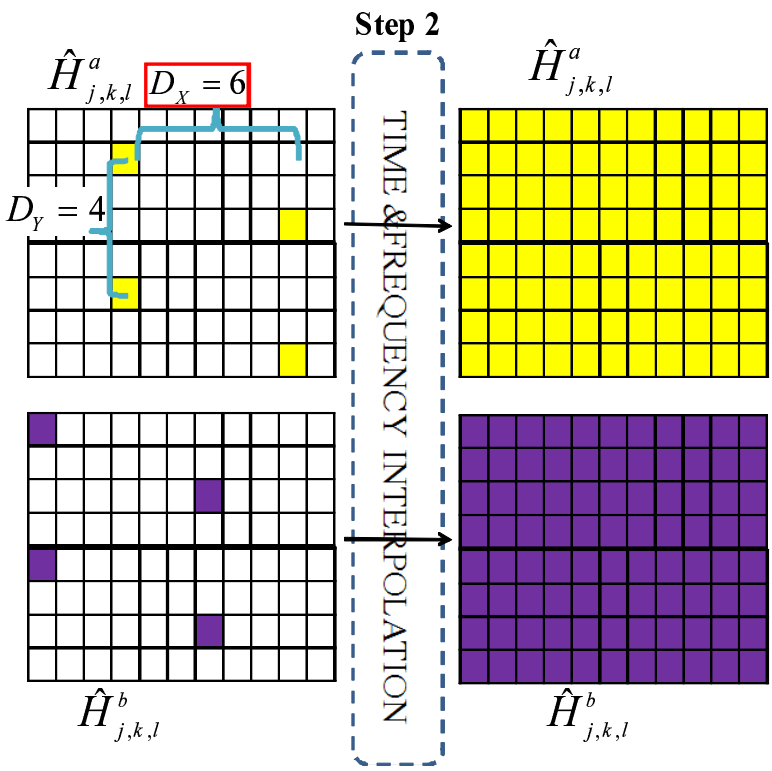

Figure 3.8: The illustration of conventional PACE for a 2×1 MISO OFDM system [16] Step 2

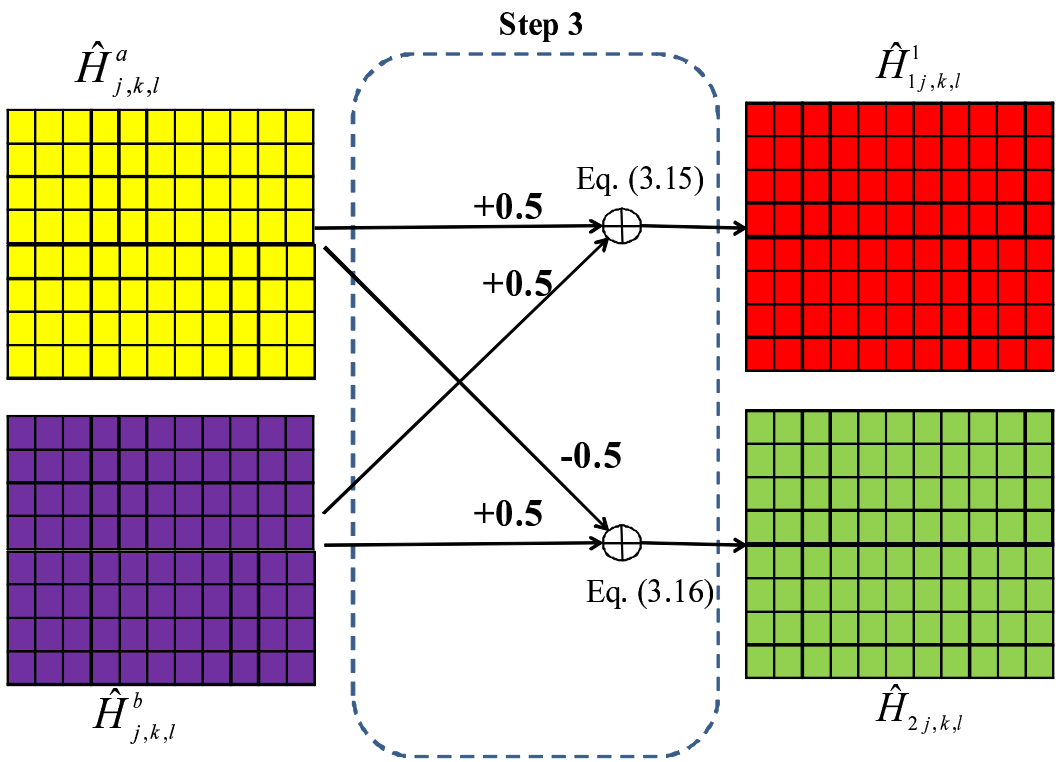

Figure 3.9: The illustration of conventional PACE for a 2×1 MISO OFDM system [16] Step 3

- **Step 1** Firstly, we separate $Y^a_{j,k,l}$ and $Y^b_{j,k,l}$. Estimate the addition and substraction of channel using the LS Method as given by (3.13)-(3.14). The process of step 1 is illustrated by Fig. 3.7.

$$\hat{H}^a_{j,k,l} = Y^a_{j,k,l}/X^a_{k,l} \approx H_{1j,k,l} - H_{2j,k,l} \tag{3.13}$$

$$\hat{H}^b_{j,k,l} = Y^b_{j,k,l}/X^b_{k,l} \approx H_{1j,k,l} + H_{2j,k,l} \tag{3.14}$$

- **Step 2** Interpolate the estimated addition and substraction of channel responses,$H^a_{j,k,l}$ and $H^b_{j,k,l}$, in time and frequency direction to obtain the estimation at all data subcarriers position. We can do the interpolate, either with 2D interpolation or 1D linear interpolation-1D frequency interpolation. The process of step 2 is illustrated by Fig. 3.8.

- **Step 3** Conduct the addition and substraction operations to obtain the estimation of channel frequency responses from both transmitters.

$$\hat{H}_{1j,k,l} = 0.5(\hat{H}^a_{j,k,l} + \hat{H}^b_{j,k,l}) \tag{3.15}$$

$$\hat{H}_{2j,k,l} = -0.5(\hat{H}^a_{j,k,l} - \hat{H}^b_{j,k,l}) \tag{3.16}$$

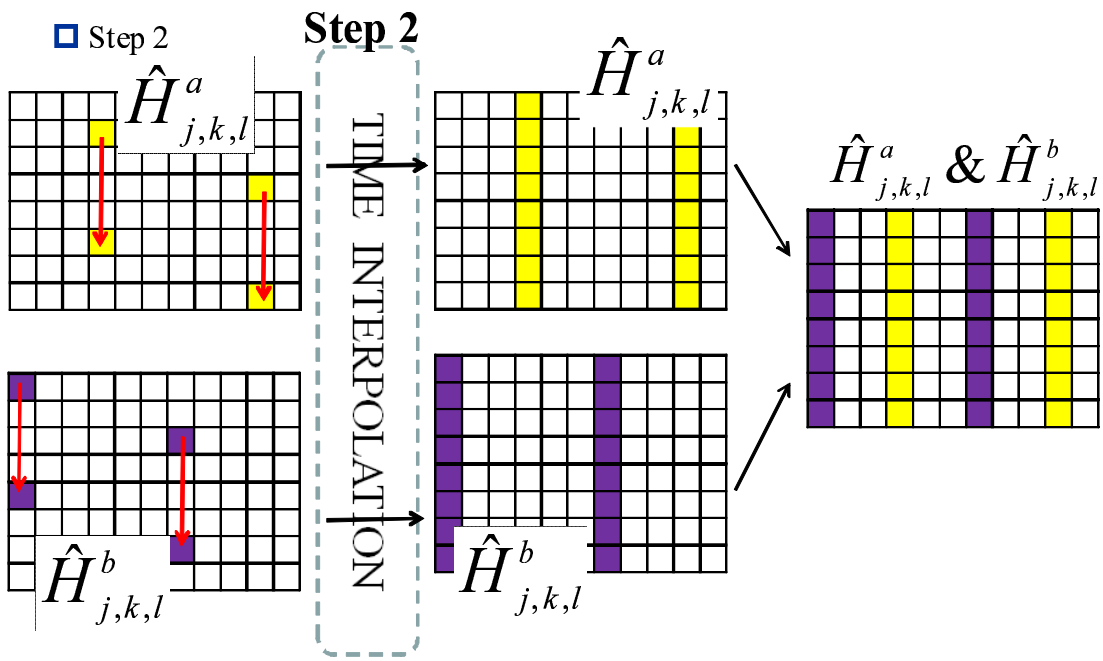

Figure 3.10: The illustration of the 2-point Averaging PACE for a 2×1 MISO OFDM system [22] step 2

The weakness of the conventional method is the larger distance among scattered pilots in frequency direction before interpolation, i.e. $D_X = 6$ which means less density of reference pilot that may decrease the performance of interpolation filter along frequency direction.

3.3.3 A 2-Point Averaging

In order to solve the problem of the conventional method [16], an averaging process can be a solution to shorten the distance among scattered pilots in frequency direction. The 2-point averaging method is the method that proposed by [22]. This method was proposed for MIMO 2×2, but can also be utilized for a 2×1 MISO. The adaptation of this method for time varying channel is defined in several steps, i.e:

- **Step 1** Estimate the addition and substraction of channel using the LS method as given by (3.13)-(3.14). The process of step 1 is illustrated by Fig. 3.7.
- **Step 2** Interpolate the estimated addition and substraction of channel responses through time direction to obtain the temporal channel estimation in subcarrier columns that contain scattered pilot. The process of step 2 is illustrated by Fig. 3.10.
- **Step 3** Conduct the two points averaging to obtain the temporal estimation of $\hat{H}_{1\,j,k,l}$ and $\hat{H}_{2\,j,k,l}$. Based on the scattered pilot pattern, we divide the addition and

substraction operations in two cases, i.e case A and B. In case A, the estimation of channel frequency responses from both transmitters are given by (3.17)-(3.18)

$$\hat{H}^{-}_{1j,k,l} = 0.5(\hat{H}^{a}_{j,k,l} + \hat{H}^{b}_{j,k+3,l}) \tag{3.17}$$

$$\hat{H}^{-}_{2j,k,l} = -0.5(\hat{H}^{a}_{j,k,l} - \hat{H}^{b}_{j,k+3,l}) \tag{3.18}$$

In case B, the estimation of channel frequency responses from both transmitters are given by (3.19)-(3.20)

$$\hat{H}^{+}_{1j,k,l} = 0.5(\hat{H}^{b}_{j,k,l} + \hat{H}^{a}_{j,k+3,l}) \tag{3.19}$$

$$\hat{H}^{+}_{2j,k,l} = 0.5(\hat{H}^{b}_{j,k,l} - \hat{H}^{a}_{j,k+3,l}) \tag{3.20}$$

The process of step 2 is illustrated by Fig. 3.11.

- **Step 4** Combine $\hat{H}^{-}_{1j,k,l}$ and $\hat{H}^{+}_{1j,k,l}$, then conduct the interpolation in frequency direction to obtain the estimation of $\hat{H}_{1j,k,l}$ in all subcarrier data position. The same process is also conducted to to obtain $\hat{H}_{2j,k,l}$. The process of step 2 is illustrated by Fig. 3.12.

The advantage of this method compared to the conventional method is the shorter distance in frequency direction before interpolation, i.e. $D_X = 3$, which means higher density of reference pilot that may increase the performance of interpolation filter along frequency direction compared to the conventional method. On the other hand, the weakness of this 2-point averaging method is the averaging process that is conducted after the interpolation in time direction. It means some channel responses are estimated using the averaging with the temporal channel estimation, not the scattered pilots themselves. Therefore, this method is really dependent on the performance of time direction interpolation. In lower SNR, the performance of time direction interpolation may decrease due to high noise level which may also decrease the performance of 2-point averaging generally.

3.3.4 The Proposed 3-Point Averaging

In this paper, we propose the channel estimation method that can optimize the performance of the interpolation filter by shortening the distance between reference pilots in frequency direction before interpolation. It also increases the number of points included in averaging process in order to produce more accurate channel estimation for rapidly time-varying channel. The channel estimation that we propose in this paper consists of several steps, i.e:

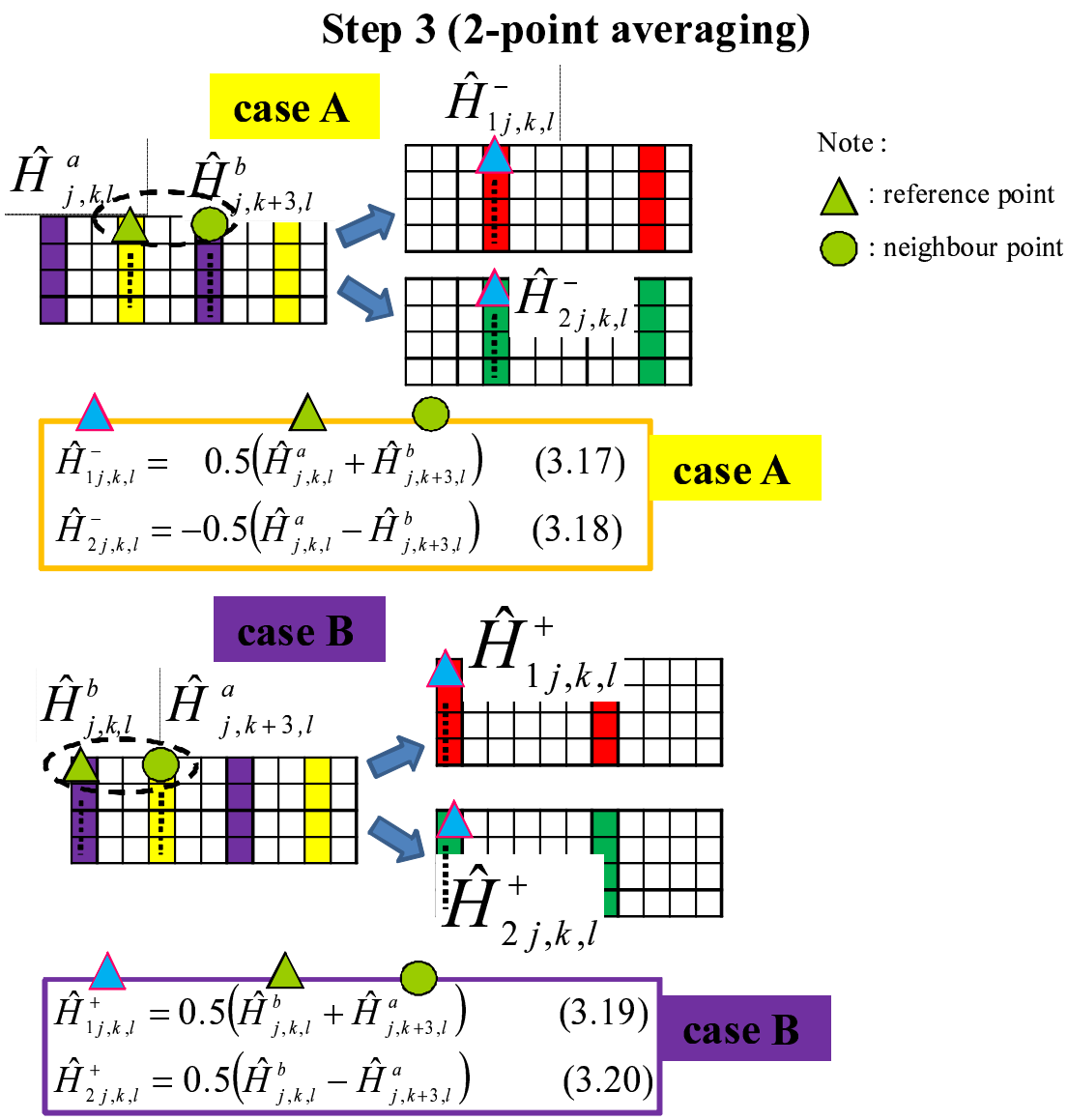

Figure 3.11: The illustration of the 2-point Averaging PACE for a 2×1 MISO OFDM system [22] step 3

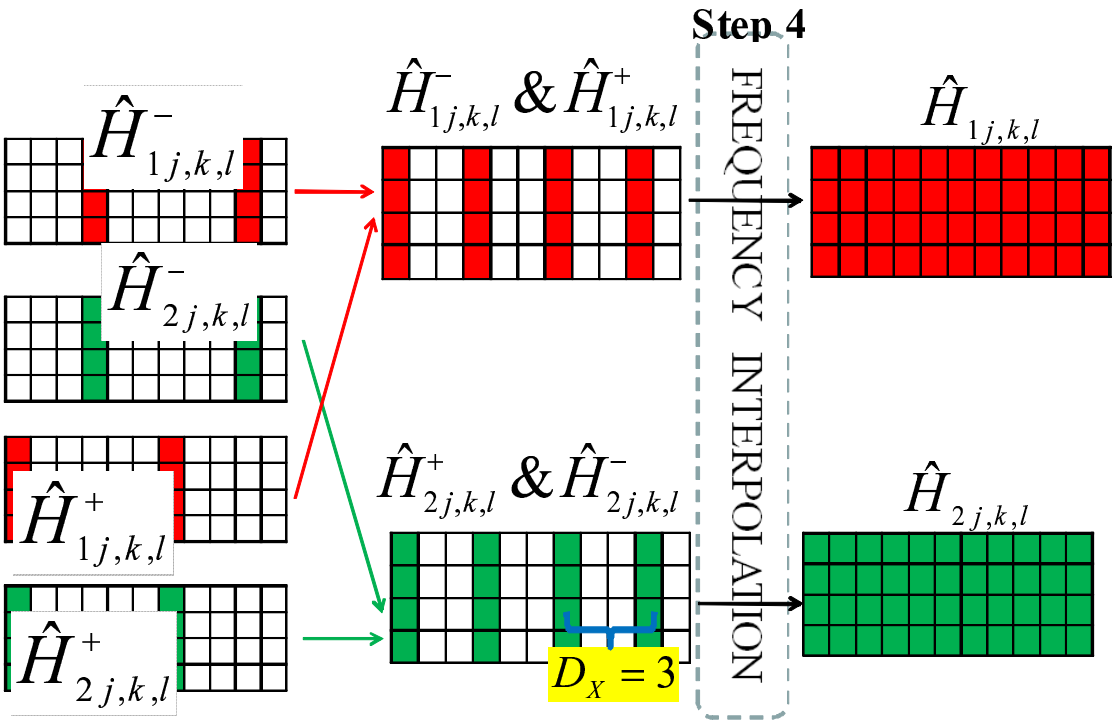

Figure 3.12: The illustration of the 2-point Averaging PACE for a 2×1 MISO OFDM system [22] step 4

- **Step 1** Estimate the addition and substraction of channel using the LS Method as given by (3.13)-(3.14). The process of step 1 is illustrated by Fig. 3.7.
- **Step 2** Estimate the channel frequency responses, $\hat{H}_{1j,k,l}$ and $\hat{H}_{2j,k,l}$ by conducting 3-points averaging operation operations. Based on the scattered pilot pattern, we divide the addition and substraction operations in two cases, i.e case A and B. In case A, the estimation of channel frequency responses from both transmitter at j-th transmitter are given by (3.21)-(3.22)

$$\hat{H}^{-}_{1j,k,l} = 0.25(\hat{H}^{b}_{j,k-3,l-1} + 2\hat{H}^{a}_{j,k,l} + \hat{H}^{b}_{j,k+3,l+1}) \tag{3.21}$$

$$\hat{H}^{-}_{2j,k,l} = 0.25(\hat{H}^{b}_{j,k-3,l-1} - 2\hat{H}^{a}_{j,k,l} + \hat{H}^{b}_{j,k+3,l+1}) \tag{3.22}$$

In case B, the estimation of channel frequency responses from both transmitter are given by (3.23)-(3.24)

$$\hat{H}^{+}_{1j,k,l} = 0.25(\hat{H}^{a}_{j,k-3,l-1} + 2\hat{H}^{b}_{j,k,l} + \hat{H}^{a}_{j,k+3,l+1}) \tag{3.23}$$

$$\hat{H}^{+}_{2j,k,l} = -0.25(\hat{H}^{a}_{j,k-3,l-1} - 2\hat{H}^{b}_{j,k,l} + \hat{H}^{a}_{j,k+3,l+1}) \tag{3.24}$$

The derivation of (3.21)-(3.24) is written in the next subsection.

- **Step 3** Combine $\hat{H}^{-}_{ij,k,l}$ and $\hat{H}^{+}_{ij,k,l}$, then conduct the interpolation in time and frequency direction to obtain the estimation of $\hat{H}_{ij,k,l}$ in all subcarrier data position. The process of step 2 is illustrated by Fig. 3.14.

The advantage of this method compared to the conventional method [16] is the shorter distance in frequency direction before interpolation, i.e. $D_X = 3$, which means higher density of reference pilot that may increase the performance of interpolation filter along frequency direction compared to the conventional method.

This method has also some advantages compared to the 2-points averaging proposed by [22]. Firstly, it does the averaging not only with the neighbour reference pilot in one side, but with the neighbours reference pilots at the both side. Utilizing more number of averaging point might increase the accuracy of the channel estimation, but considering the varying channel along time-and-frequency domain, too many point of averaging can also reduce the accuracy of estimation. In order to decide the most efficient number of averaging, we hold a computer simulation. Secondly, the averaging is not performed after time direction interpolation, thus the performance is not dependent of the time direction interpolation performance as the pointed weakness of 2-points averaging [22]. Therefore, it will be more robust in lower SNR.

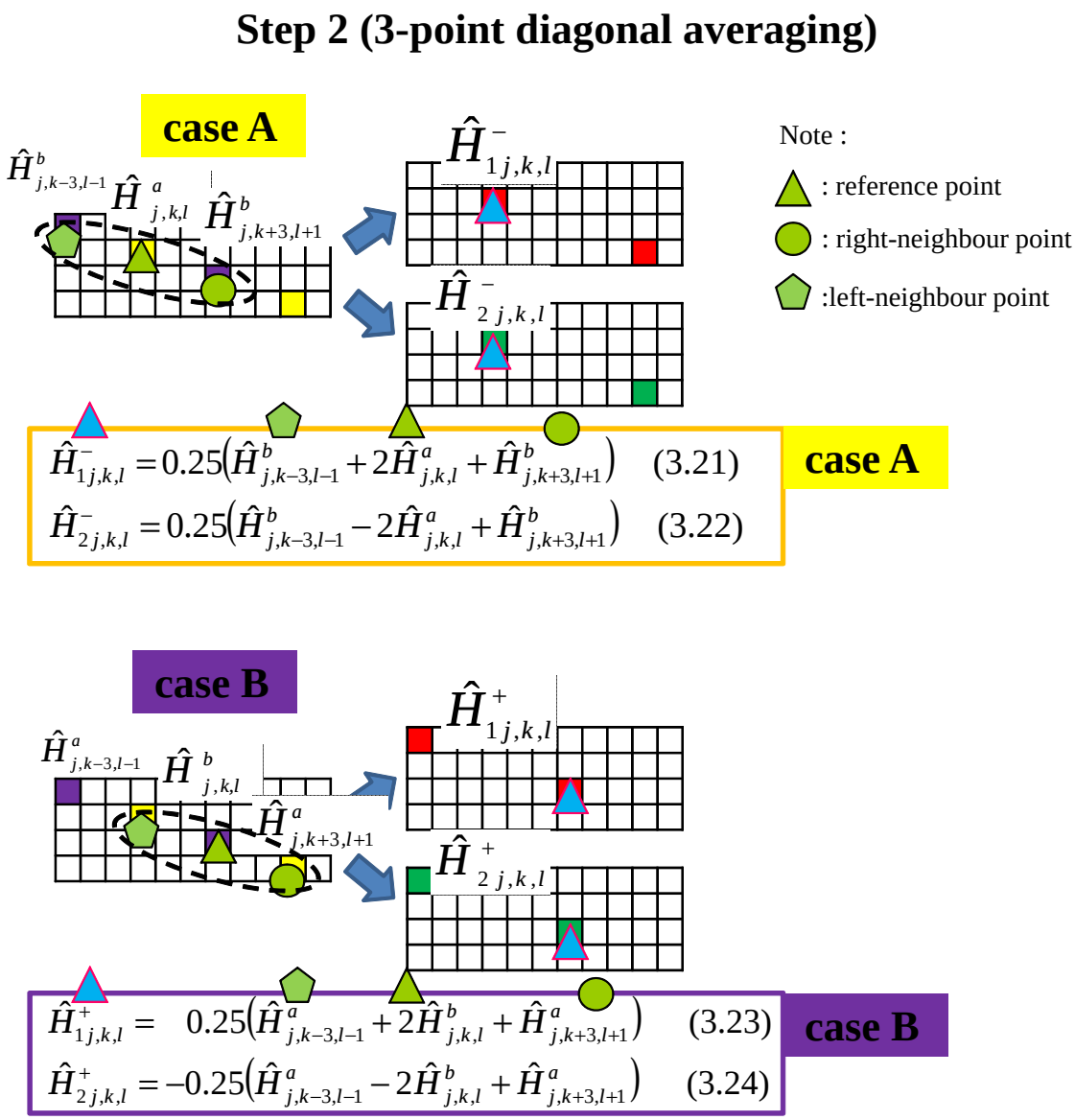

Figure 3.13: The illustration of the proposed 3-point diagonal PACE for a 2×1 MISO OFDM system step2

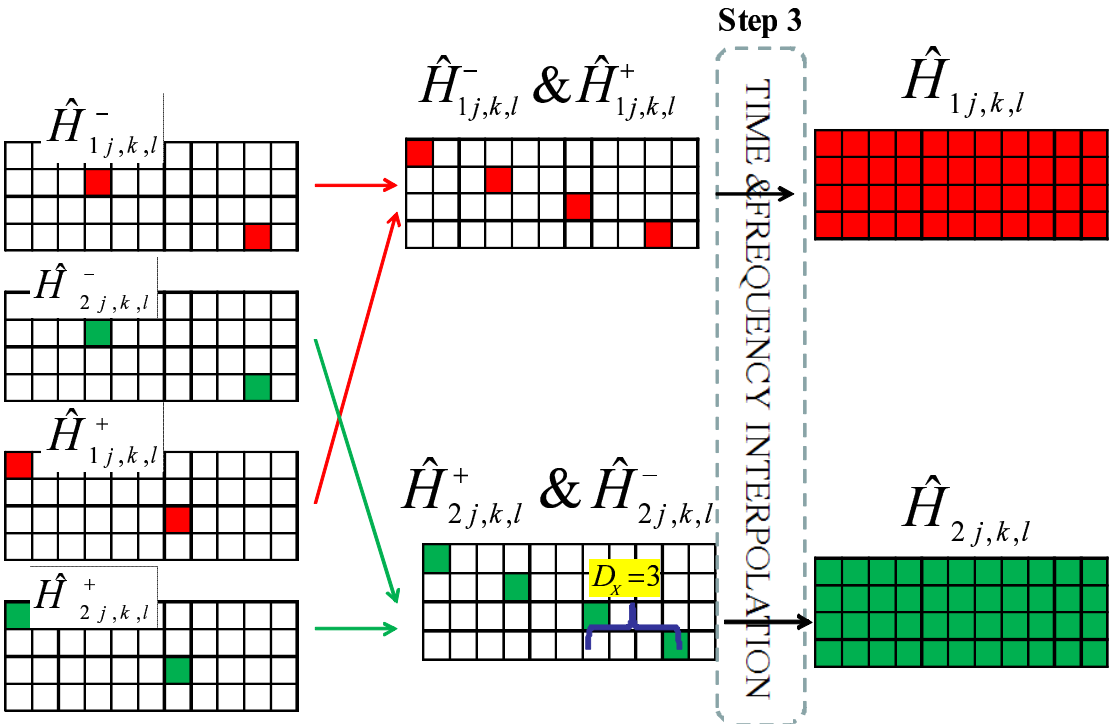

Figure 3.14: The illustration of the proposed 3-point diagonal PACE for a 2×1 MISO OFDM system step 3

The Derivation of 3-Point Averaging

The general form of (3.21) and (3.22) are shown as follow:

$$\hat{H}^{-}_{1j,k,l} = \frac{1}{C_{-1} + C_0 + C_1}(C_{-1}\hat{H}^{b}_{j,k-3,l-1} + C_0\hat{H}^{a}_{j,k,l} + C_1\hat{H}^{b}_{j,k+3,l+1}) \tag{3.25}$$

$$\hat{H}^{-}_{2j,k,l} = \frac{1}{C_{-1} + C_0 + C_1}(C_{-1}\hat{H}^{b}_{j,k-3,l-1} - C_0\hat{H}^{a}_{j,k,l} + C_1\hat{H}^{b}_{j,k+3,l+1}) \tag{3.26}$$

Since $\hat{H}^{a}_{j,k,l}$ is the substraction of $H^{1}_{j,k,l}$ and $H^{2}_{j,k,l}$ and $\hat{H}^{b}_{j,k,l}$ is the addition between them, then the coefficients summation of $\hat{H}^{a}_{j,k,l}$ and $\hat{H}^{b}_{j,k,l}$ should be equal. For 3-point averaging case, it can be defined as

$$C_0 = C_{-1} + C_1 \tag{3.27}$$

By applying (3.27), we can cancel the $H^{2}_{j,k,l}$ to get the estimation of $H^{1}_{j,k,l}$ using (3.21) and we can cancel the $H^{1}_{j,k,l}$ to get the estimation of $H^{2}_{j,k,l}$ using (3.22).

On the other hand, in order to get the best result of averaging, the summation of neighbour points at the right and left side also need to be equal. In 3-point case, it can be defined as $C_{-1} = C_1$. In order to minimize number of multipliers in hardware implementation, we consider $C_{-1} = C_1 = 1$ and $C_0 = 2$. In this manner, we only introduce one bit shift for $C_0\hat{H}^{a}_{j,k,l}$ instead of three multiplications. That is how we define coefficients for 3-point averaging, as shown by (3.21)-(3.24) The coefficient of 4-point and 5-point can also be derived in similar manner.

3.4 A 2D Non-rectangular Filter

In this paper, we propose the utilization of a 2D Filter with non rectangular spectrum as the interpolation filter for a 2×2 MIMO DVB-T2 channel estimation. Multidimensional multirate filters for non-rectangular lattices were proposed by [8] for multidimensional multirate signal processing with parallelogram-shaped passbands. In this paper, we modified the 2D filter based on the multidimensional multirate filter concept [8] to obtain the estimation of channel frequency responses. Since the DVB-T2 system utilizes the pilot pattern with parallelogram-shaped grid, the idea of 2D filter with a non-rectangular spectrum has become important in achieving a better performance for channel estimation.

3.4.1 General Lattice Expression of a 2D Sampling

In this section, we discuss about the general lattice expression of a 2D sampling that is used in 2D filter discussion. Given $\mathbf{n} = [n_1, n_2]^T$ and $\mathbf{t} = [t_1, t_2]^T$ are the rectangular

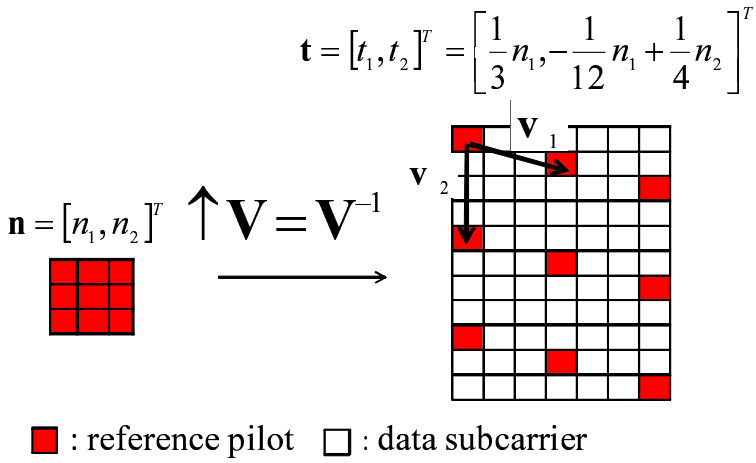

Figure 3.15: Lattice expression for upsampling in DVB-T2 scattered pilot pattern

coordinate before and after upsampling, respectively. The relation between **t** and **n** can be defined as (3.28)

$$\mathbf{t} \triangleq \begin{pmatrix} t_1 \\ t_2 \end{pmatrix} = \mathbf{V}\begin{pmatrix} n_1 \\ n_2 \end{pmatrix} = \begin{pmatrix} v_{11} & v_{12} \\ v_{21} & v_{22} \end{pmatrix}\begin{pmatrix} n_1 \\ n_2 \end{pmatrix} \tag{3.28}$$

where **V** is the sampling matrix. Every sample location **t** is of the form (3.29)

$$\mathbf{t} = n_1\mathbf{v}_1 + n_2\mathbf{v}_2 \tag{3.29}$$

where $\mathbf{v}_1 = [v_{11}, v_{21}]^T$ and $\mathbf{v}_2 = [v_{12}, v_{22}]^T$. Fig.3.15 illustrates the example of lattice expression for upsampling process in DVB-T2 scattered pilot pattern. For this pattern, the sampling matrix **V** can be expressed as (3.30)

$$\mathbf{V} = \begin{pmatrix} 3 & 0 \\ 1 & 4 \end{pmatrix}, \mathbf{v_1} = \begin{pmatrix} 3 \\ 1 \end{pmatrix}, \mathbf{v_2} = \begin{pmatrix} 0 \\ 4 \end{pmatrix} \tag{3.30}$$

In this case $\mathbf{n} = [n_1, n_2]^T$ is upsampled by matrix **V**, which means to be multiplied by $\mathbf{V}^{-1}$. Then, we get the upsampled coordinate as $\mathbf{t} = [\frac{1}{3}n_1, -\frac{1}{12}n_1 + \frac{1}{4}n_2]^T$.

3.4.2 A Design of Non-rectangular Spectrum 2D Interpolation Filter

In this section, we explain about the process of designing a 2D interpolation filter with a non-rectangular spectrum for channel estimation in DVB-T2 system. We design separated interpolation filter for time-and-frequency direction. We design separated filter by dividing **V** (3.30) into $\mathbf{V_1}$ and $\mathbf{V_2}$ as shown by (3.31)

$$\mathbf{V} = \begin{pmatrix} v_{11} & v_{12} \\ v_{21} & v_{22} \end{pmatrix} = \mathbf{V_2} \times \mathbf{V_1} \tag{3.31}$$

where $\mathbf{V_1}$ and $\mathbf{V_2}$ are defined as shown by (3.32)

$$\mathbf{V_1} = \begin{pmatrix} 1 & 0 \\ 0 & 4 \end{pmatrix}, \mathbf{V_2} = \begin{pmatrix} 3 & 0 \\ 1 & 1 \end{pmatrix}, \tag{3.32}$$

$\mathbf{V_1}$ and $\mathbf{V_2}$ denotes the sampling matrix for interpolation filter in time and frequency direction, respectively.

Firstly, we generate a 1D filter in time direction $g_1(n)$. The pass band region of 1D LPF is $[-\pi/\det(\mathbf{V_1}), \pi/\det(\mathbf{V_1})]$ where the $\det(\mathbf{V_1})$ is a determinant of matrix $\mathbf{V_1}$ that is given by (3.32). The frequency response spectrum of $g_1(n)$, i.e. $G_1(z)$ is shown in Fig. 3.16.

Secondly, we generate a 2D filter in frequency direction which consists of several steps, as shown as follow:

- **Step 1** Generate a 1D FIR LPF $g_2^{'}(n)$ which its spectrum doesn't involve aliasing when the 2D filter is later generated. The pass band region of 1D LPF is $[-\pi/\det(\mathbf{V_2}), \pi/\det(\mathbf{V_2})]$.
- **Step 2** Generate a 2D separable and rectangular spectrum filter $g_2^{''}(\mathbf{n})$ as defined by (3.33).

$$g_2^{''}(\mathbf{n}) = g_2^{'}(n)^T g_2^{'}(n) \tag{3.33}$$

- **Step 3** Obtain the impulse response of non-separable filter $g_2(\mathbf{n})$ by decimating $g_2^{''}(\mathbf{n})$ matrix with the matrix $\hat{\mathbf{V}}_2$ and scaling with $\det(\hat{\mathbf{V}}_2)$

$$g_2(\mathbf{n}) = \det(\hat{\mathbf{V}}_2) g_2^{''}(\hat{\mathbf{V}}_2 \mathbf{n}) \tag{3.34}$$

Where matrix $\hat{\mathbf{V}}_2$ is the adjoint of matrix $\mathbf{V_2}$. From here, we obtain the non-rectangular spectrum 2D filter. The frequency response spectrum of $g_2(\mathbf{n})$, i.e. $G_2(z)$ is shown in Fig.3.17.

3.4.3 Implementation of a Non-rectangular 2D Filter

A filtering process in multi-dimensional signals can be divided into several stages [8]. For two dimensional case, there are two kinds of implementation, i.e. a single-stage implementation and two-stage implementation. In this chapter, we discuss both type of implementation and the complexity of each.

Single-stage Implementation of a 2D filter

A single-stage implementation is performed by using filter $g(\mathbf{n})$ which is a product of a 2D convolution between $g_1(\mathbf{n})$ and $g_2(\mathbf{n})$ as shown by (3.35)

$$g(\mathbf{n}) = g_1(\mathbf{n}) * g_2(\mathbf{n}) \tag{3.35}$$

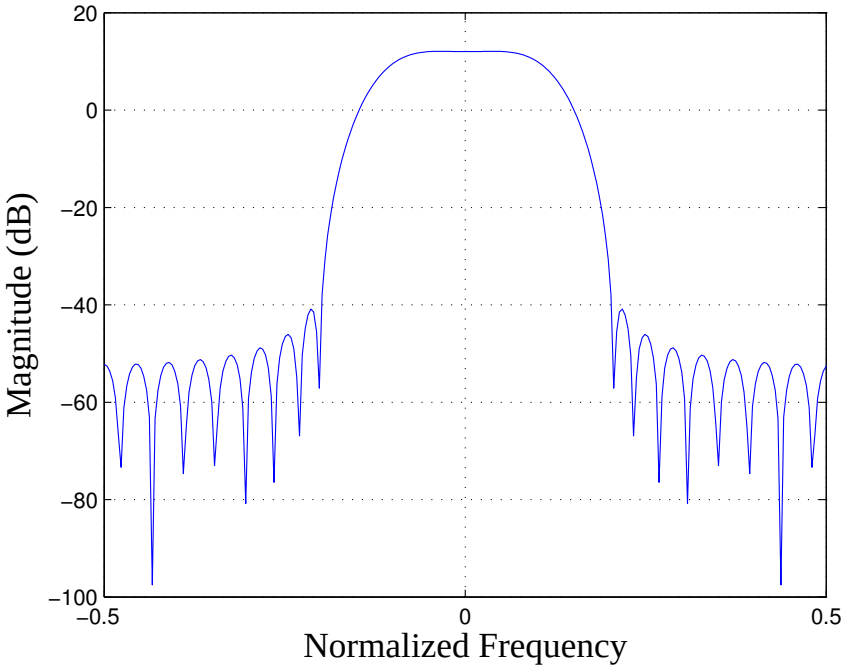

Figure 3.16: $G_1(z)$

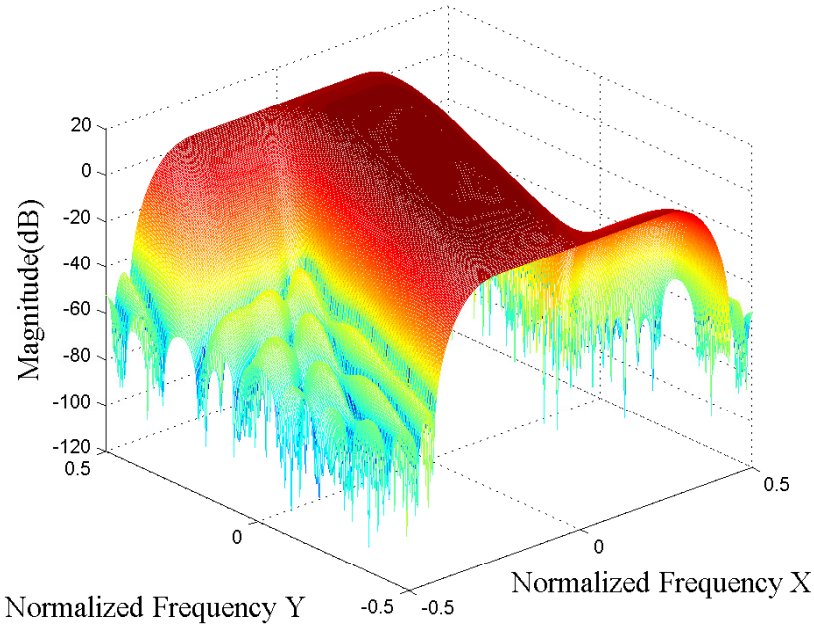

Figure 3.17: $G_2(z)$

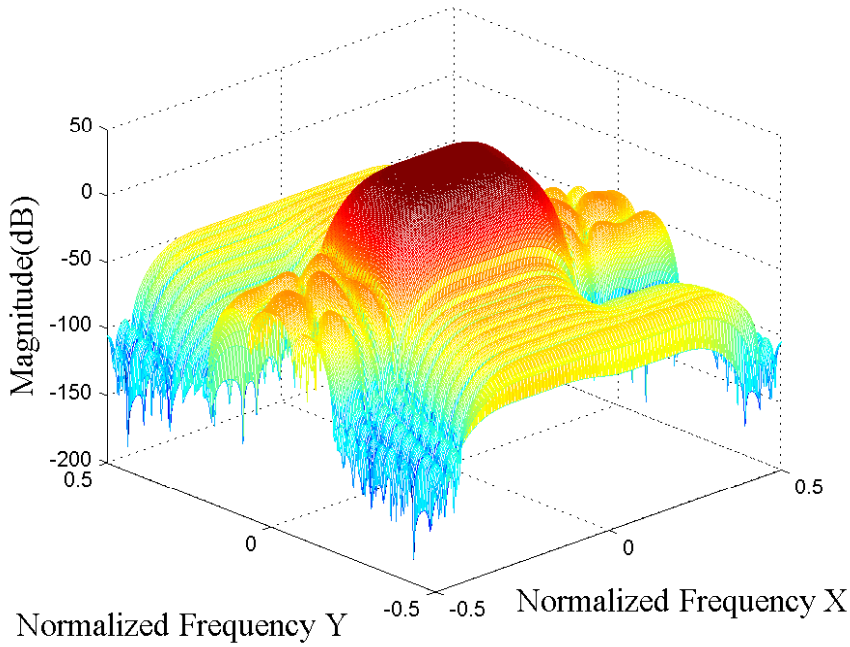

Figure 3.18: $G(z)$

The frequency response spectrum of single-stage interpolation filter $g(n)$, i.e. $G(z)$ is shown by Fig. 3.18. First, the reference pilot $p(l,k)$ is upsampled by matrix $\mathbf{V}$ (3.30).

$$a(l,k) = \mathbf{V}^{-1}p(l,k) = x(\frac{1}{3}l, -\frac{1}{12}l + \frac{1}{4}k) \tag{3.36}$$

where $a(l,k)$ is the reference pilot after upsampling. After upsampling, the reference pilot is interpolated using filter $g(\mathbf{n}) = g(n_1, n_2)$

$$q(l,k) = \sum_{n_1=0}^{N_{11}-1} \sum_{n_2=0}^{N_{12}-1} g(n_1,n_2)a_1(l-n_1, k-n_2) \tag{3.37}$$

where $q(l,k)$ is the output of single-stage filtering. N_{11} and N_{12} are the number of filter coefficients of 2D filter $g(\mathbf{n})$ in time and frequency direction, respectively. The complete process of single-stage filtering is represented in Fig. 3.19.

Two-stage implementation of a Non-Rectangular 2D Filter

In order to achieve a design with less complexity, we utilize the two-stage filtering, as shown in Fig. 3.20. The meaning of two-stage implementation is the separation between a filtering along time direction and frequency direction. In this implementation, the upsampling matrix $\mathbf{V}$ is divided into two stages as shown by (3.31).

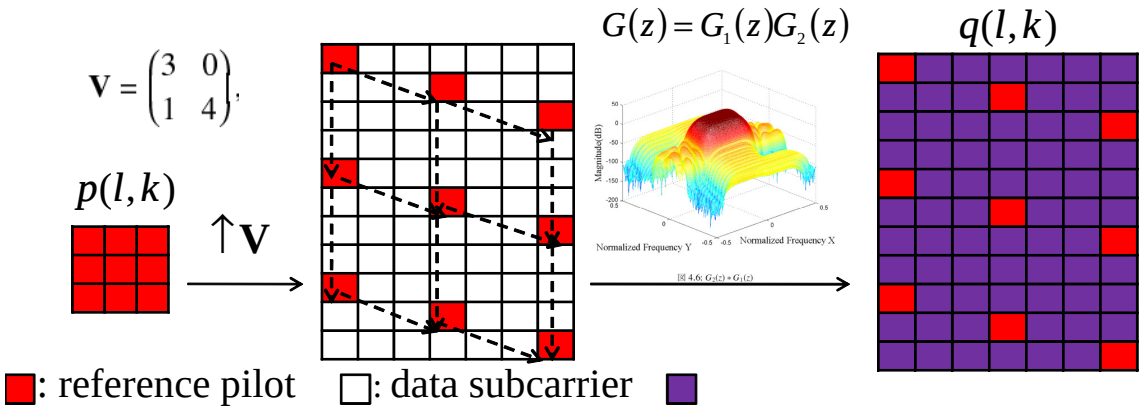

Figure 3.19: A single stage implementation

In the first-stage, the reference pilot is upsampled using matrix $\mathbf{V_1}$

$$b_1(l,k) = \mathbf{V_1}^{-1} p(l,k) = p(l, \frac{1}{4}k) \tag{3.38}$$

where $b_1(l,k)$ is the upsampled reference pilot. $b_1(l,k)$ is then filtered by filter $g_1(\mathbf{n})$

$$b_2(l,k) = \sum_{n_1=0}^{N_{21}-1} \sum_{n_2=0}^{N_{22}-1} g_1(n_1,n_2) b_1(l-n_1, k-n_2) \tag{3.39}$$

where $b_2(l,k)$ is the output of the first-stage filtering. N_{21} and N_{22} are the number of filter coefficients of 2D filter $g_1(\mathbf{n})$ in time and frequency direction, respectively. Since, the filter that we use in first stage filtering is a 1D filter, i.e. $N_{22} = 1$. We can simplify (3.39) as follow

$$b_2(l,k) = \sum_{n=0}^{N_{21}-1} g_1(n) b_1(l, k-n) \tag{3.40}$$

Therefore, the first-stage filtering denotes a 1D filtering in time-direction.

In the second-stage. the reference pilot is upsampled using matrix $\mathbf{V_2}$ as shown by

$$b_3(l,k) = \mathbf{V_2}^{-1} b_2(l,k) = b_2(\frac{1}{3}l, -\frac{1}{3}l + k) \tag{3.41}$$

where $b_3(l,k)$ is the reference pilot after upsampled by $\mathbf{V_2}$ matrix. $b_3(l,k)$ is then filtered by filter $g_2(\mathbf{n}) = g_2(n_1,n_2)$

$$q(l,k) = \sum_{n_1=0}^{N_{23}-1} \sum_{n_2=0}^{N_{24}-1} g_2(n_1,n_2) b_3(l-n_1, k-n_2) \tag{3.42}$$

where $q(l,k)$ is the output of second-stage filtering. N_{23} and N_{24} are the number of filter coefficients of 2D filter $g_2(\mathbf{n})$ in time and frequency direction, respectively.

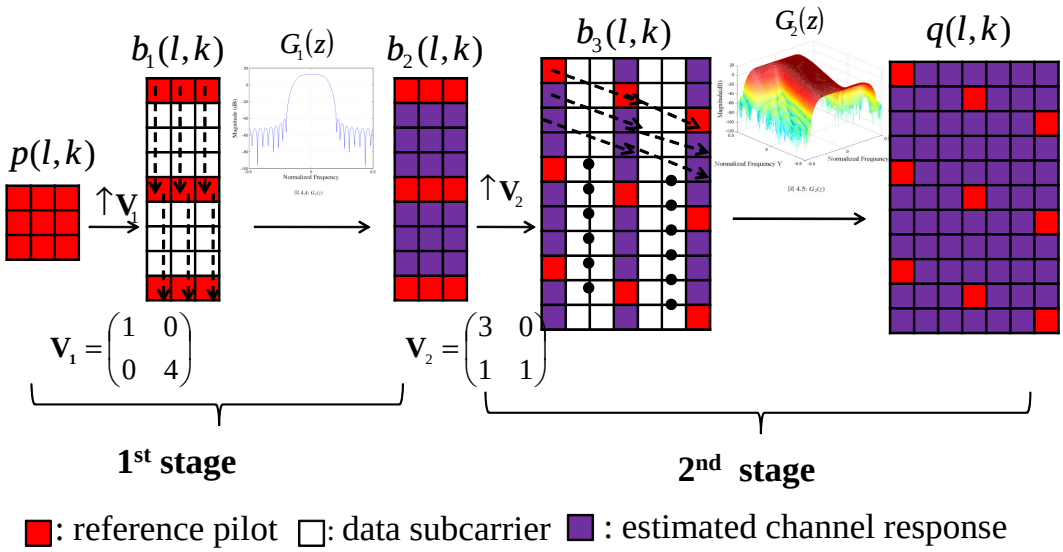

Figure 3.20: Two stage implementation

The Implementation Complexity Analysis

In terms of complexity, we compare the complexity between a single stage 2D non-rectangular interpolation filter with a two stage implementation. For number of taps: 20 taps for 1D FIR LPF time direction interpolation and 16 taps for 1D FIR LPF frequency direction interpolation. These number of filter taps is sufficient for this case. It was decided by our preliminary simulation. In two-stage implementation, the number of filter coefficients is

$$N_{21} \times N_{22} + N_{23} \times N_{24} = 20 \times 1 + 6 \times 16 = 116 \tag{3.43}$$

In single-stage implementation, since the filter $g(\mathbf{n})$ (3.35) is a product of a 2D convolution between $g_1(\mathbf{n})$ and $g_2(\mathbf{n})$, then the number of filter coefficients can be calculated as follow:

$$N_{11} \times N_{12} = (N_{21} + N_{23} - 1) \times (N_{22} + N_{24} - 1) = 400 \tag{3.44}$$

From here, we can conclude that the two stage implementation of a 2D non-rectangular filter can reduce the number of multiplication around 71% of multiplication number that is needed by the single stage implementation.

3.5 Summary

In this section we have discussed about the channel estimation for DVB-T2 system. Firstly, we have discussed about the scattered pilot pattern that we use as a reference for channel estimation process. Then, we have discussed about a channel estimation scheme

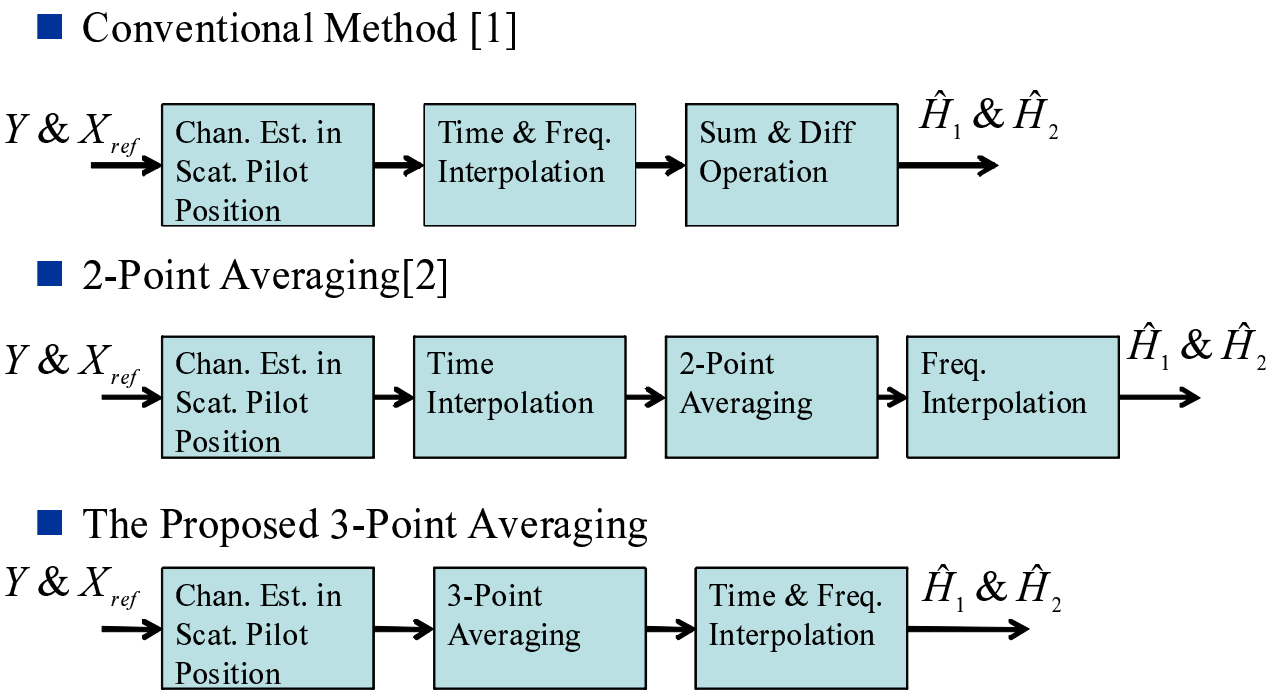

Figure 3.21: Summary of channel estimation method for MIMO DVB-T2

in SISO and MIMO case. For channel estimation in MIMO case, there are three methods that we have discussed, i.e. a conventional method [16], a 2-point averaging [22], and the proposed 3-point diagonal averaging method as shown by Fig.3.21. The strength and weakness of each methods are discussed in table 3.5

In this chapter, we have also discussed about 2D non-rectangular filter. In order to perform the robust channel estimation for paralellogram pattern of scattered pilot of DVB-T2, we have implemented the 2D non-rectangular LPF. Based on our study, in order to implement 2D non-rectangular LPF with lower complexity, we have utilized the two-stage implementation.

Table 3.5: The strength and weakness summary of every method

conventional method [16]	(-) Larger distance before frequency direction interpolation $D_x = 6$
2-point averaging [22]	(+) Smaller distance before frequency direction interpolation $D_x = 3$ (-) The performance of averaging depends on the performance of time direction interpolation which is potentially worse in lower SNR
proposed 3-point diagonal averaging method	(+) Smaller distance before frequency direction interpolation $D_x = 3$ (+) The performance of averaging doesn't depend on the performance of time direction interpolation . (+) Larger number of averaging point allow us to implement interpolation filter with lower complexity (lower number of taps) (-) Largest number of averaging point

Chapter 4

Synchronization Method for DTTB System

4.1 Synchronization Problem in Multipath Fading Channel

ISDB-T system was designed based on the OFDM. One of the main advantage of OFDM is the robustness over frequency selective fading channel because it divides the entire frequency band into a number of parallel subcarriers, each of which experiences flat channel fading. It is beneficial for terrestrial system e.g. ISDB-T which is transmitted through multipath channel and suffered performance degradation due to frequency selective fading. OFDM systems also have efficient spectrum utilization due to the overlapping spectra of subcarrier signals. It is also beneficial for ISDB-T in order to use available spectrum efficiently. However, this is only true when the orthogonality among subcarriers is preserved. If it isn't preserved, system performance will be degraded due to inter symbol interference (ISI) and inter carrier interference (ICI). In the following, synchronization errors and their effects on the received frequency-domain signals will be explained briefly.

4.1.1 Effect of Symbol Timing Offset

Before processing DFT, receiver needs to determine the start of symbol. This information will be utilized by receiver to locate the DFT window after removing the guard interval. The failure in determining the correct start of DFT window position introduces phase shift and ISI in frequency domain received signal [23]. Assume the maximum delay spread is shorter than guard interval length, there are three possibilities of DFT window position falseness, as shown in Fig. 4.1 [23]. When DFT window is earlier by θ, but it is not contaminated by delayed previous symbol, the transform received signal is free from ISI. It is called the safe DFT Window. In this case, only additional phase

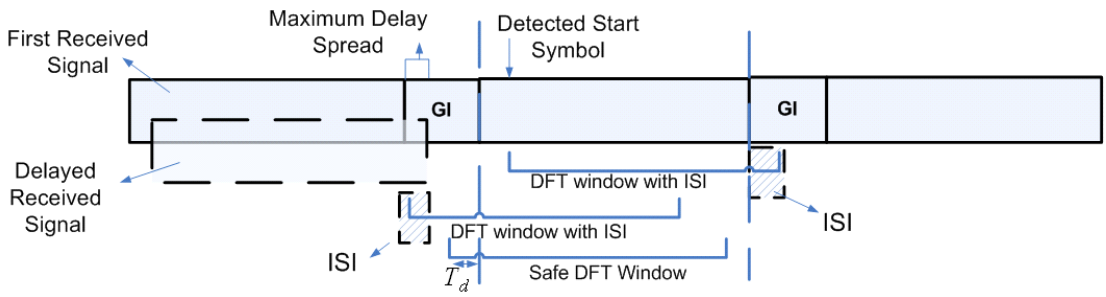

Figure 4.1: Possibility of DFT window location

shift is introduced in the transform signal, as shown in (4.1).

$$Y_{l,k} = X_{l,k} H_{l,k} e^{-j2\pi\theta k/(NT)} + W_{l,k} \tag{4.1}$$

where $Y_{l,k}$, $X_{l,k}$, $H_{l,k}$, and $W_{l,k}$ are the received frequency-domain signal, transmitted frequency-domain signal, channel response, and AWGN of the l-th OFDM symbol and k-th subcarrier, respectively. θ is the difference between the detected symbol start and the actual symbol start and T is the duration of one sample.

On the other hand, there are two possibilities when received signal can be interfered by another symbol . First possibility is when the DFT window leads by large degree and it is interfered by delayed previous symbol. The second possibility is when the DFT window lags, so it interferes with the next symbol. Both case introduce ISI and distortion to magnitude and phase of $Y_{l,k}$, as shown by (4.2)

$$Y_{l,k} = X_{l,k} H_{l,k} \frac{N - |\theta|/T}{N} e^{-j2\pi\theta k/(NT)} + ISI + W_{l,k} \tag{4.2}$$

There are three terms in (4.2). The first term is the part of received frequency-domain signals that are free from ISI. The second term is the part of received frequency domain signals which are interferred by ISI and the latter is the channel noise component. (4.2) shows that there is slight decrease in the amplitude of the first term besides the phase shift. It happens because there are $|\theta|/T$ samples that suffer interference from another symbol (second term). Therefore, only $N - |\theta|/T$ samples are from desired symbol and free from ISI.

4.1.2 Effect of Carrier Frequency Offset

CFO exists because of the mismatch of local oscillator between transmitter and receiver end. It may results on ICI and destroy the orthogonality between subcarriers [23]. The modeling of received signal that destroyed by CFO, Δf ,is given by (4.3)

$$y_{l,n} = y(t) e^{j2\pi\Delta f t} \tag{4.3}$$

Equation (4.3) shows that time-domain received signals suffer phase offset, $e^{j2\pi\Delta f t}$. The CFO can be normalized with respect to subcarrier spacing $f_s = 1/(NT)$ by defining the

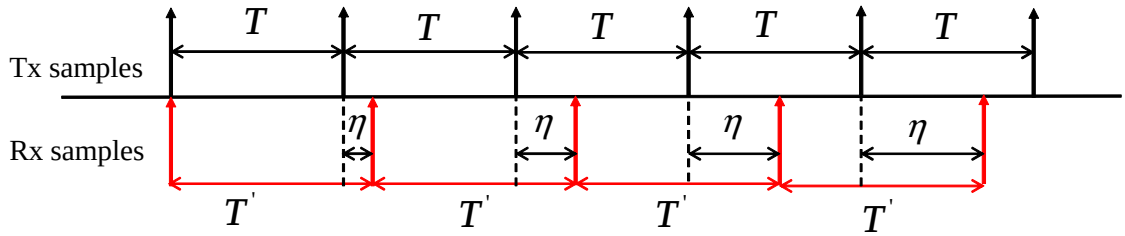

Figure 4.2: The effect of sampling frequency offset to the time-domain received signal

normalized CFO,ε, as shown by (4.4)

$$\varepsilon = \frac{\Delta f}{f_s} \tag{4.4}$$

Assume that the integer part of CFO has been estimated and compensated then the remaining CFO is within one subcarrier spacing (i.e, $|\varepsilon|\leq 0.5$). After performing DFT and discarding guard interval, the frequency-domain received signal then becomes

$$Y_{l,k} = X_{l,k}H_{l,k}\frac{sin(\pi\varepsilon)}{Nsin(\frac{\pi\varepsilon}{N})}e^{j\pi\varepsilon\frac{(N-1)}{N}} + ICI_{l,k} + W_{l,k} \tag{4.5}$$

where $X_{l,k}$ and $H_{l,k}$ are frequency-domain transmitted signals and channel response on on i-th symbol and k-th subcarrier, respectively. The second term in this equation $ICI_{l,k}$ is defined by

$$ICI_{l,k} = X_{l,k}H_{l,k}\frac{sin(\pi\varepsilon)}{Nsin(\frac{\pi\varepsilon}{N})}e^{j\pi\varepsilon\frac{(N-1)}{N}} + ICI_{l,k} + W_{l,k} \tag{4.6}$$

which is nonzero if $\varepsilon \neq 0$. Equation (4.5) shows that the frequency-domain received signals suffer amplitude degradation in every k-th subcarrier, which is introduced by $\frac{sin(\pi\varepsilon)}{Nsin(\pi\varepsilon/N)}$. They also suffer phase shift, which is introduced by $e^{j\pi\varepsilon(N-1)/N}$. But, mainly, the frequency-domain received signals is destroyed by ICI as shown by (4.6).

4.1.3 Effect of Sampling Frequency Offset

Sampling frequency offset (SFO) occurs due to a sampling frequency mismatch between the transmitter and receiver oscilators. Sampling frequency offset could introduce an intersymbol interference (ISI) and an intercarrier interference (ICI) to the signal received by digital terrestrial television broadcasting (DTTB) receiver. The demodulation of signal that contains the ISI and ICI will dramatically increase bit error rate.

Under the influence of SFO (η), the received OFDM baseband signal is sampled at a sampling period $T^{'}$= (1+η)T. Fig. 4.2 shows the shift in time-domain received signal caused by an SFO. Given the transmitted signal in l-th OFDM symbol and k-th subcarrier ($X_{l,k}$) and channel ($H_{l,k}$), the time-domain received signal under influence of SFO can be defined as (4.7)

$$\begin{aligned} y_{l,n} &= \frac{1}{N}\sum_{k=0}^{N-1} H_{l,k}X_{l,k}e^{\frac{j2\pi k[t_n-(N_g+lN_s)T']}{NT'}} + w_{l,n} \\ &= \frac{1}{N}\sum_{k=0}^{N-1} H_{l,k}X_{l,k}e^{\frac{j2\pi k[(N_g+lN_s)\eta+n(1+\eta)]}{N}} + w_{l,n} \\ n &= -N_g, ..., N-1 \end{aligned} \tag{4.7}$$

where $t_n = (N_g + lN_s)T' + nT'$ and $w_{l,n}$ is the additive white gaussian noise (AWGN). N_g and N refer to the length of guard-interval (GI) and OFDM symbol, respectively. N_s is the total length of an OFDM symbol with GI ($N_s = N + N_g$).

After the removal of GI, the receiver transforms the time-domain signal into frequency-domain signal using fast-fourier transform (FFT). The frequency-domain received signal with the presence of an SFO can be defined as (4.8)

$$\begin{aligned} Y_{l,k} &= \mathrm{FFT}(y_{l,n}) = \sum_{n=0}^{N-1} y_{l,n}e^{\frac{-j2\pi kn}{N}} \\ &= H_{l,k}X_{l,k}e^{\frac{j2\pi k\eta(N_g+lN_s)}{N}}e^{j\pi k\eta(\frac{N-1}{N})}\frac{\sin(\pi k\eta)}{N\sin(\frac{\pi k\eta}{N})} + I_{l,k} + W_{l,k} \end{aligned} \tag{4.8}$$

where $W_{l,k}$ and $I_{l,k}$ denote AWGN and intercarrier-interference (ICI) caused by an SFO, respectively. The ICI that is caused by an SFO is defined as (4.9)

$$I_{l,k} = \frac{1}{N}\sum_{m=0,m\neq k}^{N-1} H_{l,m}X_{l,m}e^{\frac{j2\pi m\eta(N_g+lN_s)}{N}}e^{j\pi[m(1+\eta)-k](\frac{N-1}{N})}.\frac{\sin(\pi[m(1+\eta)-k])}{\sin(\pi[m(1+\eta)-k]/N)} \tag{4.9}$$

From (4.8), we can observe that an SFO causes two effects,i.e. an ICI as shown by (4.9) and a phase-rotation. In this paper, we discuss how to estimate the phase rotation, to obtain the estimation of SFO.

4.2 Joint Symbol-Timing and Carrier-Frequency Synchronization

4.2.1 Maximum Likelihood based Synchronization

J.J Van beek synchronization method [24] is based on log-likelihood function. It exploits periodic part in OFDM frame structure from received signal, i.e. cyclic prefix. The appearance of cyclic prefix yields a correlation between some pairs of samples that are space N samples apart (N is DFT window size). It makes received signal, because of its probabilistic structure, contains information about time offset θ and CFO ε. It is crucial

observation that offers the opportunity for joint estimation of time and CFO. Equation (4.10) shows the estimation based on J.J Van Beek Method.

$$\Lambda(\theta, \varepsilon) = |\gamma(m)| - \rho\Phi(m) \tag{4.10}$$

where

$$\gamma(m) = \sum_{k=m}^{m+M-1} y(n)y^*(n+N) \tag{4.11}$$

$$\Phi(m) = \frac{1}{2}\sum_{k=m}^{m+M-1} |y(n)|^2 + |y(n+N)|^2 \tag{4.12}$$

$$\rho = \frac{SNR}{SNR+1} \tag{4.13}$$

m, M, N, and $y(n)$ are correlation sample index, cyclic prefix ratio×number of subcarrier, number of subcarrier, and received signal in time instant n, respectively. $\gamma(m)$ is the result of consecutive sample correlation between pairs of samples that N samples apart. $\Phi(m)$ is an energy term. Its contribution depends on the SNR (by the weighting factor ρ). The term $\Phi(m)$ will be especially used in higher SNR to normalize the autocorrelation of received signal, $\gamma(m)$

The joint ML estimation of θ and ε becomes

$$\hat{\theta}_{ML} = argmax\{\Lambda(\theta, \varepsilon)\} \tag{4.14}$$

$$\varepsilon_{ML} = \frac{1}{2\pi NT}\angle(\gamma(\hat{\theta})) \tag{4.15}$$

The start of symbol is estimated by (4.14). The terms, $\hat{\theta}_{ML}$ is the time instants when the maximum value of $\Lambda(\theta, \varepsilon)$ is detected. The autocorrelation result, $\gamma(m)$, compensated by energy term, $\Phi(m)$, results on the maximum value at the start of every symbol, as shown by Fig. 4.3 Correlation peaks are the result of correlation between Cyclic Prefix and its duplicate in last part of every symbol. In order to detect the start of symbol, we exploit peak value of the correlation result, as shown in Fig.4.4. When the amplitude is higher than threshold, a symbol start search is started. It will detect the maximum value for next M sample range (M is number of sample in Cyclic Prefix). After finding maximum peak in position, X, we can estimate the symbol start as the next M sample from detected peak position, X.

The CFO is estimated by using the phase of detected symbol start, as shown in (4.14). The terms, $\hat{\varepsilon}_{ML}$, is phase of γ in time instants $\hat{\theta}_{ML}$. However, CFO estimation using this algorithm has a limit. The limit is $\pm 1/2$ subcarrier spacing. As $\varepsilon \rightarrow 0.5$, the coarse fractional CFO estimate, may jump to -0.5 due to noise and the discontinuity of the arctangent [25]. When this happens, the estimate is no longer unbiased and, in practice, it becomes useless. Complete process for the estimation using ML function is shown in Fig.4.5

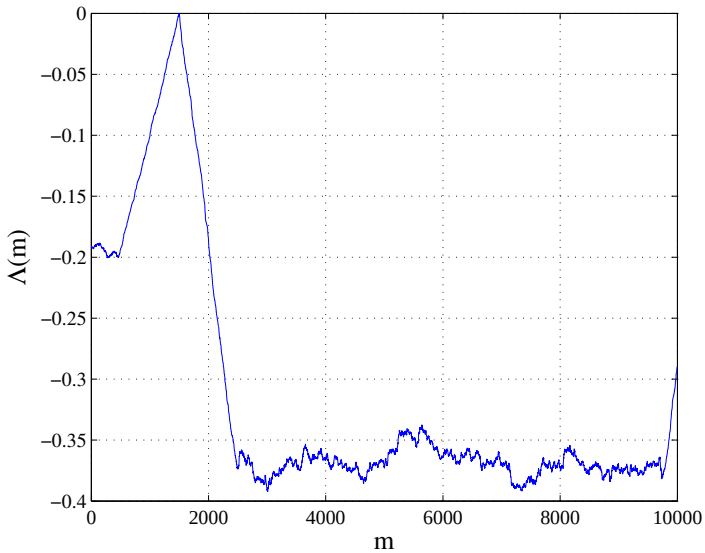

Figure 4.3: Maximum Likelihood autocorrelation results $\Lambda(m)$

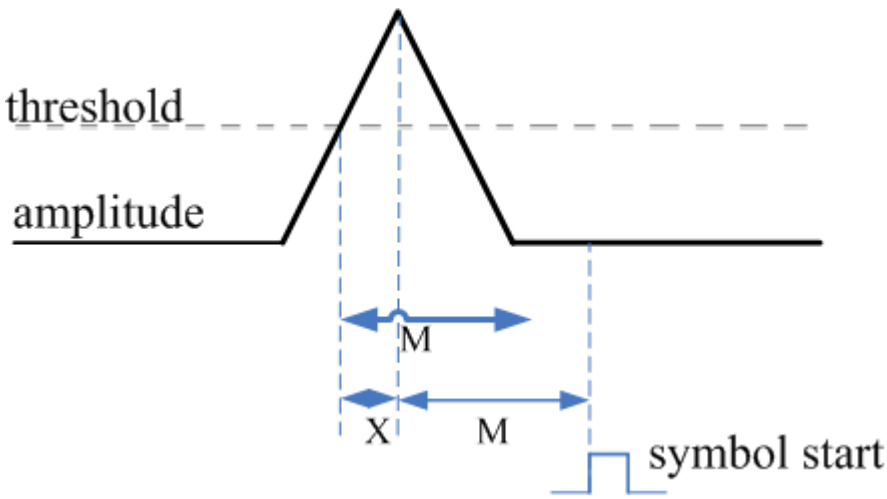

Figure 4.4: Method of finding position of a peak and a start of symbol

Table 4.1: Complexity Comparison

	ML	Simplified ML
Multiplication	$3M + 1$	M
Addition	$3M$	M

4.2.2 Simplified Maximum Likelihood based Synchronization

The Maximum Likelihood function has been simplified by D. Landstrom [26]. Simplified ML is shown by (4.16)

$$\Lambda(\theta, \varepsilon) = |re\{\gamma\}| + |im\{\gamma\}| \tag{4.16}$$

The simplification is done by removing the energy part from J.J. Van Beek ML method [24]. In order to compare the complexity, we compare the number of multiplication and addition for every m correlation samples in both algorithm. The complexity comparison is shown in table 4.1 From table 4.1, we can conclude that the number of multiplication and addition in ML are about three times of the number of multiplication and addition in Simplified ML. It means, we can design more simple hardware with Simplified ML algorithm in it. Complete process of Joint Time and Frequency Synchronization using the less complexity algorithm is shown in Fig.4.6.

4.2.3 DFT Window Shift

In order to improve the performance of Symbol Timing in Multipath fading channel, we introduce DFT Window Shift. Based on the symbol timing estimation results by Maximum Likelihood based methods, there are still exist small timing error, as shown in Fig 4.7. Mean Time Estimation Error means the average shift of symbol start estimation from the actual symbol start. From Fig. 4.7, we can conclude that the DFT window position lags compared to actual DFT window position. We can conclude that by using Maximum Likelihood based symbol timing estimation method, the received signals still suffer performance degradation caused by ISI. In order to avoid ISI, we propose the DFT window shifted to locate the DFT window position in the safe position as discussed in section II. Since, the value of mean timing estimation error always positive, we propose the backward shift DFT window position, as shown in Fig.4.8.

4.3 Sampling Frequency Offset Estimation

4.3.1 Conventional Sampling Frequency Offset Estimation

The conventional SFO estimation for the DTTB is proposed by [27]. They exploit the scattered pilot to estimate SFO. The scattered pilot is a training symbol that has a parallelogram shape pattern. It is located in the same subcarrier every four OFDM

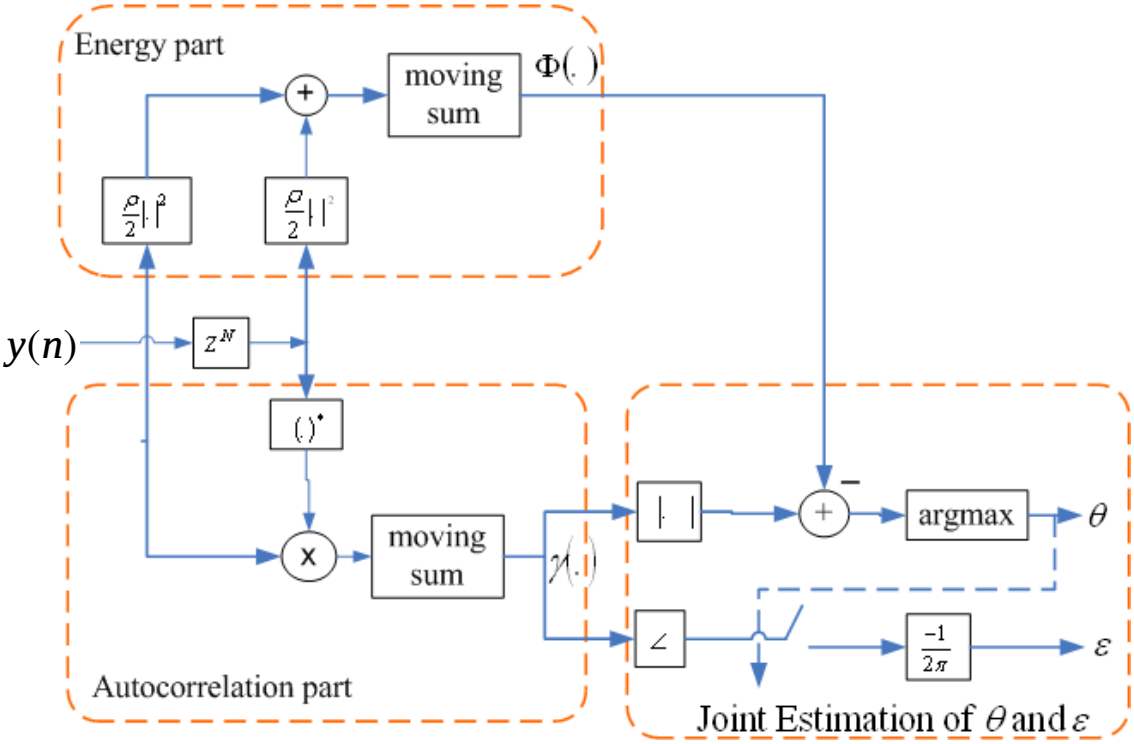

Figure 4.5: Maximum Likelihood Functional Block Diagram

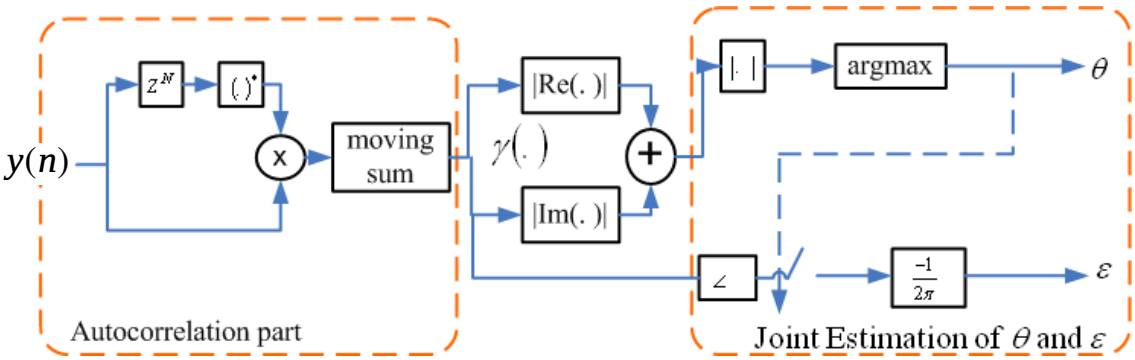

Figure 4.6: Simplified Maximum Likelihood Functional Block Diagram

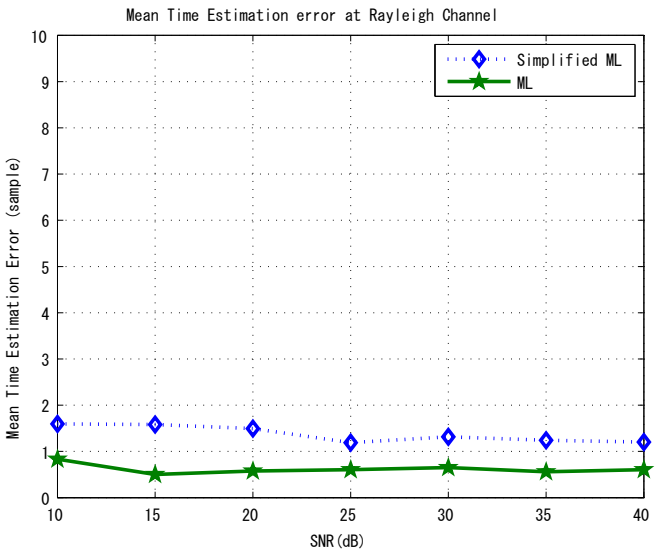

Figure 4.7: Mean Time Offset

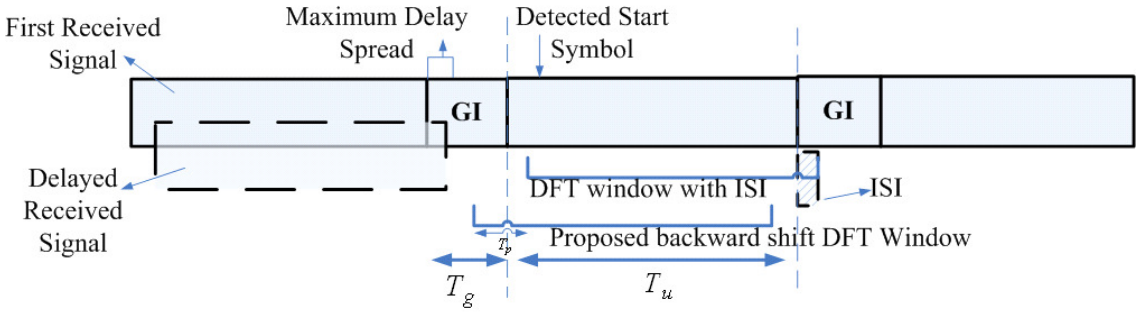

Figure 4.8: Proposed DFT Window Shift

symbols, as defined by DTTB standard [2], [12]. Every OFDM symbol consists of P number of scattered pilots.

Firstly, the conventional method calculates the phase rotation between received scattered pilots in OFDM symbol (l) and (l + 4) by applying a conjugate multiplication. From (4.8), if we ignore the ICI and AWGN, then the conjugate multiplication between them can be defined by (4.17)

$$\begin{aligned} Z_{l,k_p} &= Y^*_{l,k_p} Y_{l+4,k_p} \approx |H_{l,k_p}|^2 |X_{l,k_p}|^2 e^{\frac{j8\pi k_p \eta N_s}{N}} \\ k_p &= k_1, k_2, ..., k_P \end{aligned} \tag{4.17}$$

where k_p is a scattered pilot subcarrier. From (4.17), the phase difference ϕ_{l,k_p} can be defined as (4.18)

$$\phi_{l,k_p} = \tan^{-1}\left(\frac{Im(Z_{l,k_p})}{Re(Z_{l,k_p})}\right) = \frac{8\pi k_p \eta N_s}{N} \tag{4.18}$$

From linear equation (4.18), we can calculate η as a slope of $\phi_{l,k_p}/k_p$. Paper [27] implemented a least-square estimator to calculate η. The conventional method is shown as follow:

Step 1 Calculate the $\hat{\zeta}_{l,m}$, which is the first temporary estimation of SFO. It is calculated as a slope of ϕ_{l,k_p} against k_p using least square algorithm.

$$\begin{aligned}\hat{\zeta}_{l,m} &= \hat{\zeta}(Y^*_{l+4m,k_p} Y_{l+4(m+1),k_p}) \\ &= \frac{N}{8\pi N_s} \times \frac{P\sum_{p=1}^{P} k_p\phi_{l,k_p} - (\sum_{p=1}^{P} k_p)(\sum_{p=1}^{P} \phi_{l,k_p})}{P\sum_{p=1}^{P} k_p^2 - (\sum_{p=1}^{P} k_p)^2} \\ & l = 0, 1, 2, .., L; m = 0, 1, 2, .., M\end{aligned} \tag{4.19}$$

Step 2 Calculate the $\hat{\eta}_l$, which is the second temporary estimation of SFO. It is calculated as slope of $\hat{\zeta}_{l,m}$against m.

$$\begin{aligned}\hat{\eta}_l &= \frac{M\sum_{m=1}^{M} m\hat{\zeta}_{l,m} - (\sum_{m=1}^{M} m)(\sum_{m=1}^{M} \hat{\zeta}_{l,m})}{M\sum_{m=1}^{M} m^2 - (\sum_{m=1}^{M} m)^2} \\ & l = 0, 1, 2, .., L\end{aligned} \tag{4.20}$$

Step 3 Calculate the $\hat{\eta}$ by finding the average of $\hat{\eta}_1$,$\hat{\eta}_2$...$\hat{\eta}_L$

The drawback of this method is the implementation of least-square estimator that produces high complexity because it contains many multiplications and additions. Another drawback is the arctangent processes that are operated in every scattered pilots, resulting in $P = 469$ arctangent calculation processes in every OFDM symbol.

4.3.2 Proposed Sampling Frequency Offset Estimation

SFO, multipath fading channel, and AWGN introduce a phase rotation to the received signal. A phase rotation due to multipath fading is largely eliminated by doing conjugate multiplication between Y^*_{l,k_p} and Y_{l+4,k_p} as presented by (4.17). It leaves a small phase rotation caused by SFO, residue of multipath fading, and AWGN on received signal. In SFO estimation, we consider the phase rotation that is caused by other than SFO as a noise. Since the value of SFO is usually very small (part per millon (ppm) scale), the SFO estimation is very susceptible to a noise. Therefore, the accuracy of estimation really depends on the capability of estimator to eliminate the influence of noise.

In the conventional method, we calculate a phase rotation of every scattered pilot k_p, before doing least square operation to estimate the SFO. Therefore, the phase rotation is actually calculated from the noisy scattered pilots. In proposed method, we modified the step 1 of proposed method. In this method, we perform conjugate multiplication between adjacent pilots to calculate the phase rotation caused by SFO.

$$Z_{l,k_{p+\lambda}} Z^*_{l,k_p} \approx |H_{l,k_p}|^2 |X_{l,k_p}|^2 |H_{l,k_{p+\lambda}}|^2 |X_{l,k_{p+\lambda}}|^2 e^{\frac{j8\pi\Delta k_p \eta N_s}{N}} \tag{4.21}$$

where $\Delta k_p = k_{p+\lambda} - k_p$. To eliminate the influence of a noise, in the proposed method, we perform averaging of the real part and imaginary part of the conjugate multiplication, as presented by (4.22)

$$\hat{\zeta}_{l,m} = \frac{N}{8\pi N_s \Delta k_p (P-\lambda)} \tan^{-1}\left(\frac{\sum_{p=1}^{P-\lambda} Im(Z_{l,k_{p+\lambda}} Z^*_{l,k_p})}{\sum_{p=1}^{P-\lambda} Re(Z_{l,k_{p+\lambda}} Z^*_{l,k_p})}\right) \tag{4.22}$$

By implementing (4.22), we can eliminate the influence of noise in real and imaginary parts of Z_{l,k_p} before estimating the phase rotation using an arctangent. In the proposed method, we also reduce the arctangent process to only 1 arctangent process. It is much fewer compared to P arctangent processes in conventional method. In ISDB-T mode 3 [12], they define $P = 469$.

We can also furtherly eliminate the influence of noise by increasing the value of λ. If we set λ to be higher value, the estimated phase rotation caused by SFO becomes higher, therefore it is less subject to the noise. However, the higher λ also means fewer observation samples, then it also may decrease the accuracy of estimator. In next chapter, we decide the optimum value of λ by simulating the root mean square of an SFO estimation error. We can also increase the estimation accuracy by doing step 2 and step 3 of the conventional method.

4.4 Summary

In this thesis, we have proposed the time and frequency synchronization method for ISDB-T system for HDTV contents transmission in Multipath Fading Channel. ML synchronization method [24], the simplified version [26], and the algorithm complexity between this two algorithm have been reviewed. ML is much complex than the simplified ML, but it gives better performance itself, based on our simulation result. The effect of of a DFT window position error has also been reviewed. Based, on this knowledge, we have proposed DFT window shift to increase the performance of ML based synchronization in Multipath fading channel.

In this thesis, we have also proposed an SFO estimation method for DTTV system in multipath fading channel. Considering the low value of SFO, we have proposed the estimation method that can minimize the influence of noise in SFO estimation. The proposed method also reduces the number of arctangent process for 1 OFDM symbol significantly.

Chapter 5

Simulation and Analysis

5.1 Channel Estimation Simulation

5.1.1 Simulation Parameter

In order to confirm the performance of the proposed channel estimation method, we conducted computer simulation to simulate mean square error (MSE) and bit error rate (BER) performance. We compared the performance of the three method that we discussed in chap. 3, i.e. the proposed 3-point diagonal averaging method, conventional method [16], and 2-point averaging method [22]. For a channel model, we used the Typical Urban 6 path channel (TU6) that was defined by COST 207 [28]. The power delay profile of this channel model is described in table 5.1. This channel model reproduces the terrestrial propagation in an urban area. The complete parameters of simulation are shown in table 5.2.

We conducted the simulation within very high speed mobile environment $v = 240$ [km/h] and $v = 360$ [km/h] in order to prove the robustness of the proposed system in high speed train environment(commercial speed ≈ 300 [km/h]). On other hand, in order to check the performance of fixed DVB-T2 system, we also conducted simulation in fixed condition ($v = 0$ [km/h]). The maximum doppler frequency is derived based on (5.1).

$$F_d = \frac{F_c}{c} v \tag{5.1}$$

where F_d, F_c, c, and v are maximum doppler frequency [Hz], carrier frequency [Hz], speed of light (3×10^8) [m/s], and mobile velocity [km/h], respectively. In this simulation, the carrier frequency used is 470 [MHz] - the lowest UHF carrier used in DVB-T2.

Table 5.1: Typical Urban Power and Delay Profile (TU6) [28]

Tap number	1	2	3	4	5	6
Delay (μs)	0.0	0.2	0.5	1.6	2.3	5.0
Power (dB)	-3	0	-2	-6	-8	-10

Table 5.2: Simulation Parameter

Modulation	QAM-64
Bandwidth	8 MHz ($T_s = 7/64\mu s$)
FFT size	2K
GI length	1/ 8
Channel model	COST207 TU6 [28]
Channel encoding/decoding	No
Maximum doppler frequency	0Hz (0 [km/h]),104 Hz(240 [km/h]), 156Hz(360 [km/h])
Carrier frequency	470 MHz
Pilot pattern	PP1(MISO)

Applying a doppler frequency F_d = 104 [Hz] corresponds to a v = 240 [km/h]. In the same manner, doppler frequency F_d = 156 [Hz] corresponds to a v = 360 [km/h]

As the interpolation filter, we utilized a 2D non-rectangular spectrum filter which the performance was confirmed to be better than the conventional 2×1D FIR LPF in previous work result [9].

5.1.2 MSE and BER Simulator Block Diagram

As shown by table 5.2, we employ the OFDM based DVB-T2 system without channel encoding/decoding. The complete description of the MSE BER simulator is shown by Fig. 5.1. The system consists of two transmit antenna with J receive antenna. The binary data are first mapped according to the modulation that is used by the signal mapper. Then, the mapped data are processed by the MIMO encoder to generate input for each transmitter antenna. After that, the reference pilots are inserted into the data. The reference pilot will be further utilized to conduct the channel estimation, especially the scattered pilots.

An OFDM baseband symbol is generated by modulating complex data using the inverse fast fourier transform (IFFT). In order to prevent inter symbol interference (ISI), guard interval (GI) which is chosen to be larger than delay spread is inserted at the beginning of each symbol. The symbol is then transmitted through multipath fading channel. The receiver consists of a complementary process of transmitter, in order to recover the transmitted information.

The mean squared error (MSE) of channel estimation is calculated by comparing the estimated channel value with the real channel value produced by channel generator, as shown by Fig. 5.1. The bit error rate (BER) is calculated by comparing the binary data input of mapper in transmitter with binary data output of demapper in receiver.

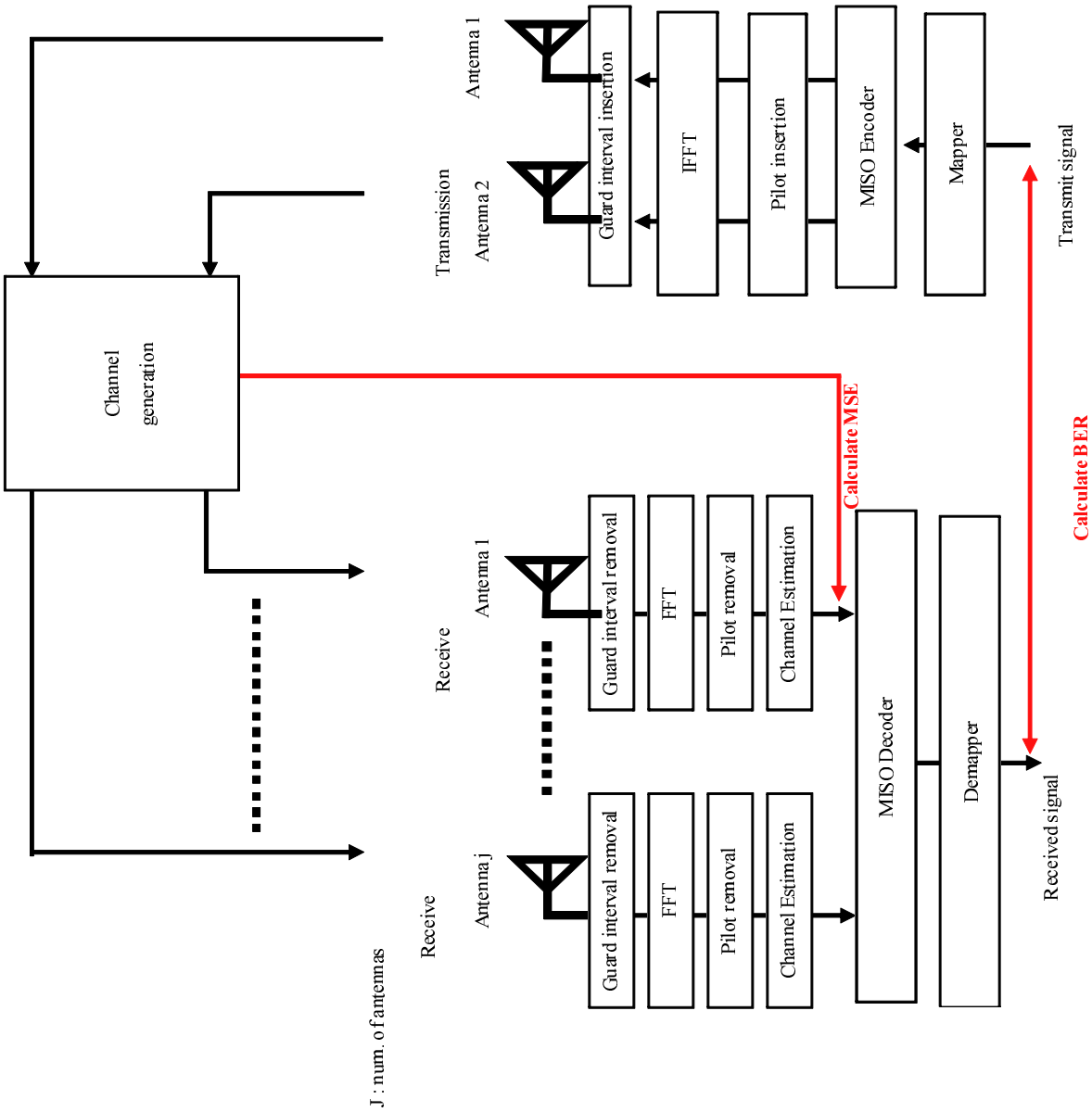

Figure 5.1: MSE BER Simulator for DVB-T2 System

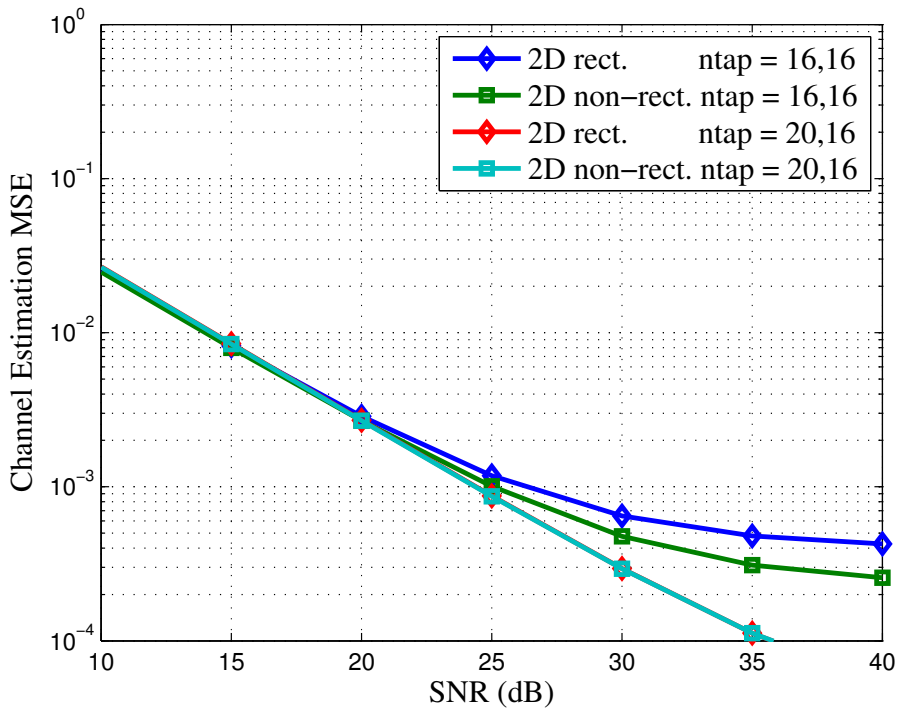

Figure 5.2: MSE vs SNR for SISO 1×1 case with $f_d = 0$ Hz (0 [km/h])

5.1.3 Performance Analysis of a 2D Non-rectangular Filter

SISO case

Fig.5.2-5.10 show the MSE vs SNR performance of the channel estimation methods. The MSE is defined as the mean squared difference between the channel frequency responses of transmitter channel $H_{ij,k,l}$ and the estimated channel frequency responses $\hat{H}_{ij,k,l}$. It is given by (5.4)

$$\hat{H}_{ij,k,l} = [|H_{ij,k,l} - \hat{H}_{ij,k,l}|^2] \tag{5.2}$$

where $H_{ij,k,l}$ is the channel value from i-th transmitter to j-th receiver in k-th subcarrier and l-th OFDM symbol.

In this simulation we have compared the performance of 2D non-rectangular filter with 2D rectangular filter. From the simulation results, for the implementation of number of taps = 20,16 means 20 taps for filtering in time-direction and 16 taps for filtering in frequency-direction. Based on the simulation results, we can see that for number of taps = 20,16 the difference between 2D non-rectangular filter and 2D rectangular filter is not really significant. The difference is getting significant at number of taps = 16, 16. From this simulation, for 1×1 SISO case, we can conclude that the 2D non-rectangular filter can perform much better compared to the 2D rectangular filter especially in lower number of taps.

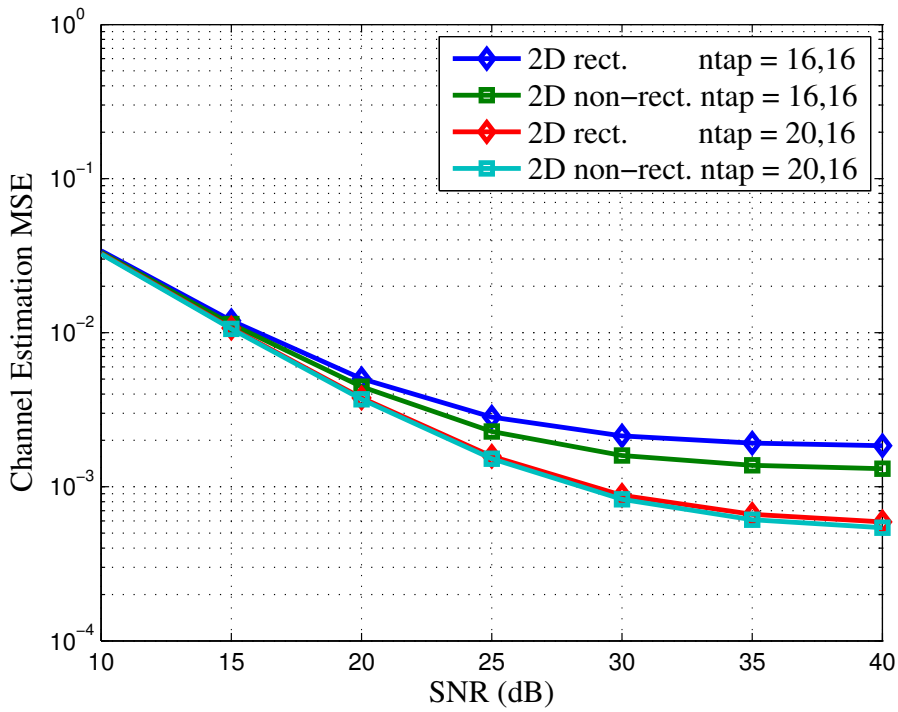

Figure 5.3: MSE vs SNR for SISO 1×1 case with f_d = 104 Hz (240 [km/h])

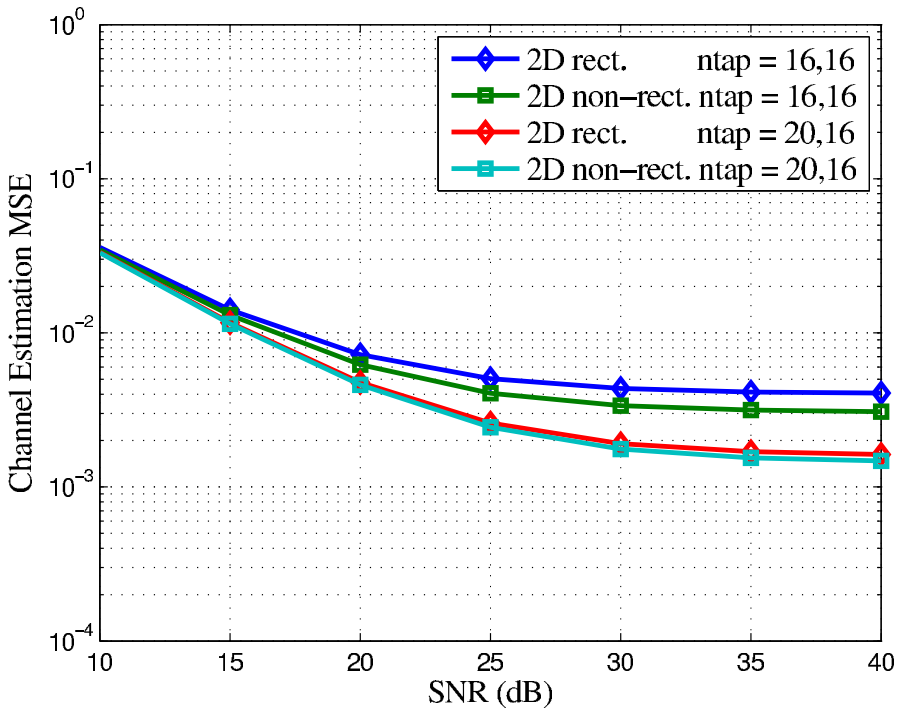

Figure 5.4: MSE vs SNR for SISO 1×1 case with f_d = 156 Hz (360 [km/h])

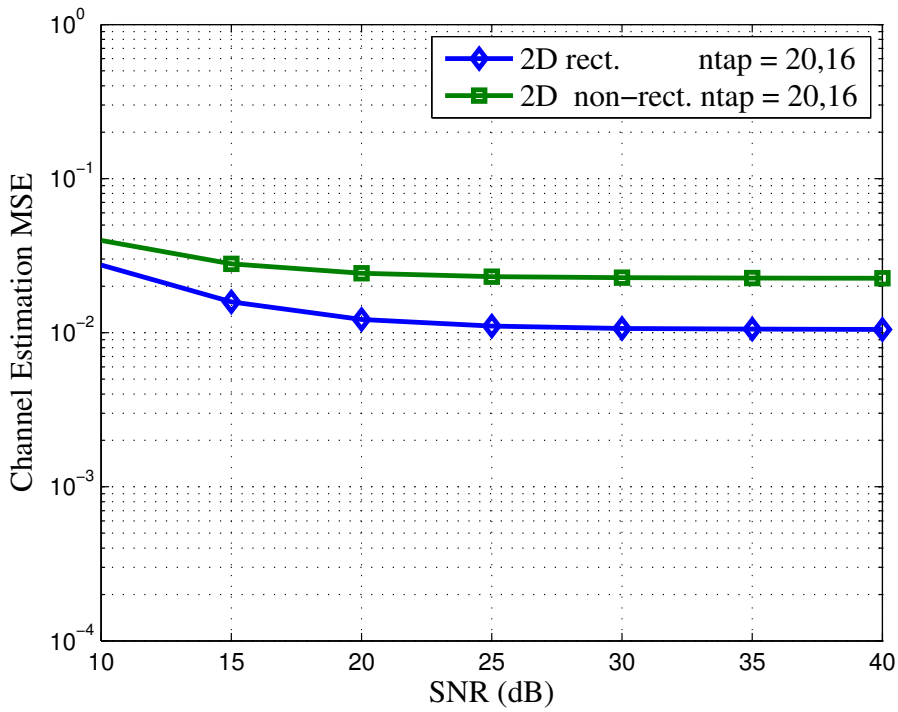

Figure 5.5: MSE vs SNR for MISO 2×1 case with the Conventional Method [16] at f_d = 0 Hz (0 [km/h])

A 2×1 MISO with the Conventional Method [16]

In this simulation we have compared the performance of 2D non-rectangular filter with 2D rectangular filter at 2×1 MISO system with conventional method [16]. It turns out for this case, both filter perform very bad at number of taps = 20,16. It is caused by the larger distance between scattered pilot along frequency direction that makes the low number of taps filter that we use in this implementation is not enough to get the optimal performance. In this case, we can also notice that the performance of 2D non-rectangular is worse than the 2D rectangular.

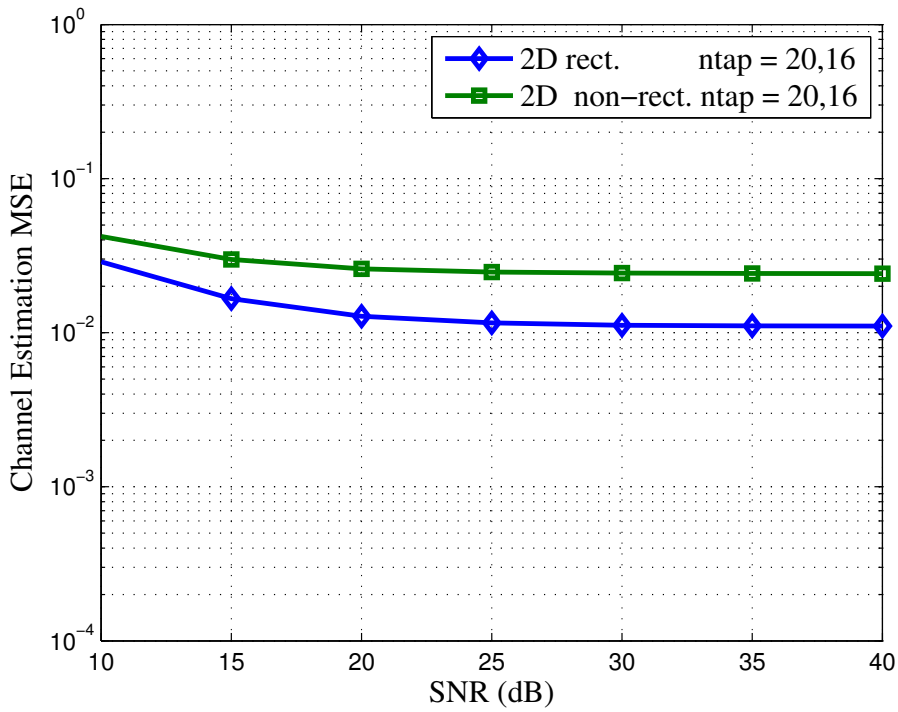

Figure 5.6: MSE vs SNR for MISO 2×1 case with the Conventional Method [16] at f_d = 104 Hz (240 [km/h])

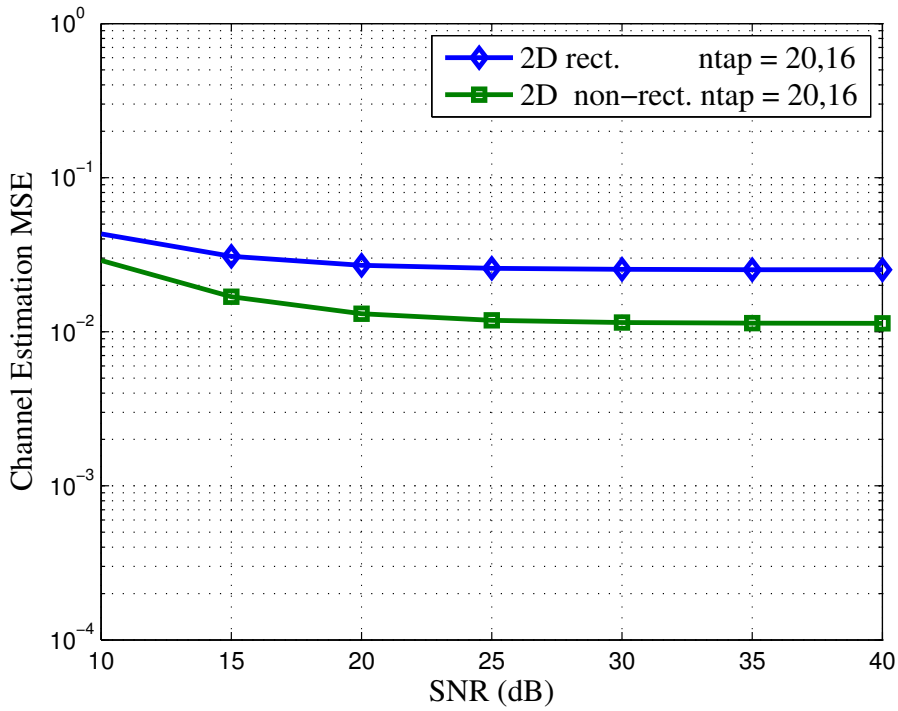

Figure 5.7: MSE vs SNR for MISO 2×1 case with the Conventional Method [16] at f_d = 156 Hz (360 [km/h])

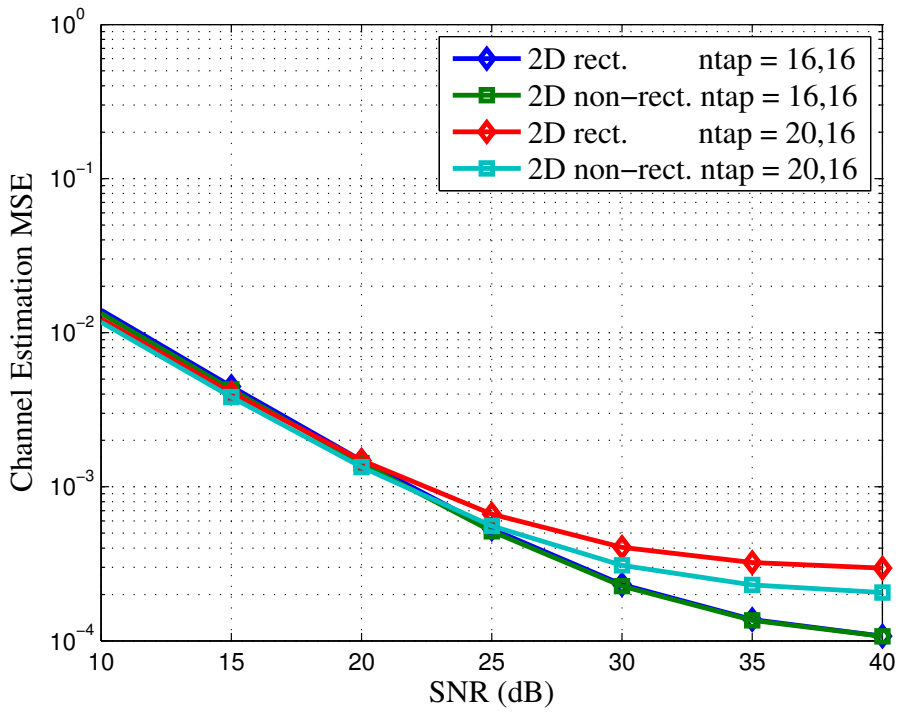

Figure 5.8: MSE vs SNR for MISO 2×1 case with the Proposed 3-Point Averaging at f_d = 0 Hz (0 [km/h])

A 2×1 MISO with the Proposed 3-Point Averaging Method

Since a 2×1 MISO case with the conventional method [16] doesn't perform very well, in this simulation we have compared the performance of 2D non-rectangular filter with 2D rectangular filter at 2×1 MISO system with the proposed 3-point diagonal averaging method. It turns out the characteristic of performance of both filter in this case resembles the performance at 1×1 SISO case. Based on the simulation results, we can see that for number of taps = 20,16 the difference between 2D non-rectangular filter and 2D rectangular filter is not really significant. The difference is getting significant at number of taps = 16, 16. From this simulation, for 2×1 MISO case with the proposed 3-point diagonal method, we can conclude that the 2D non-rectangular filter can perform much better compared to the 2D rectangular filter especially in lower number of taps.

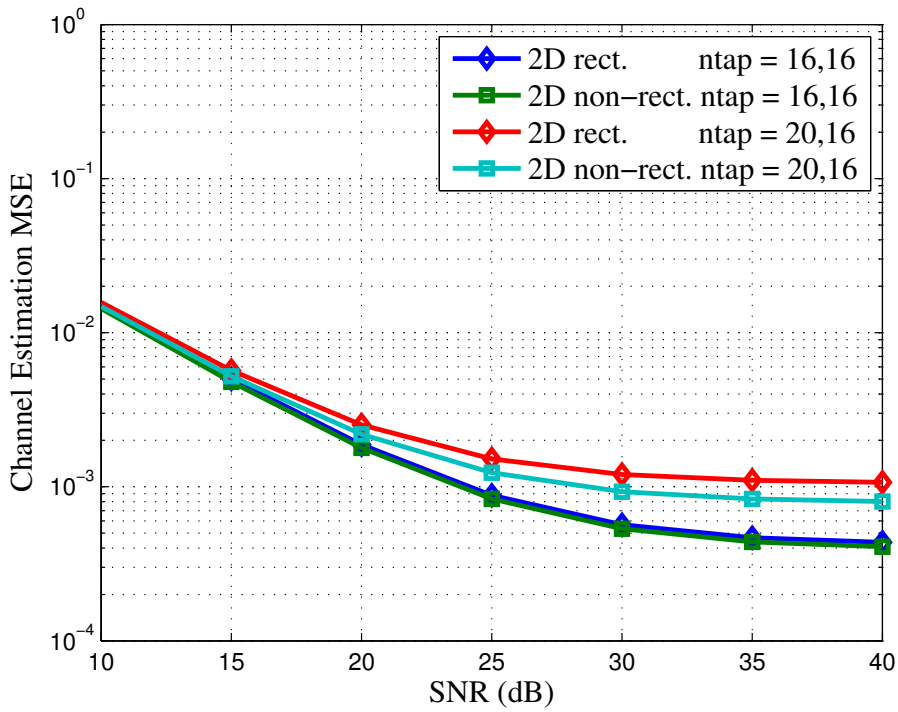

Figure 5.9: MSE vs SNR for MISO 2×1 case with the Proposed 3-Point Averaging at f_d = 104 Hz (240 [km/h])

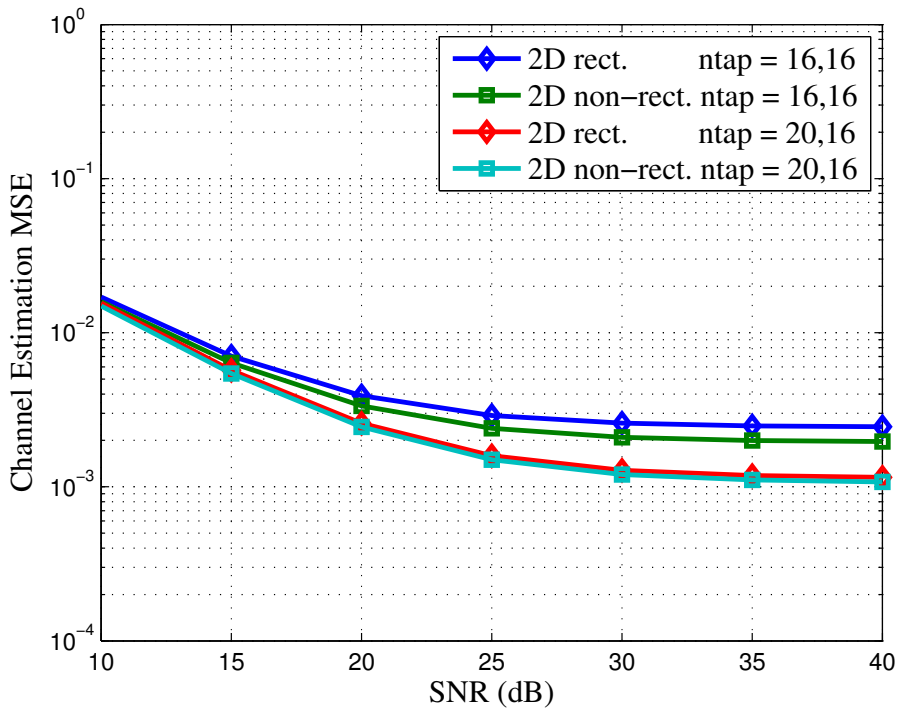

Figure 5.10: MSE vs SNR for MISO 2×1 case with the Proposed 3-Point Averaging atf_d = 156 Hz (360 [km/h])

5.1.4 Performance Analysis of The Proposed 3-Point Averaging

The MSE Performance

We compared the performance of the three method that we discussed in chap.4, i.e. the proposed 3-point diagonal averaging method, conventional method [16], and conventional 2-point averaging method [22] in a 2×1 MISO system. We also compared the performance of more than 3-point averaging (4-point and 5-point averaging) to confirm the most effective points number of averaging. We have simulated some combinations of coefficients for 4-point and 5-point case. We pick the best results of them to be compared with the 3-point averaging result. More detail explanation about 4 and 5 point averaging is given in chap. 7. Fig.5.11 shows that the proposed 3-point diagonal averaging method outperforms the conventional and the 2-point averaging. The 3-point diagonal averaging method also outperforms the 4 and 5-point averaging. It means 3-point is the most effective averaging points number for this condition. In this case, 2-point is not sufficient to provides enough accuracy of estimation. On the other hand, 4-point and 5-point averaging also provides less accuracy of averaging due to the variation of channel along time and frequency domain.

The BER Performance

Fig.5.13- Fig.5.15 show the BER vs SNR performance of the channel estimation methods. In this simulation results, the result of a 1×1 SISO, a 2×1 MISO, a 2×2 MIMO, and a 2×4 MIMO are included to verify if the proposed channel estimation can optimize a diversity gain that is provided by Alamouti scheme in a 2×2 MISO system. Based on the simulation results, The proposed 3-points diagonal averaging method is very effective in optimizing the diversity gain provided by the Alamouti scheme.

First, we evaluate the performance of the proposed channel estimation method in optimizing the diversity gain provided by transmitter diversity. In this case, we compare BER performance between a 2×1 MISO system estimated by the proposed method with an SISO system estimated by the conventional SISO channel estimation. For v = 0 [km/h], the proposed method can give SNR improvement around 2.5 dB for a 2×1 MISO at uncoded BER= 2×10^{-2} compared to an SISO with conventional channel estimation. For v = 240 [km/h]The proposed method can give SNR improvement around 3 dB for a 2×1 MISO at uncoded BER= 2×10^{-2} compared to an SISO with conventional channel estimation. At last, for v = 360 [km/h]The proposed method can give SNR improvement around 7 dB for a 2×1 MISO at uncoded BER= 2×10^{-2} compared to an SISO with conventional channel estimation. It means the proposed method can optimize the diversity gain provided by transmitter diversity, i.e. Alamouti scheme and the gain is only getting larger in higher doppler frequency.

Then, we evaluate the performance of the proposed channel estimation method in optimizing the diversity gain provided by receiver diversity. For v = 0 [km/h], the proposed method can give SNR improvement around 3 dB for a 2×4 MIMO at uncoded BER= 2×10^{-3} compared to a 2×2 MIMO with the same method. For v = 240 [km/h]The

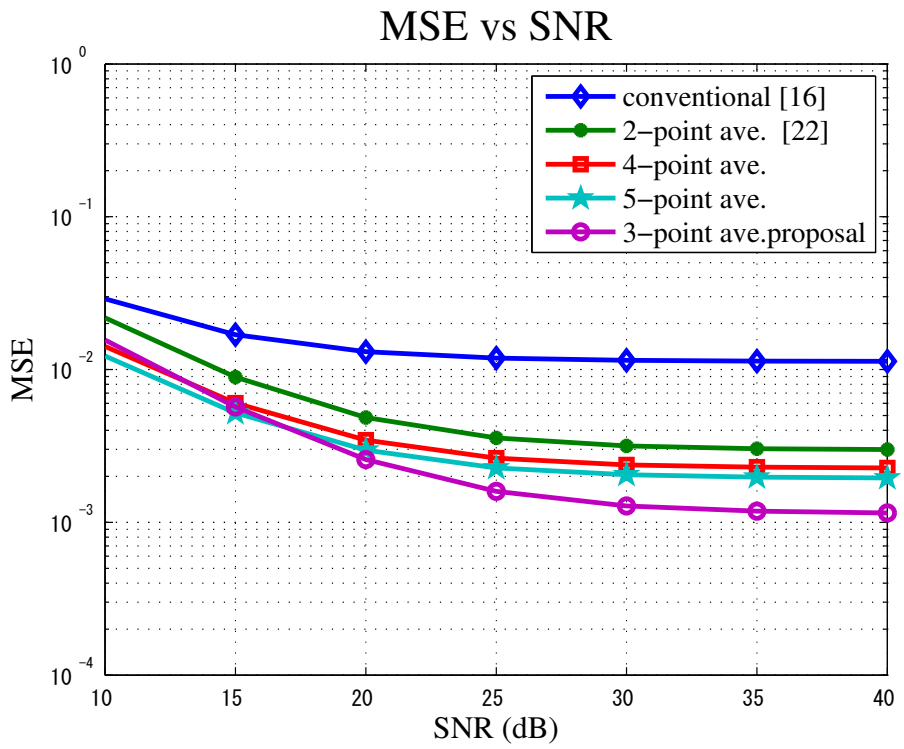

Figure 5.11: MSE vs SNR for f_d = 156 Hz (360 [km/h])

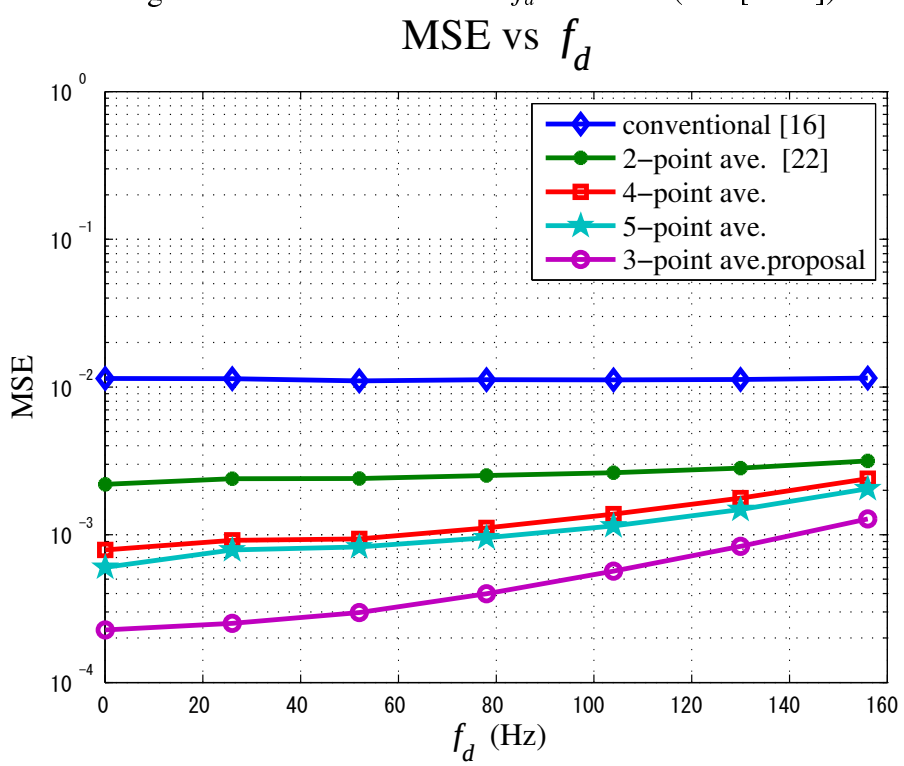

Figure 5.12: MSE vs f_d for SNR = 30 dB

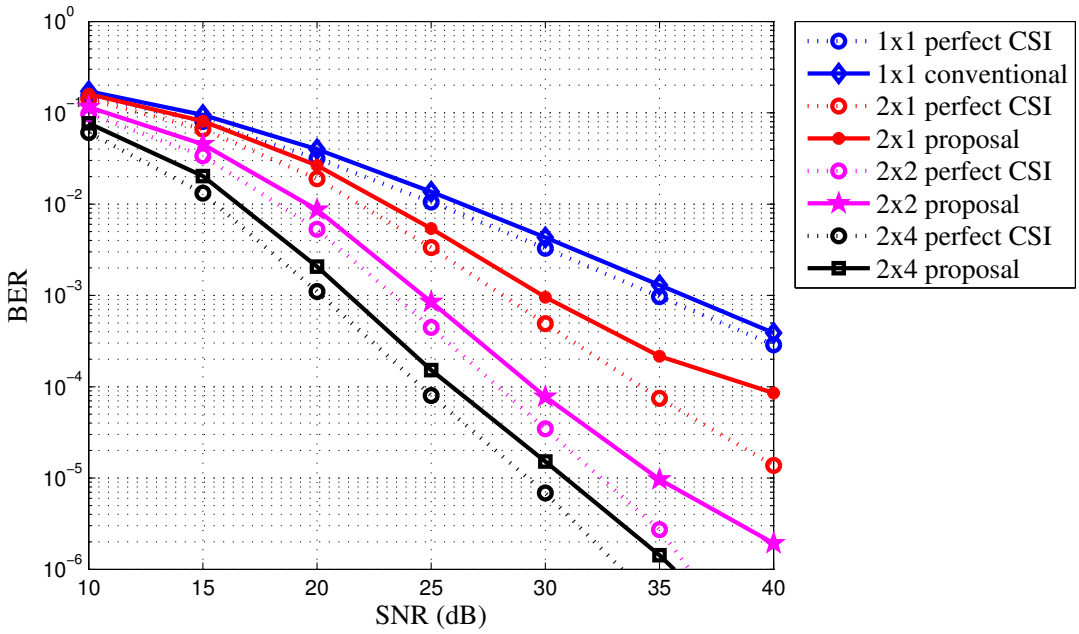

Figure 5.13: BER vs SNR for f_d = 0 Hz (0 [km/h])

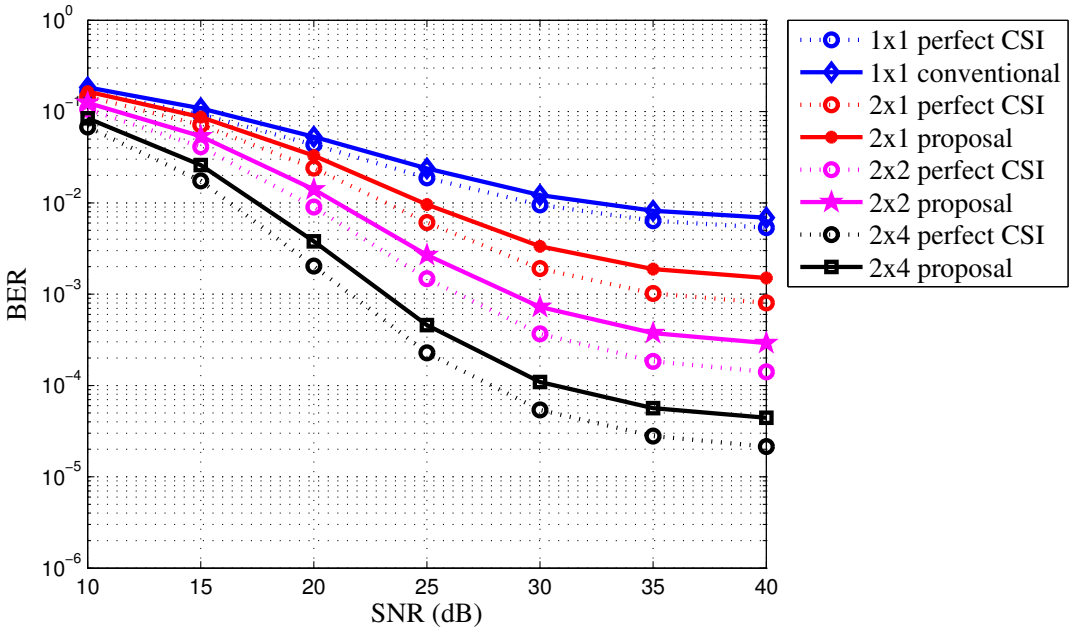

Figure 5.14: BER vs SNR for f_d = 104 Hz (240 [km/h])

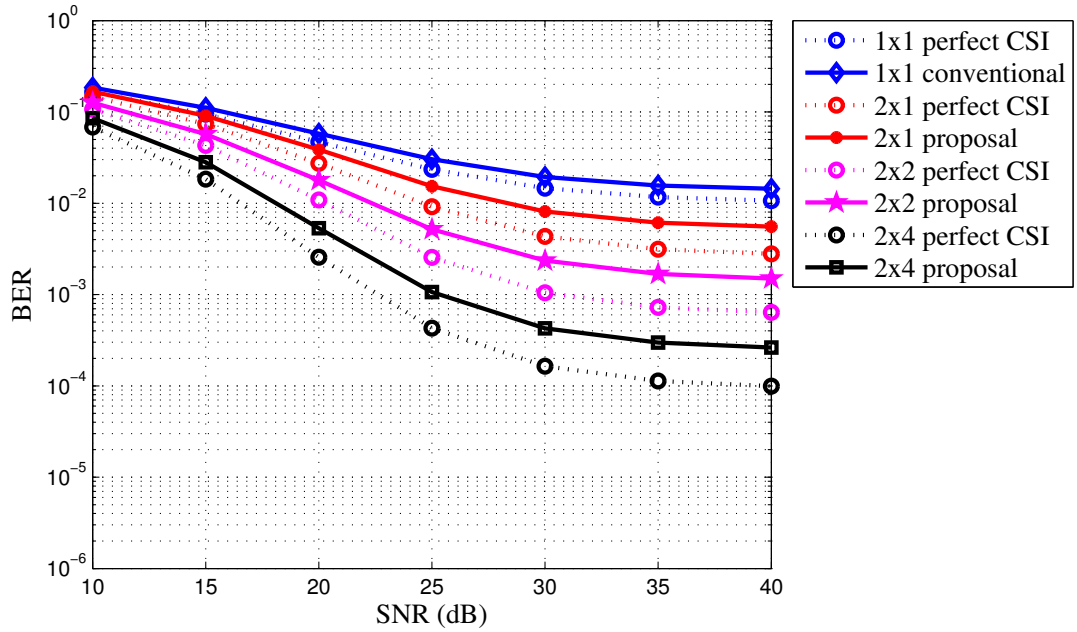

Figure 5.15: BER vs SNR for f_d = 156 Hz (360 [km/h])

proposed method can give SNR improvement around 5 dB for a 2×4 MIMO at uncoded BER= 2×10^{-3} compared to a 2×2 MIMO with the proposed method. For v = 360 [km/h]The proposed method can give SNR improvement around 8 dB for a 2×4 MIMO at uncoded BER= 2×10^{-3} compared to a 2×2 MIMO with a proposed method. It means the proposed method can optimize the diversity gain provided by receiver diversity scheme, i.e. MRC and the gain is only getting larger in higher doppler frequency. The proposed method perfomance also close to the performance of system with ideal channel knowledge (perfect CSI).

5.1.5 Complexity Analysis of The Proposed 3-Point Averaging

In this section we perform a complexity comparison among the three method that we discussed in sec.3.3, i.e. the proposed 3-point diagonal averaging method, conventional method [16], and 2-point averaging method [22] in a 2×1 MISO system. We also included the complexity of 4-point and 5-point averaging as a comparison. As an interpolation filter, we utilized a two-stages implementation of a non-rectangular 2D filter. Fig.5.16 shows that the conventional method [16] with number of taps = 20,32 (20 taps in time direction and 32 taps in frequency direction) can achieve the same performance with the proposed 3-point diagonal averaging method with number of taps = 20,16. On the other hand, the 2-point averaging method [22] achieve the maximum performance at number of taps = 20,32. The 2-point averaging method [22] still could not match the

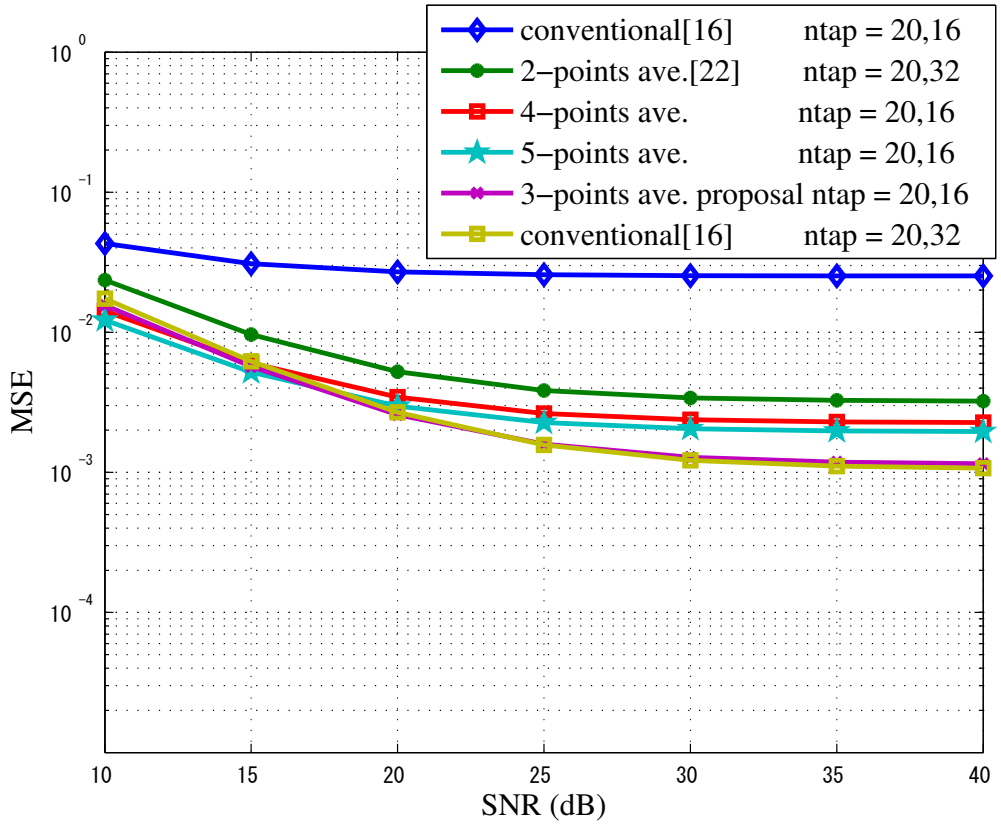

Figure 5.16: Performance comparison with different number of filter taps

performance of the proposed method eventhough it is implemented with 32 taps in frequency direction. It means the 2-point averaging is not robust for rapidly time-varying channel.

Therefore we compare the architecture of each system with their maximum performance, i.e. conventional method [16] with number of taps = 20,32; 2-point averaging method with number of taps = 20,32; proposed method 3-point averaging, 4-point, and also 5-point averaging with number of taps = 20,16. The result is shown in table 5.3.

Based on data shown by table 5.3, eventhough proposal 3-point diagonal averaging method contains the the largest number of addition in averaging process, but it can reduce the number of additions and multiplications in 2D interpolation process. Totally, it can reduces the number of additions and multiplications around 50% compared to the implementation of the conventional method [16] and 2-point averaging method [22]. The 3-point averaging also contains 33% and 50% less number of additions in averaging process, compared to 4-point and 5-point averaging, respectively. Based on this result, we can conclude that our solution, i.e. 3-point averaging is more efficient than increasing number of filter taps of conventional method in terms of complexity. On other hand, the 3-point averaging is also the most efficient averaging interpolation method

Table 5.3: Complexity Comparison

Method	Averaging	2D Interpolation	
	Number of addition per 1 OFDM symbol	Number of addition per 1 OFDM symbol	Number of multiplication per 1 OFDM symbol
Conventional [16]	0	51957	53568
2-point ave. [22]	569	51957	53568
Proposal 3-point ave.	1138	25381	27040
4-point ave.	1707	25381	27040
5-point ave.	2276	25381	27040

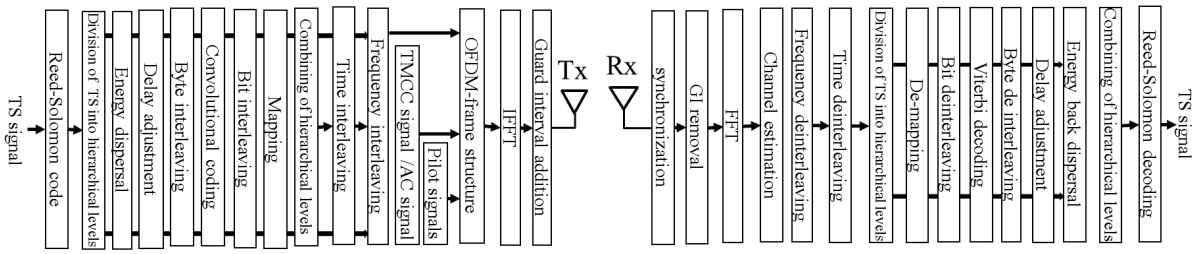

Figure 5.17: ISDB-T Simulator Block Diagram

compared to the 2-point, 4-point, and 5-point averaging.

5.2 Synchronization Method Simulation

5.2.1 Symbol-Timing and Carrier Frequency Synchronization Simulation

Simulation Parameter

We have done the simulation with the Integrated System Digital Broadcasting-Terrestrial (ISDB-T) system , a digital terrestrial television standard developed by Japan. The block diagram of simulator is shown by Fig. 5.17. In this simulation, We use mode 3 of ISDB-T transmission mode. ISDB-T introduces three transmission mode according to the space between carrier frequencies width. Mode 3 introduces 1 KHz subcarrier spacing (0.99206 KHz) width and number of carrier per symbol is 5617 carrier. The DFT size is 8192 and we use guard interval ratio = $1/8(1/8 * 8192 = 1024)$. Complete simulation system parameter is shown in table 5.4 . Similar to channel estimation simulation, for a channel model, we used the Typical Urban 6 path channel (TU6) that was defined by COST 207 [28]. For the error synchronization, We make the model of synchronization error according to (5.3)

$$r(n) = s(n - \theta)e^{j2\pi\varepsilon n} \tag{5.3}$$

Table 5.4: Simulation Parameter

Spacing between carrier frequencies	0.99206 KHz
Number of carrier per symbol	5617 carrier
FFT size	8K (8192)
GI length	1/ 8
Modulation	QAM-64
Convolutional code	3/4
Effective symbol length	1.008 ms

Table 5.5: Channel and Synchronization Error Parameter

Multipath Channel Model	TU6 channel
Fading	Rayleigh block fading
Time offset(θ)	1500 samples
Normalized CFO(ε)	0.3(300 [Hz] CFO)

$r(n)$, $s(n-\theta), \theta$, and ε are received signal in time instants n, transmitted signal in time instant n delayed by θ sample , time offset [sample], and normalized CFO [Hz], respectively. According to CFO explanation in section II, We know that only less than 0.5 subcarrier spacing = ± 500 Hz frequency shift that can be detected by the algorithm. Therefore, We choose 300 Hz as the CFO value (normalized by subcarrier spacing value, 1 KHz,it becomes ε =0.3). Complete channel model and synchronization error parameter is shown in table 5.5.

Simulation Results

In this section, We present simulation results for synchronization system performance in receiving HDTV contents in Multipath Fading environment. Firstly we simulate the performance comparison of symbol timing estimation using Maximum Likelihood and Simplified Maximum Likelihood algorithm as shown in Fig. 4.7 in chap. 4. The performance of Maximum Likelihood is only slightly better than the simplified Maximum Likelihood. Secondly, We simulate the perfomance comparison of CFO estimation between both algorithms by comparing RMS (Root Mean Squared) Error of CFO estimation from both algorithm. RMS error of CFO estimation means the root mean squared difference between detected CFO and actual CFO. Fig. 5.18 shows that the performance of ML is better than the simplified ML in in estimating CFO, especially in higher SNR. Therefore, based on the Mean Symbol Timing Estimation error and RMS CFO simulation, we can conclude that the performance of ML is better than Simplified ML.

Secondly, we simulate BER performance of proposed method. First, We look for the appropriate backward shift value for our system. As we know, since we need to put the DFT window starting from any points inside Guard Interval, so we will move the DFT window backward from the previous detected position. In order to know how many

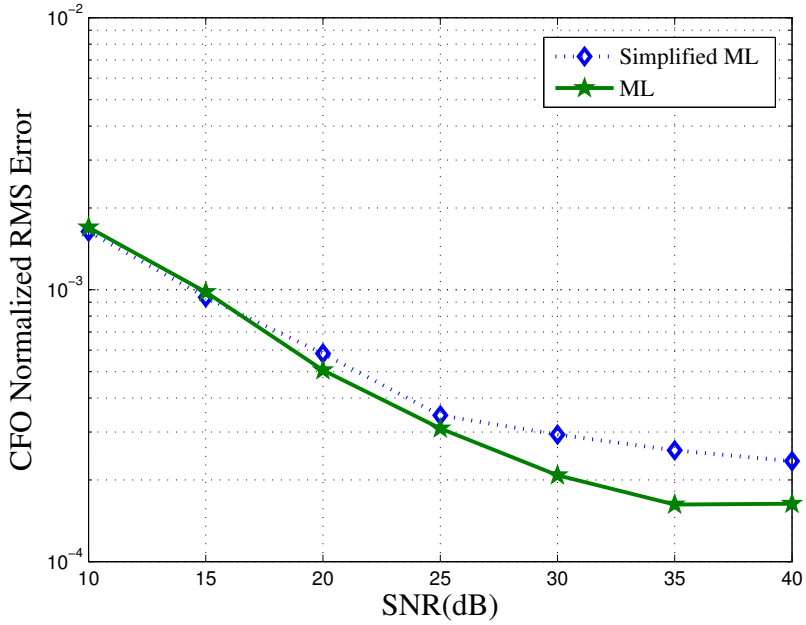

Figure 5.18: Root Mean Square of Normalized CFO Estimation Error)

shift that we need to get the the best BER result, we need to consider about the value of Cyclic Prefix and maximum delay spread. From system simulation parameter shown by table 5.4 and channel model delay characteristic shown by table 5.1, we know that the cyclic prefix size is 1024 and maximum delay spread is 5μs (41 time sample). ISI can be removed if $T_p = T_g/2$ is set for all transmission mode combinations in ISDB-T, except for mode 1 with GI mode 1/32 (GI length = 7.875μs). In this simulation, since $T_g = 1024$, then $T_p = 512$. In this simulation, we want to compare the performance of conventional Maximum Likelihood based Synchronization and Maximum Likelihood based Synchronization equipped with DFT window shift. As a comparison, we also plot the BER performance of system in perfect synchronization mode, which means the mode where the time offset and CFO can be perfectly detected and recovered

Fig. 5.19 shows that the simplified Maximum Likelihood itself could not produce a good BER performance. It happens because the timing estimation shows the positive value as shown in Fig. 4.7 in chap. 4 that makes the received signal contains ISI. On the other hand, the combination between Simplified Maximum Likelihood and proposed DFT window shift produce good BER performance, which is almost close to the performance of perfect synchronization.

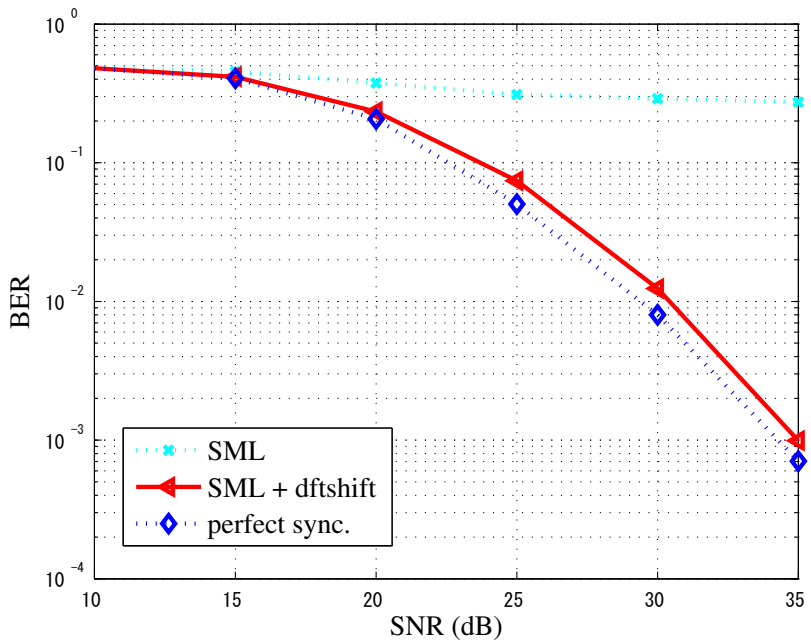

Figure 5.19: BER vs SNR in Rayleigh Channel)

5.2.2 Sampling-Frequency Synchronization Simulation

Simulation parameter

In order to compare the performance of conventional method and proposed method, we conducted computer simulations by implementing ISDB-T system mode 3 [12]. For a channel model, we utilized the Typical Urban 6 path channel (TU6) that was defined by COST 207 [28]. The power delay profile of this channel model is shown in table 5.1. This channel model reproduces the terrestrial propagation in an urban area. The complete parameters of simulation are shown in table 5.6. In this simulation, we also included the timing offset and carrier frequency offset (CFO). The estimation and compensation of symbol-timing and carrier-frequency offset is implemented based on the autocorrelation function of time-domain received signal and the dftshift method. To implement the arctangent process, we employ cordic based arctangent with 16 iteration.

λ decision

We conduct a simulation to calculate the value of λ that can maximize the performance of the proposed method. In this simulation, we decide the value of λ by simulating the root mean square (RMS) of estimation error, as presented as follow

$$\mathrm{RMS}(\hat{\eta}) = \sqrt{E[(\eta - \hat{\eta})^2]} \tag{5.4}$$

Table 5.6: Simulation Parameter

Mode	Mode 3
Modulation	QAM-64 (12seg) QPSK(1seg)
Convolutional code	3/4(12seg) 2/3(1seg)
Bandwidth	8 MHz (T_s = 7/64μs)
FFT size	8K
GI length	1/ 8
Channel model	COST207 TU6 [28]
Carrier frequency	470 MHz
SFO	10 ppm
Time offset	5000 sample
Carrier Freq. Offset	300 Hz

where η and $\hat{\eta}$ are the SFO and the estimation of SFO, respectively. As shown by Fig. 5.20, λ = 135 shows the smallest RMS of estimation error, while the larger λ make the estimation accuracy become worse because of less observation sample. Using λ = 135, the estimation method can achieve RMS SFO =2×10^{-2} ppm in SNR=35 dB. For performance comparison, we use the best λ for the proposed method.

Performance comparison

In this subsection, we compare the performance of conventional method [27] and proposed method. We conducted bit-error rate (BER) simulations to compare the performance of conventional and proposed method. For 1 OFDM symbol observation (L=1,M=1), the proposed method can produce performance gain around 7 dB at BER= 3×10^{-2} compared to conventional method. The performance of conventional method can be improved by utilizing more OFDM symbols. Based on our simulation, the conventional method can achieve the similar performance with proposed method by employing 10 OFDM symbols (L=2, M=5).

We also verify the performance of proposed method in different value of SFO. Considering the low value of SFO, we simulated the performance of conventional method and proposed method in SFO = 1-30 ppm with SNR = 35 dB. This simulation result is shown by Fig. 5.22. Fig. 5.22 shows that the estimation using proposed and conventional method remain constant in selected range of SFO. In this result, we can also confirm that the conventional method can achieve the similar performance with proposed method by employing 10 OFDM symbols (L=2, M=5).

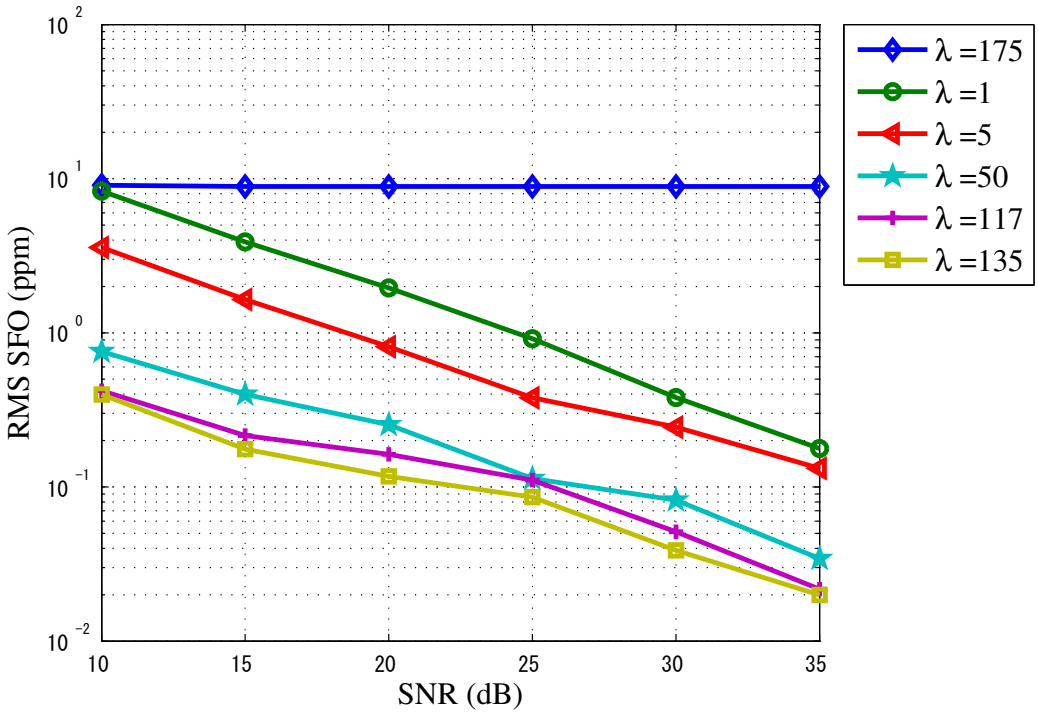

Figure 5.20: λ value decision for proposed method based on root mean square of error simulation

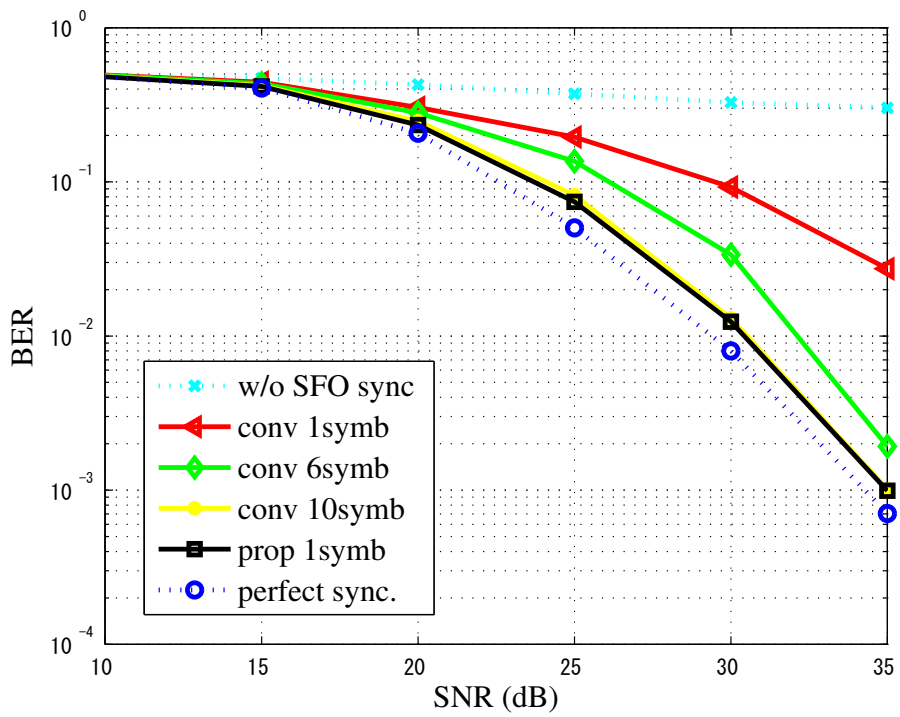

Figure 5.21: BER vs SNR performance

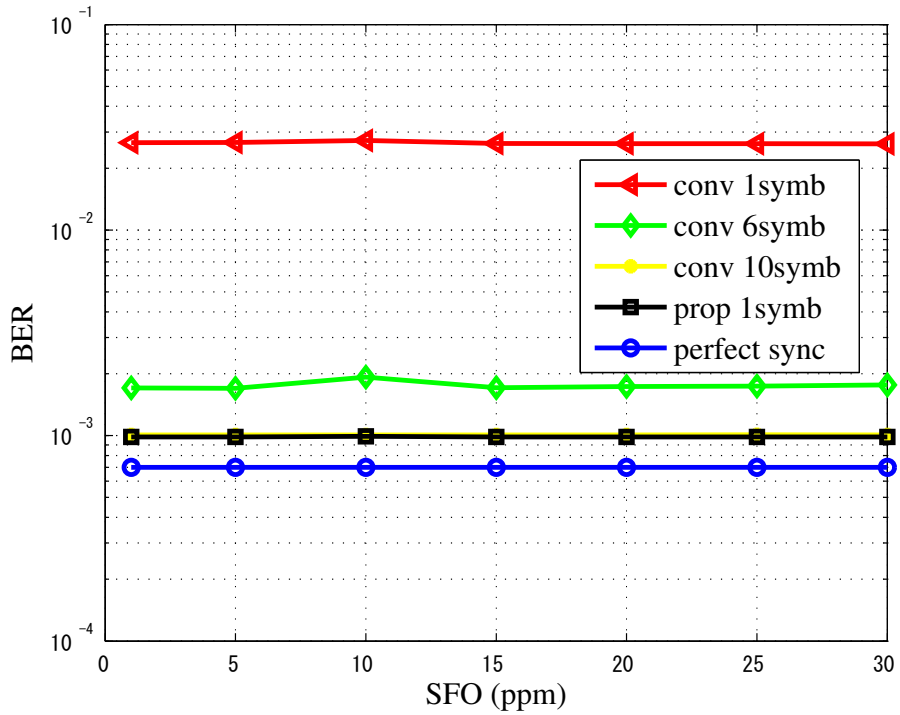

Figure 5.22: BER vs SFO performance

Complexity calculation

In this section,we compare the implementation complexity among the conventional method and the proposed method. In order to make the fair comparison of the implementation complexity of both method, firstly we need to separate the constant from (4.19). After simplification, we can implement (4.19) as shown by (5.5)

$$\hat{\zeta}_{l,m} = C_{11} \times \left[P \sum_{p=1}^{P} k_p \phi_{l,k_p} - C_{21} (\sum_{p=1}^{P} \phi_{l,k_p}) \right] \tag{5.5}$$

where C_{11} and C_{21} are constants that can be stored in the memory. Both constants are defined as follow

$$C_{11} = \frac{N}{8\pi N_s (P \sum_{p=1}^{P} k_p^2 - (\sum_{p=1}^{P} k_p)^2)} \tag{5.6}$$

$$C_{21} = \sum_{p=1}^{P} k_p \tag{5.7}$$

Table 5.7: Algorithm complexity comparison

Method	eq.	Multiplier		Adder	
Conventional [27] (L=2, M=5)	(4.17)	$4P\times L\times M$	23488	$2P\times L\times M$	146327
	(4.18)	-		$48P\times L\times M$	
	(5.5)	$(P+3)\times L\times M$		$(2P-1)\times L\times M$	
	(5.8)	$M+3$		$2M-1$	
Proposed (L=1,M=1, λ = 135)	(4.17)	$4(P-\lambda)\times L\times M$	2673	$2(P-\lambda)\times L\times M$	2050
	(4.22)	$(4(P-\lambda)+1)\times L\times M$		$(4(P-\lambda)+46)\times L\times M$	

While (4.20) can be simplified as follow

$$\hat{\eta}_l = C_{12} \times \left[M \sum_{m=1}^{M} m\hat{\zeta}_{l,m} - C_{22}(\sum_{m=1}^{M} \hat{\zeta}_{l,m}) \right] \tag{5.8}$$

where C_{12} and C_{22} are defined by (5.9) and (5.10), respectively.

$$C_{12} = 1 \Big/ \left(M \sum_{m=1}^{M} m^2 - (\sum_{m=1}^{M} m)^2 \right) \tag{5.9}$$

$$C_{22} = \sum_{m=1}^{M} m \tag{5.10}$$

In this manner, we can make a fair complexity comparison between the conventional and proposed method.

Generally, the complexity comparison is described in table 5.7. In this comparison, we consider the 16 iteration of cordic for arctangent in our implementation. 16 iteration of 1 cordic process contains 48 adders. Since the conventional method using 10 symbols achieves the similar performance with proposed method using 1 OFDM symbols, then in the comparison we compare the complexity between both conditions. From table 5.7, we can see that in order to produce similar performance, the proposed method produces much lower computational complexity. The proposed method can reduce number of multiplier around 90% and adder around 99% compared to the conventional method. The number of adder reduces drastically because the proposed method only employ 1 arctangent process per OFDM symbol, compared to conventional method that employs P = 469 arctangent processes per OFDM symbols.

5.3 Summary

In this chapter, I have shown the simulation results to confirm the peformance of the proposed method in channel estimation and synchronization. In sec. 5.1, I have shown the simulation results of my proposed channel estimation. Firstly, we simulated the performance of interpolation filter that we utilize, i.e. a 2D non-rectangular filter. We utilized

the two-stages implementation of a 2D filter with nonrectangular spectrum. Based on the simulation results, it is shown that the performance of 2D non-rectangular filter is better than 2D rectangular filter, especially in lower number of taps.

Secondly, we show the performance of the proposed 3-point diagonal averaging method. Based on the MSE simulation results, the proposed methods can give SNR improvement until 12 dB at MSE = 3×10^{-3} compared to the 2-points averaging [22] for receiver with v = 360 [km/h].

Since the conventional method shows the worst performance among three methods, we can confirm the importance of the averaging method to increase the performance of system by shortening the distance between reference pilot along frequency direction before interpolation in a MIMO channel estimation.

On the other hand, we have also done the BER simulation to prove the performance of the proposed channel estimation method in optimizing the diversity gain provided by Alamouti scheme and maximal-ratio combining scheme. First, we have evaluated the performance of the proposed channel estimation method in optimizing the diversity gain provided by transmitter diversity. For v = 360 [km/h], The proposed method can give SNR improvement around 7 dB for a 2×1 MISO at uncoded BER= 2×10^{-2} compared to an SISO with conventional channel estimation. Based on the simulation results, we can confirm that the proposed method can optimize the diversity gain provided by transmitter diversity, i.e. Alamouti scheme and the gain is only getting larger in higher doppler frequency.

Then, we have evaluated the performance of the proposed channel estimation method in optimizing the diversity gain provided by receiver diversity. For v = 360 [km/h]The proposed method can give SNR improvement around 8 dB for a 2×4 MIMO at uncoded BER= 2×10^{-3} compared to a 2×2 MIMO with a proposed method. Based on the simulation results, we can confirm that the proposed method can optimize the diversity gain provided by receiver diversity scheme, i.e. MRC and the gain is only getting larger in higher doppler frequency. In terms of complexity, a combination of a proposed 3-point diagonal averaging with two-stages non-rectangular 2D filter also contains the smallest number of additions and multiplications among available method. Therefore, we can conclude that the proposed 3-point diagonal averaging is the most efficient averaging scheme in this case.

In this thesis, we have also proposed a symbol-timing, carrier-frequency, and sampling-frequency synchronization method for ISDB-T system for HDTV contents transmission in Multipath Fading Channel. For joint symbol-timing and carrier-frequency synchronization, ML synchronization method [24], the simplified version [26], and the algorithm complexity between this two algorithm have been reviewed. ML is much complex than the simplified ML, but it gives better performance itself, based on our simulation result. The effect of of a DFT window position error has also been reviewed. Based, on this knowledge, we propose DFT window shift to increase the performance of ML based synchronization in Multipath fading channel. According to simulation result, proposed synchronizer, combination between DFT window shift method and Simplified ML can get good performance and less complexity synchronization algorithm.

For sampling-frequency synchronization, we have proposed an SFO estimation method for DTTV system in multipath fading channel. Considering the low value of SFO, we have proposed the estimation method that can minimize the influence of noise in SFO estimation. The proposed method also reduces the number of arctangent process for 1 OFDM symbol significantly. Simulation result shows that the proposed method produces much better performance compared to the conventional method when both using 1 OFDM symbol. In terms of complexity, the proposed method can reduce the number of multiplier around 90% and adder around 99% compared to the conventional method when both produce similar performance.

Chapter 6

Conclusion and Future Work

In this thesis, we report the study about the next generation of digital terrestrial television system. In chap. 2, we have discussed about the digital terrestrial television standard, especially, DVB-T2. We have also discussed about the importance of mobile reception of digital terrestrial television system in high speed environment, such as high speed train (TGV, Maglev, etc with commercial speed $\approx$ 300 km/h). In this case, the inclusion of MIMO scheme become necessary to increase the reception performance of high speed digital terrestrial television. In chap. 2, we have discussed the antenna diversity method for DVB-T2, i.e. modified Alamouti scheme (transmitter diversity) and maximal-ratio combining (receiver diversity).

In chap. 3, In we have discussed about the channel estimation for DVB-T2 system. Firstly, we have discussed about the scattered pilot pattern that we use as a reference for channel estimation process. Then, we have discussed about a channel estimation scheme in SISO and MIMO case. For channel estimation in MIMO case, there are three methods that we have discussed, i.e. a conventional method [16], a 2-point averaging [22], and the proposed 3-point diagonal averaging method. In this chapter, we have also discussed about 2D non-rectangular filter. In order to perform the robust channel estimation for paralellogram pattern of scattered pilot of DVB-T2, we have implemented the 2D non-rectangular LPF. Based on our study, in order to implement 2D non-rectangular LPF with lower complexity, we have proposed the two-stage implementation.

In chap. 4, we have proposed the time and frequency synchronization method for ISDB-T system for HDTV contents transmission in Multipath Fading Channel. ML synchronization method [24], the simplified version [26], and the algorithm complexity between this two algorithm have been reviewed. ML is much complex than the simplified ML, but it gives better performance itself, based on our simulation result. The effect of of a DFT window position error has also been reviewed. Based, on this knowledge, we have proposed DFT window shift to increase the performance of ML based synchronization in Multipath fading channel. Considering the low value of SFO, we have proposed the estimation method that can minimize the influence of noise in SFO estimation. The proposed method also reduces the number of arctangent process for 1 OFDM symbol significantly.

In chap 5, we show simulation results for proposed channel estimation and synchronization methods. Based on the simulation results for receiver with v=360 [km/h], the proposed 3-points averaging produce the best performance among the available method. In terms of complexity, a combination of a proposed 3-point diagonal averaging with two-stages non-rectangular 2D filter also contains the smallest number of additions and multiplications among available method. Therefore, we can conclude that the proposed 3-point diagonal averaging is the most efficient averaging scheme in this case.

We have also shown simulation results for a symbol-timing, carrier-frequency, and sampling-frequency synchronization method for ISDB-T system for HDTV contents transmission in Multipath Fading Channel. For joint symbol-timing and carrier-frequency synchronization, ML synchronization method [24], the simplified version [26], and the algorithm complexity between this two algorithm have been reviewed. ML is much complex than the simplified ML, but it gives better performance itself, based on our simulation result. According to simulation result, proposed synchronizer, combination between DFT window shift method and Simplified ML can get good performance and less complexity synchronization algorithm. For sampling-frequency synchronization, we have also performed performance comparison between conventional and proposed SFO estimation method. Simulation result shows that the proposed method produces much better performance compared to the conventional method when both using 1 OFDM symbol. In terms of complexity, the proposed method can reduce the number of multiplier around 90% and adder around 99% compared to the conventional method when both produce similar performance.

For future works, we will conduct an FPGA implementation of the proposed channel estimation method.

Chapter 7

Appendix A: The Derivation of 4-point and 5-point Averaging

As a comparison to the proposed 3-point averaging, we introduce 4-point and 5-point averaging. In this section. we explain the derivation of 4-point and 5-point averaging. The general form to calculate $\hat{H}^{1a}_{k,l}$ and $\hat{H}^{2a}_{k,l}$ with 4-point averaging is shown by (7.1)-(7.2), respectively.

$$\hat{H}^{1a}_{k,l} = \left(1\Big/\sum_{n=-1}^{2} C_n\right)\left(C_{-1}\hat{H}^{b}_{k-3,l-1} + C_0\hat{H}^{a}_{k,l} + C_1\hat{H}^{b}_{k+3,l+1} + C_2\hat{H}^{a}_{k+6,l+2}\right) \tag{7.1}$$

$$\hat{H}^{2a}_{k,l} = \left(1\Big/\sum_{n=-1}^{2} C_n\right)\left(C_{-1}\hat{H}^{b}_{k-3,l-1} - C_0\hat{H}^{a}_{k,l} + C_1\hat{H}^{b}_{k+3,l+1} - C_2\hat{H}^{a}_{k+6,l+2}\right) \tag{7.2}$$

For 5-point averaging, The general form to calculate $\hat{H}^{1a}_{k,l}$ and $\hat{H}^{2a}_{k,l}$ is shown by (7.3)-(7.4), respectively.

$$\hat{H}^{1a}_{k,l} = \left(1\Big/\sum_{n=-2}^{2} C_n\right)\left(C_{-2}\hat{H}^{a}_{k-6,l-2} + C_{-1}\hat{H}^{b}_{k-3,l-1} + C_0\hat{H}^{a}_{k,l} + C_1\hat{H}^{b}_{k+3,l+1} + C_2\hat{H}^{a}_{k+6,l+2}\right) \tag{7.3}$$

$$\hat{H}^{2a}_{k,l} = \left(1\Big/\sum_{n=-2}^{2} C_n\right)\left(-C_{-2}\hat{H}^{a}_{k-6,l-2} + C_{-1}\hat{H}^{b}_{k-3,l-1} - C_0\hat{H}^{a}_{k,l} + C_1\hat{H}^{b}_{k+3,l+1} - C_2\hat{H}^{a}_{k+6,l+2}\right) \tag{7.4}$$

Similar to 3-point averaging, in order to achieve the equal summation of $\hat{H}^{a}_{k,l}$ and $\hat{H}^{b}_{k,l}$, the coefficient of averaging of 4-point and 5-point averaging is shown by (7.5)-(7.6), respectively.

$$C_0 + C_2 = C_{-1} + C_1 \tag{7.5}$$

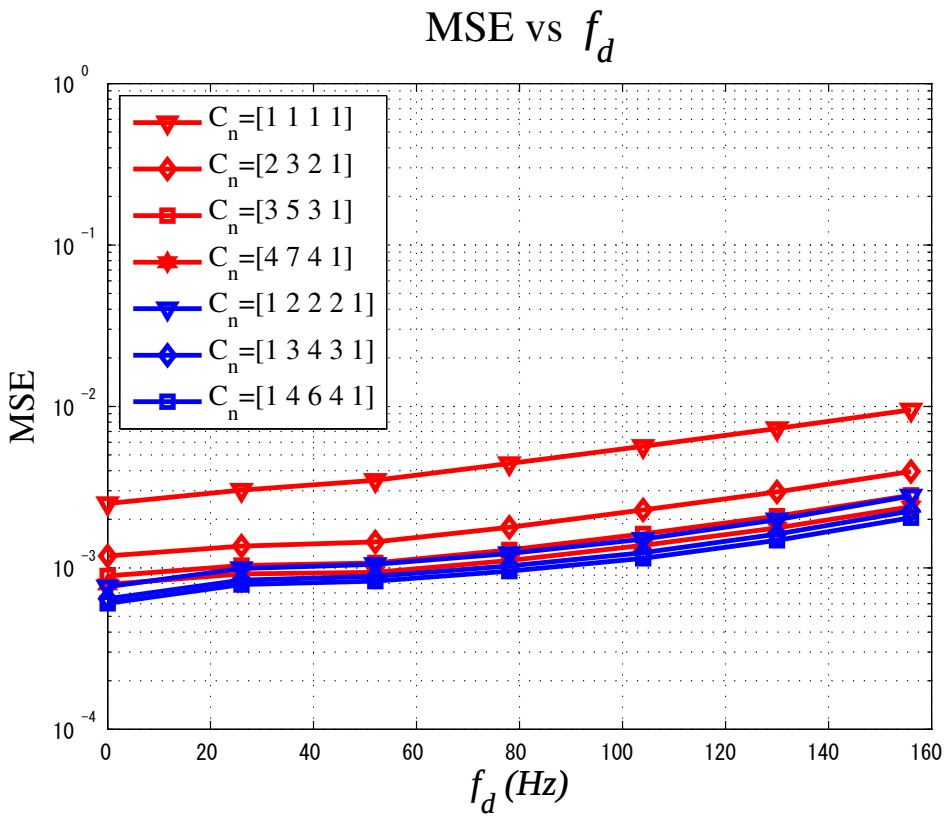

Figure 7.1: Coefficient Decision of 4-point and 5-point averaging (SNR=30dB)

$$C_{-2} + C_0 + C_2 = C_{-1} + C_1 \tag{7.6}$$

Unlike the 3-point averaging, in case of 4-point and 5-point averaging, there are some combinations of coefficients that can be implemented. In this paper, we have simulated some combinations of coefficients and use the best result of simulation to be compared with the proposed 3-point averaging as shown by Fig. 7.1. Based on the simulation result, it shows that $C_n = [C_{-1}C_0C_1C_2] = [4741]$ and $C_n = [C_{-2}C_{-1}C_0C_1C_2] = [14641]$ are the best coefficient combination among the simulated coefficients combinations.

Acknowledgement

First of all, I would like to thank my supervisor, Professor Hiroshi Ochi for his guidance, support, and advice during my study in Kyushu Institute of Technology. I also want to thank Ass. Professor Kurosaki for his support and advice in my research.

Secondly, I want to thank judges panel in my dissertation defense,, i.e. Prof. Inoue, Prof. Shuichi Ohno, and Prof. Kenji Kawahara. I want to thank them for their constructive comments and suggestions.

I also want to thank all of Ochi lab members for their cooperation and support during my study in Kyushu Institute of Technology.

I gratefully acknowledge financial supports from Kyushu Institute of Technology, Assuran International Scholarship Foundation, and Radrix,inc. I really appreciate the financial support from them that helps me alot to finish my PhD program.

Last but not least, I would like thank for my parents Benar Darius Ginting Soeka and Rahel Barus. Thank you for always give me a moral support during my PhD study. I also want to thank all of my sisters, Meltharyna, Shona Meilyna, and Lorenz Rulyna that never stop to cheer and support me everytime. I also want to thank all of my family for being my source of inspiration and spirit. For the love, encouragement, support that they always give to me.

References

[1] ETSI EN 302 705 V1.1.1, ”Digital Video Broadcasting(DVB);Frame structure channel coding and modulation for a second generation digital terrestrial television broadcasting system (DVB-T2),” Sep. 2009.

[2] ETSI EN 300 744 V1.6.1, ”Digital Video Broadcasting (DVB); Framing structure, channel coding, and codulation for digital terrestrial television,” Jan. 2009.

[3] S.M. Alamouti, ”A simple transmit diversity technique for wireless communication,”IEEE J. Sel. Areas Commun.,vol.16,no.8,pp.1451-58,Oct.98.

[4] Y.Li, N. Seshadri, and S. Ariyavisitakul, ”Channel estimation for OFDM systems with transmitter diversity in mobile wireless channels,”IEEE J. Sel. Areas Commun.,vol.17,no.3,pp.461-470, Mar.1999.

[5] Y. Gong, K. Letaief, ”Low rank channel estimation for space-time coded wideband OFDM systems,”in Proc. IEEE. Vehic. Technology Conf.(VTC’2001-Fall),Atlantic City,USA,pp.722-776,2001.

[6] Y. Li, ”Simplified channel estimation for OFDM Systems with multiple transmit antennas, ”IEEE Trans. Wireless Commun.,vol.1,no.1, pp.67-75,Jan. 2002.

[7] G. Auer, ”Channel estimation in two dimensions for OFDM systems with multiple transmit antennas,”Proc. IEEE Global Telecomm. Conf. (Globecom’03),San Fransisco,USA,vol.1,pp.322-326,2003.

[8] P.P Vaidyanathan, ”Multirate systems and filter banks,” Prentice Hall, 1993.

[9] Y. Sakaguchi, M. Kurosaki, S. Kinjo, H. Ochi, ”Channel estimation method using nonrectangular lattice filter for mobile digital terrestrial television broadcasting, ”in Proc. IEEE. Vehic. Technology Conf.(VTC’2007-Spring),Baltimore,USA, pp.3051-3055,April 2007

[10] Y. Sakaguchi, Y. Nagao, M. Kurosaki, H. Ochi, ”A study on channel estimation using two-dimensional interpolation filters for mobile digital terrestrial television broadcasting, ”IEICE Trans. Fundamentals,vol.E91-A,no.4,pp.1150-1154,April 2008.

[11] http://www.dvb.org

[12] ARIB STD-B31 1.6. ”Transmission system for digital terrestrial television broadcasting, ” Association of Radio Industries and Businesses, 2005.

[13] http://www.dibeg.org

[14] ATSC Doc. A53, ATSC Digital Television Standard, September 1995.

[15] Digital Video Broadcasting (DVB); Second generation framing Structure, channel Coding, and modulation systems for broadcasting, interactive services, news gathering, and other broadband satellite applications, European Telecomm. Standards Inst. (ETSI) EN 302 307 V1.2.1, Aug. 2009.

[16] DVB Document A 133. ”Digital Video Broadcasting (DVB); Implementation guidelines for a second generation digital terrestrial television broadcasting system (DVB-T2),” Dec. 2009.

[17] L. Vangelista, et al. ”Key Technologies for Next-Generation Terrestrial Digital Terrestrial Digital Television Standard DVB-T2, ” IEEE Communications Magazine. Oct. 2009.

[18] K. Nybom, J. Sandqvist, T. Soininen, J. Bjorkqvist, and J. Lilius. A software based implementation of the DVB-T2 bit interleaved coding and modulation transmission chain. Technical Report 931, Turku Center of Computer Science, March 2009.

[19] S. H. Han and J. H. Lee, ”An overview of peak-to-average power ratio reduction techniques for multicarrier transmission,” IEEE Wireless Commun., vol. 12, no. 2, Apr. 2005, pp. 56-65.

[20] Digital Video Broadcasting (DVB). 2nd Generation Terrestrial: The worlds most advanced Digital Terrestrial TV system. Technical report, 2009.

[21] Gershmann,A.B., Sidiroupoulos, N.D., ” Space-time processing for MIMO communications”, Wiley, June 2005.

[22] C. Gomez-Calero, L. Cuellar Navarette, L. de Haro, R. Martinez, ”A 2×2 MIMO DVB-T2 system: design, new channel estimation scheme, and measurements with polarization diversity,”IEEE. Trans. Broadcast, vol.57,no.2,pp.195-203,June 2011.

[23] Tzi Dar Chiueh, Pei-Yun Tsai. OFDM baseband receiver for wireless communications. Wiley December 2007.

[24] J.J Van Beek, M. Sandell, P.O. Borjesson. “ ML estimation of time and frequency offset in OFDM systems,”IEEE Transactions on Signal Processing Vol. 45 No. 7 July 1997.

[25] PH. Moose,"A technique for orthogonal frequency division multiplexing frequency offset correction," IEEE Transactions On Communications, Vol. 42, No 10, October 1994.

[26] D. Landstrom, S. Johansson, P. Nillson,"Silicon realization of an OFDM synchronization algorithm,"Proceedings of ICECS, pp. 319-322 .1999.

[27] Hou-Shin Chen,"Novel sampling clock offset estimation for DVB-T OFDM,"IEEE VTC 2003-Fall, vol.4, pp.2272-2276, Oct. 2003.

[28] Commission of the European Communities, "COST 207: Digital land mobile radio communications,"Luxembourg: Final Report,Office for Official Publications of the European Communities, 1989.

Papers

1. Transaction Manuscripts(Reviewed)

[1] Nico Surantha, Tatsumi Uwai, Yuhei Nagao, Masayuki Kurosaki, Baiko Sai, Hiroshi Ochi,"A Channel Estimation for a MISO DVB-T2 System in High Speed Environments," RISP Journal of Signal Processing, Vol. 17, No. 5, pp.179-188, 2013.

[2] Nico Surantha, Yuhei Nagao, Masayuki Kurosaki, Hiroshi Ochi,"Sampling Frequency Offset Estimation for Digital Terrestrial Television Broadcasting System," IEICE Communication Express, Vol. 2, No. 5, pp. 224-230, May 2013.

2. International Conference Proceeding (Reviewed)

[1] Nico Surantha, Yuhei Nagao, Masayuki Kurosaki, Hiroshi Ochi,"A Computationally Efficient Sampling Frequency Offset Estimation for OFDM-Based Digital Terrestrial Television Systems," IEEE International Symposium on Personal, Indoor, and Mobile Radio Communications (PIMRC) 2013, London, UK, Sept 2013.

[2] Nico Surantha, Tatsumi Uwai, Yuhei Nagao, Masayuki Kurosaki, Baiko Sai, Hiroshi Ochi,"Pilot Aided Channel Estimation for a 2×2 MIMO DVB-T2 System in High Speed Mobile Environment," IEEE Vehicular Technology Conference-Fall 2012, Sept. 2012.

[3] Nico Surantha, Tatsumi Uwai, Yuhei Nagao, Masayuki Kurosaki, Baiko Sai, Hiroshi Ochi,"Symbol Timing Synchronization for ISDB-T System in Multipath Fading Channel," Proc. The 13th IEEE International Conference of Advanced Communication Technology (ICACT2011), No.10C-01, Phoenix Park, Korea, February 13-16, 2011.

[4] Nico Surantha, Tatsumi Uwai, Yuhei Nagao, Masayuki Kurosaki, Hiroshi Ochi, "Joint Time-and-Frequency Synchronization for ISDB-T Receiver in Multipath Fading Channel" Proc. IEICE Smart Info-Media System Conference in Asia (SISA) 2010, No. RS2-8 CDROM, Manila, Philippines, September 8-9 (9), 2010.

Author

Nico Surantha

Born, July 24 1985, Jakarta, Indonesia
Elementary School, Graduated 1997, Pangudi Luhur Elementary School, Jakarta, Indonesia
Junior High School, Graduated 2000, Pangudi Luhur Junior High School, Jakarta, Indonesia
Senior High School, Graduated 2003, 70 Public Senior High School, Jakarta, Indonesia.
Bachelor of Engineering, Graduated 2007, Bandung Institute of Technology, Bandung, Indonesia.
Master of Engineering, Graduated 2009, Bandung Institute of Technology, Bandung, Indonesia.
Doctor of Engineering, Graduated 2013, Kyushu Institute of Technology, Iizuka, Japan.